KTH Architecture and
the Built Environment

Undifferenced GPS for Deformation Monitoring

Johan Vium Andersson

Licentiate thesis in Geodesy

Royal Institute of Technology (KTH)
Department of Transport and Economics
Division of Geodesy
100 44 Stockholm

June 2006

Abstract

This thesis contains the development of a deformation monitoring software based on undifferenced GPS observations. Software like this can be used in alarm systems placed in areas where the earth is unstable. Systems like this can be used in areas where people are in risk of getting hurt, like in earthquake zones or in land slide areas, but they can also be useful when monitoring the movements in buildings, bridges and other artefacts.

The main hypotheses that are tested are whether it is possible to detect deformations with undifferenced observations and if it is possible to reach the same accuracy in this mode as when working in a traditional mode where the observations are differenced.

The development of a deformation monitoring software based on undifferenced GPS observations is presented. A complete mathematical model is given as well as implementation details. The software is developed in Matlab together with a GPS observation simulator. The simulator is mainly used for debugging purposes.

The developed software is tested with both simulated and real observations. Results from tests with simulated observations show that it is possible to detect deformations in the order of a few millimetres with the software. Calculations with real observations give the same results. Further, the result from calculations in static mode indicates that the commercial software and the undifferenced software diverge a few millimetres, which probably depends on different implementations of the tropospheric corrections. In kinematic mode the standard deviation is about 1 millimetre larger in the undifferenced mode than in the double differenced mode. An initial test with different observation weighting procedures indicates that there is a lot of potential to improve the result by applying correct weights to the observations. This is one of the aims in the future work within this project.

This thesis are sponsored by the Swedish Research Council for Enviroment, Agricultural Sciences and Spatial Planning, FORMAS within the framework “Monitoring of construction and detection of movements by GPS ref no. 2002-1257”

Keywords: deformation monitoring, GPS, modified NGS-parameters, undifferenced GPS-observations, Kalman filter

Acknowledgements

First and foremost, I want to express my gratitude to my supervisors Professor Lars E Sjöberg and Ph.D. Milan Horemuz, how have helped, supported and encouraged me through my entire thesis work. Their knowledge and experience have been a true help for me during these three years.

I also want to thank all my former and present colleagues and the Ph.D.-students at the division of Geodesy for all the support and for the interesting discussions we had during lunches and coffee breaks.

I am thankful to the Swedish Research Council for Enviroment, Agricultural Sciences and Spatial Planning, FORMAS, for sponsoring this research.

I further wish to thank Michael Skoglund at the Swedish National Road Administration and Bo Jonsson at the National land survey for letting me access the ftp-archive with GPS-observations from the permanent reference stations in Gothenburg. It saved me a lot of headache and several hours of work.

I am also indebted to my former and future colleagues at WSP Sweden AB for the encouragement to continue my study as well as for the economical support provided for participation in the meetings of the Nordic Geodetic Commission and all the internal events and meetings at WSP.

Finally I want to express my gratitude to my family and friends that have been patient with me being hard to reach and difficult to meet. But without you being there, this work would have been difficult to finish.

Contents

1 Introduction

Everything on earth is in motion. The main part of these motions is very slow and we can not sense them with our human senses. Other motions are larger and more hazardous, as earth quakes and land slides, and if we are unlucky be killed by them. Most of these dangerous motions are preceded by slow motions of the type that we cannot sense. By the use of special sensors, it is possible to detect these small motions and predict when a catastrophe is to come. This is what this thesis is about the developing of a system which can detect small motions and alarm if something unpredicted is about to happen.

There are several different types of sensors that can be used to detect slow and small motions. They either work in relative or in absolute mode. In relative mode all sensors are placed on the object that is moving and the sensors sense relative changes among each other. Absolute sensors, on the other hand, are placed both on the moving object and on some non moving objects away from the moving object. The benefit of the absolute method is that the absolute change is sensed but a problem is that there is often a long distance between the moving and the fix objects.

During a long time motion monitoring has been a subject for surveying engineers. Several different techniques have been used to measure movements as triangulation with total stations, precise levelling, close range photogrammetry, laser scanning and with satellite methods as GPS, DORIS and SLR. Common within all these methods are that they are measured in repeated campaigns and the result is presented determined after the campaign is finished.

If an alarm function is wanted or if the motions must be monitored all of the time, the mentioned systems will not fulfil the needs, since they do not operate in real-time. A type of sensors that have become very popular during the last 15 years for motion and deformation monitoring are the GPS-receivers. The GPS-technology has some good properties; one is that it possible to measure baselines with a high accuracy over long distances without any demand of a line-of-sight between the receivers. This makes it possible to perform absolute motion and deformation monitoring where the distance between the moving area and the fix points are long.

There are several different movement and deformation monitoring systems available on the market today like

- GRAZIA, developed at Graz University of Technology, Gassner et al. (2002)
- GOCA, (GPS based online control and alarm system) developed at Gachhochschule Kalsruhe, Jäger and Kälber (2004)

- RT-MODS2- Real-Time Monitoring Of Dynamic Systems, developed at Istambul Technical University, Ince and Sahin (2000)
- GNPOM, Geodetic Navstar - Permanent Object Monitoring, Geo++®, (www.geopp.de)
- Motion Tracker, by Trimble (www.trimble.com)

The deformation monitoring systems can be separated into three categories according to their way of using the observations. The first category is the post processing category, where Motion tracker from Trimble belongs. The observations from the GPS-receivers in this category are stored in observation files that are placed in a file library. The baselines are calculated with a given time interval and the result is stored in a database from which one can perform the deformation analyses. This is not a true real-time system but still a system that perform deformation analyses automatically, however with a little time delay.

The second category uses the result calculated in the receivers in RTK-mode (Real Time Kinematic) for deformation monitoring. RT-MODS2 and GOCA are typical softwares of this category. In RT-MODS2 the coordinates from the RTK solution are directly used in the deformation monitoring. GOCA uses the same information but instead of taking the coordinates directly, it first performs an adjustment of all the observations from the same epoch in a traditional network adjustment. The benefit of this approach is that outliers can be detected as well as movements in the static receivers. A problem with this approach is that the correlations among the baselines are not treated correctly.

The third category is the one that uses raw data; all observations are sent into the central computer, where the calculations are performed. GRAZIA and GNPOM are softwares that follow this approach. The differences between these softwares are that GARZIA is based on double differenced observations while GNPOM is based on undifferenced observations. More about the mathematical principles of the differenced and the undifferenced approaches follows in the next chapter of the thesis.

The goal with the project, which this thesis is a part of, is to build a system for real-time movement detection at mm level, based on GPS observations. The system will consist of two or more GPS receivers, data-links between them and a central computer with software developed to detect deformation and an alarm system.

As one part of the research a software based on undifferenced GPS observations is developed. The reason for developing a new software is to fully understand each step in this type of software and to have a platform for further research within the area. For the evaluation, the software is developed in object oriented Matlab code, which in the

future will be converted into a programming language that is more adapted for real-time applications.

1.1 Author's contribution

This thesis describes the fundamental process in developing a deformation monitoring software. The author has contributed with a software, based on undifferenced GPS observations, that are able to calculate coordinates and detect deformations.

In the beginning of the second chapter, the observation equations for GPS observations are introduced. Thereafter follows a comparison of the undifferenced and double differenced algorithms to compare their advantages and disadvantages. The theory of each of these technologies is mainly known information summarised to motivate the undifferenced solution.

The undifferenced model we use is described in Chapter 3 together with deterministic models of all unknown parameters that are estimated in the software. The Kalman filter described in this chapter is a known general mathematical approach for solving the state parameters of a dynamic system. The author has to find a suitable dynamic model for each parameter and derive corresponding transmission and process noise covariance matrix. This part of the thesis is performed in collaboration with supervisor Milan Horemuz.

In Chapter 4, follows a description of the implementation details. Two new algorithms are presented in this chapter: first an algorithm that unifies the calculation methods for the satellite coordinates, presented by Horemuz et al. (2006), and then an algorithm that makes it possible to use GPS-antenna calibrations from NGS (U.S. National Geodetic Survey) in an arbitrary direction. The author has contributed in the paper where he implemented the algorithm in Matlab and did the numerical calculations. The new antenna orientation algorithm is developed by the author.

To study the performance and simplify the debugging procedure, a simulator is generated, which is described in Chapter 5. The contribution of the author in this chapter was to implement the same type of stochastic and deterministic models in the simulator.

A series of calculations are done with the developed software, the result from these are presented in Chapter 6. The author has here compared the result from the developed software with the result from commercial softwares. Initial tests with different weighting models are also done here.

Finally in Chapter 7, summary and conclusions and some proposals for further research are presented.

2 Observation Equations

Three types of observations can be done with a geodetic GPS-receiver: pseudorange, phase and Doppler observations. These observations are done with the receivers in epochs with a fix time interval i.e. each second. The pseudorange observations are based on the PRN-code message that is modulated on the carrier wave, the phase observations are based on the fractional part of the carrier phase and an integer number representing full wavelengths from a reference time t_0 and the Doppler count observations, represent the difference between nominal and the received frequencies between two observation epochs. The purpose of this chapter is to derive the observation equations for both pseudoranges and phase observations and to introduce the error sources that influence them along their travel path from the satellite to the receiver. The Doppler observations are not used in this thesis and are therefore not described further within the report. The derivation of the observation equations follows the derivation given by Leick (2004) and Hoffmann-Wellenhof et al.(2001). When this is done two different approaches of positioning with GPS-observations are introduced: differential and undifferenced positioning. At the end of this chapter the advantages and disadvantages of each approach are discussed to motivate why the use of the undifferenced approach in this thesis.

2.1 Pseudorange observations

Pseudorange observations are based on the PRN-code message that is sent out from each satellite modulated on the carrier phase signal. The main idea with the pseudorange observations is to determine the true travelling time from the satellite to the receiver and then to multiply it with the speed of light, to determine the distance between the satellite and the receiver. The travelling time is determined in the receivers by generating a replica of the PRN-code message in the receiver and then maximising the correlation between the incoming signal and the generated signal by time shifting the latter in the instrument. The total time shift will then correspond to the travelling time from satellite to receiver. The pseudorange P_A^S between a satellite antenna S and a receiver antenna A can be expressed as:

$$P_A^S(t_A) = (t_A - t^S)c \tag{1}$$

where t_A and t^S are nominal times of reception in the receiver and emission of the signal from the satellite, respectively c is a constant which represents the speed of light in vacuum. From now on we use subscripts for the receivers and superscript to for the satellites. Nominal times in the receiver t_A and satellite t^S are related to true GPS-times $t_{A,GPS}$ and t^S_{GPS} respective as

$$\begin{aligned} t_{A,GPS} &= t_A - \delta t_A \\ t^S_{GPS} &= t^S - \delta t^S \end{aligned} \tag{2}$$

where δt_A and δt^S are the delays in the receiver and satellite clocks with respect to GPS-time. Additional subscripts are used in the time variables to distinguish between true GPS-time and nominal time. Combining the results in Eqs. (1) and (2) we get:

$$\begin{aligned} P^S_A(t_A) &= \left(t_{A,GPS} - t^S_{GPS}\right)c + c\delta t_A - c\delta t^S \\ &= \rho^S_A\left(t_{A,GPS}\right) + c\delta t_A - c\delta t^S \end{aligned} \tag{3}$$

where $\rho^S_A\left(t_{A,GPS}\right)$ is introduced as the true geometric travel distance for the emitted signal in true GPS-time $t_{A,GPS}$. Since the $t_{A,GPS}$ at the receiver is unknown, the geometric distances are linearised around the known nominal receiver time t_A. This is done with expansion into a Taylor series:

$$\rho^S_A(t_{A,(GPS)}) = \rho^S_A\left(t_A\right) + \dot{\rho}^S_A\left(t_A\right)\delta t_A + \underbrace{\frac{\ddot{\rho}^S_A\left(t_A\right)}{2!}\delta t_A^2 + \ldots}_{\text{HOT}} \tag{4}$$

where $\dot{\rho}^S_A, \ddot{\rho}^S_A, \ldots$ are the first and second order time derivatives of the geometric distance according to the nominal receiver time t_A. Ignoring the higher order terms (HOT) in Eq.(4), the geometric distance can be written as:

$$\rho^S_A\left(t_{A,GPS}\right) = \rho^S_A\left(t_A\right) + \dot{\rho}^S_A\left(t_A\right)\delta t_A \tag{5}$$

and the code pseudorange observation can be rewritten by combining Eqs.(3) and (5) as:

$$P^S_A\left(t_A\right) = \rho^S_A\left(t_A\right) + \left(\dot{\rho}^S_A\left(t_A\right) + c\right)\delta t_A - c\delta t^S \tag{6}$$

here $\dot{\rho}^S_A$ is the radial velocity along the vector between the satellite and the receiver. This velocity has a maximum value of approximately 800 m/s according to Leick (2004). If the clock delay δt_A is about $10\,\mu s$, the radial influence of $\dot{\rho}^S_A$ has a maximal value of 8 millimetres, which is significant in the case of relative positioning with phase observations.

2.2 Phase observations

To describe the phase observations we start by studying how the incoming signal is processed in the GPS receivers. When a GPS receiver A is started at nominal time t_0, it generates a carrier with nominal frequency f_A and phase $\varphi_A\left(t_A\right)$, based on the receiver clock. Incoming signals from a satellite is reconstructed in the receiver with a carrier frequency f^S_i and phase $\varphi^S\left(t_A\right)$ based on the satellite clock. The instrument records the

sum of all changes between the phase of the incoming signal and the receiver generated phase. This sum can be expressed in GPS-time as follows:

$$\varphi_A^S\left(t_{A,GPS}\right) = \varphi^S\left(t_{A,GPS}\right) - \varphi_A\left(t_{A,GPS}\right) \tag{7}$$

The receiver and satellite clocks are related to true GPS-time as described in Eq.(2).

Taking the clock errors in the satellite clock into account as well as the travelling time for the incoming satellite signal we get the following phase for the incoming signal given in GPS-time.

$$\varphi^S\left(t_{A,GPS}\right) = f^S\left(\left(t_A + dt^S\right) - t_\rho\right) \tag{8}$$

The travelling time t_ρ is determined by dividing the true geometric distance ρ_A^S with the speed of light c. The phase in the receiver is given in GPS-time as:

$$\varphi_A\left(t_{A,GPS}\right) = f_A t_A + f_A dt_A \tag{9}$$

According to Hoffmann-Wellenhof et al. (2001 p.89), the deviation of the frequencies, f^S and f_A, from a nominal frequency f is in the order of a fraction part of Hz, so for the moment we may treat all the frequencies as the same $(f = f_A = f^S)$, and come back to the issues about the frequency later on. The satellite clock error is even smaller, at the range of milliseconds, and is therefore ignored. With these assumptions we can rewrite the phase equations at epoch t_A as:

$$\varphi_A^S\left(t_{A,GPS}\right) = fdt^S - ft_\rho - fdt_A = -f\left(\frac{\rho_A^S}{c}\right) - f\left(dt_A - dt^S\right) \tag{10}$$

The observed phase difference does not tell anything about the total number of phases which is used to determine the distance from the receiver to the satellite. There is an unknown integer number N_A^S missing in Eq.(10), which represents the amount of whole cycles between the satellite and the receiver. This number of whole cycles, also known as the phase ambiguities, is constant from the initialization of the instrument where the phase signal is locked to the receiver generated phase, if the signal is not lost or the tracking interrupted. Using the well-known physical relation between wavelengths and frequencies, $f = c\lambda^{-1}$, which can be found in any basic textbook containing the fundamentals of physics, like Halliday et al (2001), we can Eq.(10) as:

$$\varphi_A^S\left(t_{A,GPS}\right) = -\frac{\rho_A^S}{\lambda}\left(t_{A,GPS}\right) - \frac{c \cdot t_{A,GPS}}{\lambda} + N_A^S \tag{11}$$

Since the true time $t_{A,GPS}$ at the receiver is unknown, the geometric distance is linearised around the known nominal receiver time t_A, with Taylor expansion described

in Eq.(4). Then we arrive in the following observation equation expressed for the nominal time in the receiver and converted from cycles to a distance in metres:

$$\begin{aligned}\Phi_A^S\left(t_{A,GPS}\right) &= \lambda_i \varphi_A^S\left(t_A\right) \\ &= \rho_A^S\left(t_A\right) + \left(-\dot{\rho}_A^S\left(t_A\right) + c\right)\delta t_A - c\delta t^S + \lambda N_A^S\end{aligned} \tag{12}$$

The observation equations for the code and phase observations in Eqs.(6) and (12) would be complete, if there where no additional error sources involved. In reality there are some additional systematic and random errors that have to be added to get the complete observation equations. The errors can be divided, as in Table 1, into three groups depending on their source.

Table 1. Additional errors that affect the GPS observables

Satellite	$\delta\mathbf{o}^S$ - orbital errors a^s - satellite clock errors HD^S - hardware delays in the satellite AO – antenna offset in the satellite
Atmosphere	I - ionospheric delay T - tropospheric delay (wet and dry)
Receiver	MPA – Multipath APC - antenna phase centre variations HD_A - hardware delays in the receiver ε - random errors for the satellite / receiver combination

Taking these errors into account the complete equation for pseudoranges reads:

$$\begin{aligned}P_{A,i}^S\left(t_A\right) = \rho_A^S\left(t_A\right) + \left(-\dot{\rho}_A^S\left(t_A\right) + c\right)\delta t_A - c\delta t^S + \frac{\mathbf{R}_A^S}{\left|\mathbf{R}_A^S\right|}\cdot\delta\mathbf{o}^S + HD_{i,P}^S\left(t_A\right) + AO_{A,i}^S\left(t_A\right) \\ + I_{A,i}^S\left(t_A\right) + T_A^S\left(t_A\right) + MPa_{A,i,P}^S\left(t_A\right) + APC_{A,i}^S\left(t_A\right) + HD_{A,i,P}\left(t_A\right) + \varepsilon_{A,i,P}^S\end{aligned} \tag{13}$$

and phase observables

$$\Phi^{S}_{A,i}(t_A) = \lambda_i \varphi^{S}_{A,i}(t_A) = \rho^{S}_{A}(t_A) + \left(-\dot{\rho}^{S}_{A}(t_A) + c\right)\delta t_A - c\delta t^{S} + \lambda_i N^{S}_{A,i} + \frac{a^{s}}{f_i}\rho^{s}_{A}(t_A)$$
$$+ \frac{\mathbf{R}^{S}_{A}}{\left|\mathbf{R}^{S}_{A}\right|}\cdot \delta \mathbf{o}^{S} + HD^{S}_{i,\Phi}(t_A) + AO^{S}_{A,i}(t_A) - I^{S}_{A,i}(t_A) + T^{S}_{A}(t_A) + MPA^{S}_{A,i,\Phi}(t_A) \quad (14)$$
$$+ APC^{S}_{A,i}(t_A) + HD_{A,i,\Phi}(t_A) + \varepsilon^{S}_{A,i,\Phi}$$

Subscript i can be L_1 or L_2, denoting the dependence of the variable on the observation frequency and subscript P denotes code measurement, i.e. the error term with this subscript is not equal to the corresponding error affecting the phase pseudoranges. In front of the orbital error, in Eq.(14), is a mapping function $\mathbf{R}^{S}_{A}/\left|\mathbf{R}^{S}_{A}\right|$ based on the vector $\mathbf{R}^{S}_{A}$ which contains the vector components of the relative position between the receiver and the satellite. A further discussion and analysis of all these error sources will be done in detail in Section 3.2, and it is therefore not discussed here.

To reach millimetre accuracy with GPS one must use phase observations and find the correct value of the unknown ambiguities N^{S}_{A}. Mathematical it is normal to use least square adjustment to estimate a solution to the unknown parameters, described i.e. by Bjerhammar (1973). One of the requirements in this approach is that no linear dependencies are allowed between the estimated parameters, since the solution then becomes singular.

The parameters in the observation equation Eq.(14) show a linear dependency. The ambiguities are linear dependent with the clock errors and the hardware delays. To solve this problem there are some various methods, which can be used as a solution. Two of them are presented in the subsequent sections of this chapter: the differenced and the undifferenced solution.

2.3 Phase differences

By the use of data from two satellites and two receivers one can eliminate the parameters that are singular as mentioned in the end of previous section. This is done in two steps: first two single differences (SD) are created which then are combined in a double difference (DD) observation, and both the steps will now be explained with a start with the single difference.

2.3.1 Single differences

Assume that we have observations from two receivers (*k* and *m*) to the same satellite *p* during an epoch t as in Figure 1. The two observation equations are combined into one equation for the SD as

$$\Phi^{p}_{km}(t) = \Phi^{p}_{k}(t) - \Phi^{p}_{m}(t) \tag{15}$$

By inserting the observation equations from Eq.(14) for receivers k and m into Eq.(15) we get the following expression for the single difference

$$\begin{aligned}\Phi^{p}_{km}(t) = \rho^{p}_{km}(t) + \dot{\rho}^{p}_{km}(t)\delta t_{km} + c\delta t_{km} + \lambda N^{p}_{km} + \frac{a^{p}}{f}\rho^{p}_{km}(t) + \frac{\mathbf{R}^{p}_{km}}{\left|\mathbf{R}^{p}_{km}\right|}\cdot\delta\mathbf{o}^{p} + AO^{p}_{km}(t) \\ -I^{p}_{km}(t) + T^{p}_{km}(t) + MP^{p}_{km,\Phi}(t) + APC^{p}_{km}(t) + HD_{km,\Phi}(t) + \varepsilon^{p}_{km,\Phi}\end{aligned} \tag{16}$$

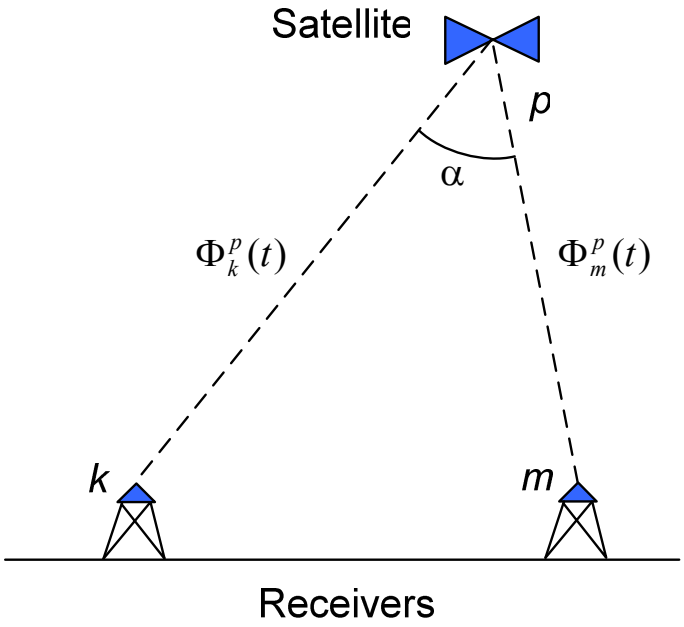

Figure 1. A single difference is generated by combining observations from two receivers, in this case k and m, to one satellite p

By forming the single differences all the errors related to the satellites are eliminated. The remaining parameters that occur in Eq.(16) are combinations of the original parameters. The new subscript km indicates the receivers from which the observations originate, and the superscripts tell the same about the satellites. For example, the new single difference of the geometric distance is given by

$$\rho^{p}_{km}(t) = \rho^{p}_{k}(t) - \rho^{p}_{m}(t) \tag{17}$$

All of the differentiated parameters in Eq.(16) can be formed in a similar way. If the distance between the receivers k and m is shorter than 100 km, then the orbital error $\delta\mathbf{o}^{p}$ and the satellite antenna offset AO can be ignored in Eq.(16). The reason to this is that the orbital error is mapped to the geometrical vector between satellite and receiver. If the receivers are placed close to each other, then the angle between the two vectors (α in Figure 1) will be small and the orbital error will become much the same at both stations and eliminated in the single differencing procedure. The same discussion can

be applied to AO. The term with a^p can be neglected, since its contribution is at 0.01 mm level, if a^p is one millisecond. With these parameters removed, Eq.(16) are rewritten into:

$$\begin{aligned}\Phi^{p}_{km}(t) = \rho^{p}_{km}(t) + \dot{\rho}^{p}_{km}(t)\delta t_{km} + c\delta t_{km} + \lambda N^{p}_{km} - I^{p}_{km}(t) \\ + T^{p}_{km}(t) + MP^{p}_{km,\Phi}(t) + APC^{p}_{km}(t) + HD_{km,\Phi}(t) + \varepsilon^{p}_{km,\Phi}\end{aligned} \tag{18}$$

2.3.2 Double differences

Double differences are generated by combining two single differences from a pair of receivers to two satellites as in Eq.(19), where the single differences between receiver k and m to satellite q and p are combined into a double difference.

$$\Phi^{pq}_{km}(t) = \Phi^{p}_{km}(t) - \Phi^{q}_{km}(t) \tag{19}$$

which also can be written with the use of Eq.(18) as:

$$\begin{aligned}\Phi^{pq}_{km}(t) = \rho^{pq}_{km}(t) + \dot{\rho}^{pq}_{km}(t)\delta t_{km} + \lambda N^{pq}_{km} - I^{pq}_{km}(t) + T^{pq}_{km}(t) + MP^{pq}_{km,\Phi}(t) \\ + APC^{pq}_{km}(t) + \varepsilon^{pq}_{km,\Phi}\end{aligned} \tag{20}$$

Figure 2 shows a principle figure of a double difference combination

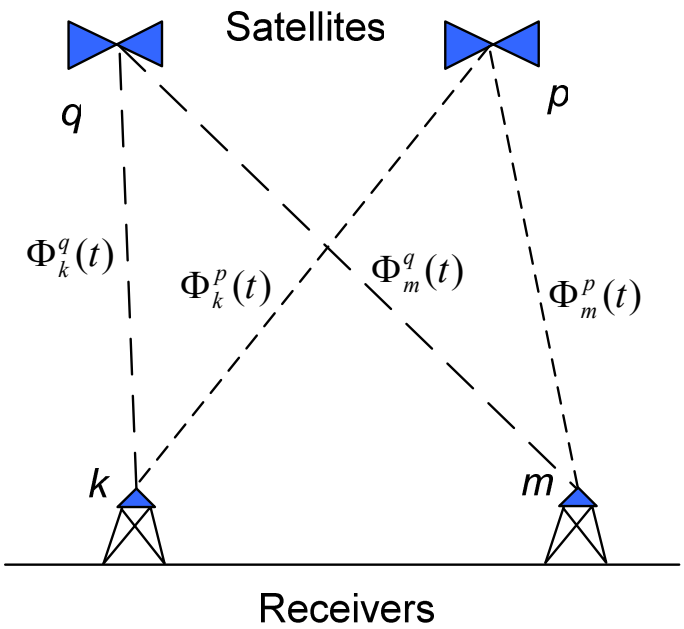

Figure 2. Double differences where two single differences are combined

The double differencing procedure eliminates the receiver errors, both the hardware delays and the clock offset are removed since they occur in both single differences. The remaining double differenced variables in the double difference equation are

$$
\begin{aligned}
\rho_{km}^{pq}(t) &= \rho_{km}^{p}(t) - \rho_{km}^{q}(t) \\
\dot{\rho}_{km}^{pq}(t) &= \dot{\rho}_{km}^{p}(t) - \dot{\rho}_{km}^{q}(t) \\
N_{km}^{pq} &= N_{km}^{p} - N_{km}^{q} \\
I_{km}^{pq}(t) &= I_{km}^{p}(t) - I_{km}^{q}(t) \\
T_{km}^{pq}(t) &= T_{km}^{p}(t) - T_{km}^{q}(t) \\
MP_{km,\Phi}^{pq}(t) &= MP_{km,\Phi}^{p}(t) - MP_{km,\Phi}^{q}(t) \\
APC_{km}^{pq}(t) &= APC_{km}^{p}(t) - APC_{km}^{q}(t) \\
\varepsilon_{km,\Phi}^{pq} &= \varepsilon_{km,\Phi}^{p} - \varepsilon_{km,\Phi}^{q}
\end{aligned}
\tag{21}
$$

where the new subscript for the parameters indicates the receiver combination and the superscript the satellite combination.

The singularity in the original observation equation is removed with the double differences, but correlations between the observations are introduced for all other parameters in the double difference observation equation.

2.3.3 Correlations

In the previous section we eliminated the singularity in the phase observables mathematically by combining observations from two receivers. The benefit of this procedure is that the unknown parameters related to the satellite and the receiver clocks and hardware delays are removed. To get a complete overview of the result after the differencing one must also study the stochastic part of the double differences. Let us denote the phase observations at an arbitrary receiver R to the three satellites o, p and q, as

$$
\mathbf{\Phi}(t) = \begin{bmatrix} \Phi_R^o(t) & \Phi_R^p(t) & \Phi_R^q(t) \end{bmatrix}^T \tag{22}
$$

The superscript T symbolises the transpose of the vector. Each phase observation is assumed to be normal distribution with zero expectation value and variance σ^2. The variance of each observation depends on the error sources along the signal path from satellite to receiver. It increases with the travelling distance through the atmosphere and is therefore directly correlated with the elevation angle. At low elevation angles the distance through the atmosphere are longer than at high elevation angles. The stochastic nature of the observations and the correlation will be explained in detail in Chapter 3 and will not be discussed further here. Instead we assume that all observations are uncorrelated with equal variance σ_0^2. The pure mathematical correlation matrix can therefore be written as:

$$
\mathbf{C}_\Phi(t) = \sigma_0^2 \mathbf{I} \tag{23}
$$

where **I** is an unit matrix. With the use of the observation equations, single and double difference equations (18) and (20), we can derive the correlation matrices for each level of differences. This is done in the following subsections.

2.3.3.1 Single differences

Single differences are generated with observations from two receivers, combined as in Eq.(15). To give an example how the single differences can be generated we use observations from two receivers (k and m) to three satellites (o, p and q). Their observations are given in two vectors, one fore each receiver, as in Eq.(22). To simplify the notation we ignore the time index t and write the single difference combination $\mathbf{\Phi}_{SD}$ in matrix notation as:

$$\mathbf{\Phi}_{SD} = \mathbf{A}_{SD}\mathbf{\Phi}_{SD} \tag{24}$$

where

$$\mathbf{\Phi}_{SD} = \begin{bmatrix} \mathbf{\Phi}_{km}^{o} \\ \mathbf{\Phi}_{km}^{p} \\ \mathbf{\Phi}_{km}^{q} \end{bmatrix} \quad \mathbf{A}_{SD} = \begin{bmatrix} 1 & -1 & 0 & 0 & 0 & 0 \\ 0 & 0 & 1 & -1 & 0 & 0 \\ 0 & 0 & 0 & 0 & 1 & -1 \end{bmatrix} \quad \mathbf{\Phi}_{SD} = \begin{bmatrix} \mathbf{\Phi}_{k} \\ \mathbf{\Phi}_{m} \end{bmatrix} \tag{25}$$

$\mathbf{A}_{SD}$ is the design matrix which correspond to two the single differences according to Eq.(15). The stochastic model is formed by the law of error propagation of covariance

$$\mathbf{C}_{SD} = \mathbf{A}_{SD}\mathbf{C}_{\Phi}\mathbf{A}_{SD}^{T} \tag{26}$$

This gives the covariance matrix for the three single differences. By combining Eqs. (26) and (23) we get the following covariance matrix for the single differences

$$\mathbf{C}_{SD} = \mathbf{A}_{SD}\left(\sigma_0^2\mathbf{I}\right)\mathbf{A}_{SD}^{T} = \sigma_0^2\mathbf{A}_{SD}\mathbf{A}_{SD}^{T} = 2\sigma_0^2\mathbf{I} \tag{27}$$

The identity matrix **I** indicates that there is no off-diagonal elements different than zero in the covariance matrix, and by that, one can make the conclusion that no correlations between single differences exist. The size of the matrix **I** depends on the number of single differences that can be formed, or in other words the number of common satellites at receiver k and m. The condition that only the common observations can be used implies that all other observations are useless. Eq.(27) is a general expression for the covariance matrix of the single differences when two receivers are used.

2.3.3.1.1 Single differences in a multipoint solution

In the case when three or more receivers are used in a multipoint solution the situation becomes a little more complicated. Additional correlations are introduced when observations are used to form more than one single difference. This will be described with the following example: Assume that observations are collected at three receivers (k, l and m) to the satellite p at epoch t, as in Figure 3.

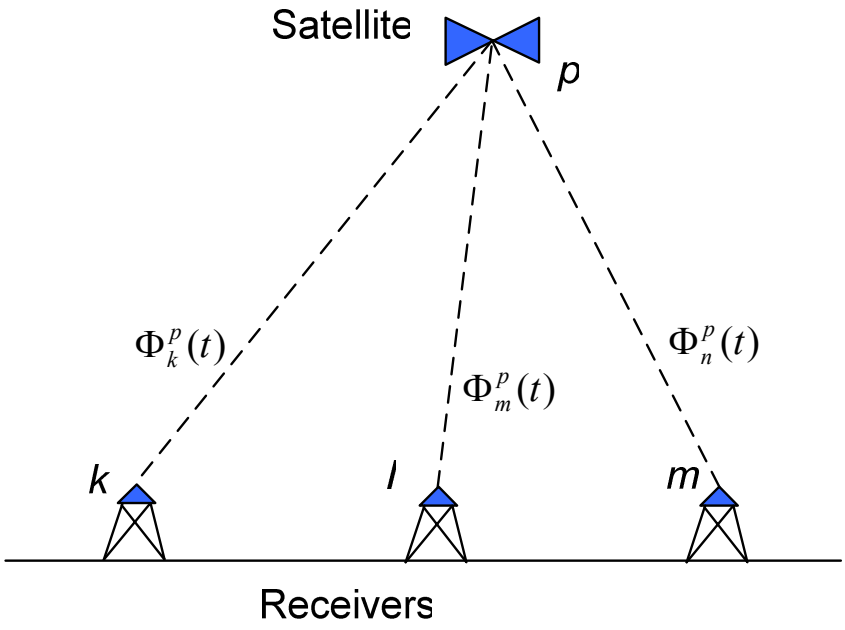

Figure 3. Three receivers *k*, *l* and *m* records observations the same epoch t to one common satellite *p*

With the use of these observations we can form two single differences with Eq.(24). This gives the following observation and design matrices

$$\mathbf{\Phi}_{SD,MP} = \begin{bmatrix} \mathbf{\Phi}_{kl}^{p} \\ \mathbf{\Phi}_{km}^{p} \end{bmatrix} \qquad \mathbf{\Phi} = \begin{bmatrix} \Phi_{k}^{p} & \Phi_{l}^{p} & \Phi_{m}^{p} \end{bmatrix}^{T} \qquad \mathbf{A}_{SD,MP} = \begin{bmatrix} 1 & -1 & 0 \\ 1 & 0 & -1 \end{bmatrix} \tag{28}$$

the additional subscript MP indicates multipoint solution. The correlations are brought forward by the covariance matrix

$$\mathbf{C}_{SD,MP} = \mathbf{A}_{SD,MP}\left(\sigma_0^2\mathbf{I}\right)\mathbf{A}_{SD,MP}^{T} = \sigma_0^2\begin{bmatrix} 2 & 1 \\ 1 & 2 \end{bmatrix} \tag{29}$$

The off diagonal elemants in the covariance matrix in Eq.(29) are not zero as in the case when only two receiver were used. This means that there are correlations introduced between the observations at single difference level in a multipoint solution.

2.3.3.2 Double differences

To derive the correlation for the double differences we follow the same steps as we did with the single differences and starts with the case where only two receivers are used. The general matrix expression of the double differences can be formed as:

$$\mathbf{\Phi}_{DD} = \mathbf{A}_{DD}\mathbf{\Phi}_{SD} \tag{30}$$

Where $\mathbf{\Phi}_{DD}$ is the vector with double differences and $\mathbf{A}_{DD}$ the design matrix which describes the linear combination of the single differences in $\mathbf{\Phi}_{SD}$. If the result from the single differences is used, Eqs. (25) and (27), the double differences can be described as:

$$\mathbf{\Phi}_{DD} = \begin{bmatrix} \mathbf{\Phi}_{km}^{op} \\ \mathbf{\Phi}_{km}^{oq} \end{bmatrix} \quad \mathbf{A}_{DD} = \begin{bmatrix} 1 & -1 & 0 \\ 1 & 0 & -1 \end{bmatrix} \quad \mathbf{\Phi}_{SD} = \begin{bmatrix} \mathbf{\Phi}_{km}^{o} \\ \mathbf{\Phi}_{km}^{p} \\ \mathbf{\Phi}_{km}^{q} \end{bmatrix} \tag{31}$$

One of the single differences is chosen as the reference. In this case we use the first $\mathbf{\Phi}_{km}^{o}$,where satellite is used as a reference satellite. When choosing the reference satellite, it is preferable to chose one with a high elevation angle, since the influence of atmospheric error source, like the ionosphere and troposphere is at minimum. One can also expect that in most cases the risk of loosing the connection to the satellite, caused by buildings and natural objects, is lower at high elevation angles than at low.

The covariance matrix of the DD can be derived, with the law of error propagation of covariance's, in the same manner as in the case of single differences:

$$\mathbf{C}_{DD} = \mathbf{A}_{DD}\mathbf{C}_{SD}\mathbf{A}_{DD}^{T} \tag{32}$$

resulting in

$$\mathbf{C}_{DD} = \mathbf{A}_{DD}\mathbf{C}_{SD}\mathbf{A}_{DD}^{T} = 2\sigma_0^2 \begin{bmatrix} 2 & 1 \\ 1 & 2 \end{bmatrix} \tag{33}$$

The correlations between the observations in the double differences are evident when studying the off diagonal elements in the matrix in Eq.(33).

2.3.3.2.1 Double differences in a multipoint solution

As can be seen in Eq.(33) there are correlations between all double differences in the way here as in the case of multipoint single differences. The correlation between the observations will become even more complicated in the multipoint solution corresponds to the case of single differences. This is obvious when taking the multipoint correlation explained in Eq. (29) into account. We are not going to explain

the multipoint covariance matrices here, but instead we give a reference to Beutler et al. (1986). They describe how the multipoint covariance matrix can be formed both in the case when identical observations are made at all receivers and when it is not. The paper gives a general description with the same assumption as we did in Eq.(23), i.e. that all observations have the same variance. Since this is usually not the case, it is common to use one and the same satellite as a reference satellite. The reference satellite is selected according to minimum variance to minimise the variance in the DD combinations, since it is preferable to have at least one satellite with low noise level in each DD.

One can not assume that common satellites are available in each epoch at all receivers. There might be obstacles that are blocking the signal at some of the receivers but not on the others. In the worst case observations to a satellite is only done at one receiver. In this case, the observation must be ignored in the double difference approach since it is impossible to generate any double differences.

With a change in the observation scheme, the covariance matrix must be redefined. If another satellite than the reference is lost, it is quite simple to adjust the covariance matrix to the new situation, but in the case the reference receiver is lost, one need to create a complete new covariance matrix based on another reference satellite. In the dual receiver case it is rather easy to adjust the covariance matrix, but in a multipoint solution it becomes more complicated because of the correlation between the receivers.

2.3.3.3 Correlation in time

So far, the correlation has only been studied within one epoch. Usually more than one epoch are used when positions are determined with GPS. To connect them in time one need to construct a covariance matrix for all observations. In many applications one assumes that there is no correlation between the epochs. This gives the following shape of the covariance matrix where all of diagonal elements (matrices) are set to zero.

$$C(t)=\begin{bmatrix} C(t_1) & 0 & \cdots & 0 \\ 0 & C(t_2) & & 0 \\ \vdots & & \ddots & \\ 0 & 0 & & C(t_n) \end{bmatrix} \tag{34}$$

This assumption holds, only if all the error sources in the observation equations are eliminated in the differencing procedure. Some of them are completely eliminated (the clock errors and the hardware delays), but there are still some parameters which are not, such as the troposphere, ionosphere, multipath and antenna phase centre variations. These parameters are unique for each receiver and they also depend on the observation site. Physical models for each of them have been developed to reduce as much as

possible of their influence as described in Chapter 3, but the models are not completely correct, so there will still be some errors left after they are applied on the observation equations. It is the time correlation for these remaining errors that will make the correlation equation Eq.(34) incorrect. The outcome of an incorrect correlation model will result in a non-optimal adjustment and wrong variances in the final result.

2.4 Undifferenced solution

There is a linear dependency in the phase observation equation between the clock parameters and the ambiguities. One way to eliminate these dependencies is to use the differential solution, which is done above but there is an alternative method based on raw phase observations called an undifferenced approach, where all the systematic errors are estimated independently of each epoch in a state vector. The method is usually called a state space model approach.

The state space approach is based on the fact that all the parameters in the observation equation are independently correlated in time. Take as an example the satellite hardware delay. It has some kind smooth stochastic process in time and would not make large jumps from epoch to epoch.

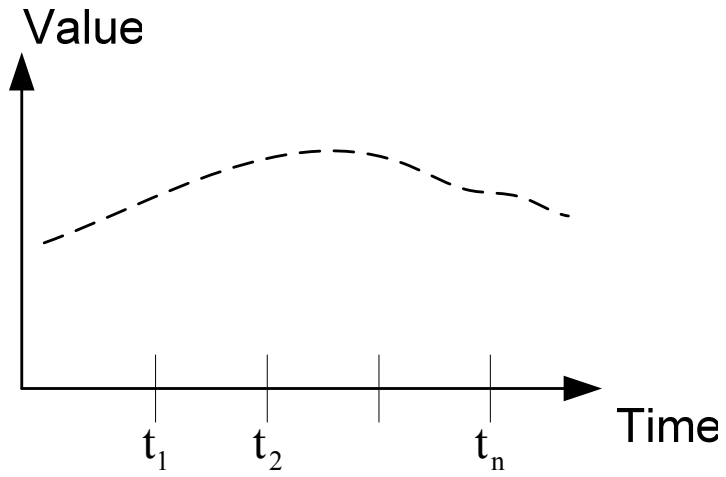

Figure 4. Parameter values are normally changing smoothly during time and do not make any sudden jumps

With this knowledge about the stochastic processes it is possible to create a model for each error parameter that describes how the parameter is expected to change from epoch to epoch. Most of the unknown parameters in the raw observations Eq.(14) have both a stochastic and a deterministic part. The deterministic parts are the same as have been used in the double differenced approach and are removed from the observations before the estimation of the stochastic part. In the undifferenced approach is it directly the parameter between a receiver and a satellite that are estimated and no correlations

are therefore introduced. The number of unknowns in the state vector depends on the number of receivers, the number of modelled parameters and the number of observations at each receiver. Further more, the undifferenced approach will not cause any problem when the actual observations at each receiver vary as is the case when using double differences. In the former case, if a satellite is observed only at one receiver, then additional unknown parameters will be added to the state vector.

The estimations of the parameters is, in this report, based on a Kalman filter, which is a sequential filter technique that takes into account the dynamics of the parameters. The Kalman filter estimates the state space parameters by considering the states of the parameters between observation epochs, and it uses the appropriate stochastic processes to update their variances. The Kalman filter is explained in detail in Section 3.1 together with the deterministic and stochastic models of each unknown parameter.

2.5 Double differences vs. undifferenced data

The two most important observables are described in the earlier sections, are undifferenced GPS observations and the double differenced observations. In this section we compare the methods in discussing their advantages and disadvantages.

We start with the double differences, where several observations are used to eliminate the unknown clock errors and hardware delays in the satellites and receivers. The elimination implies that parameters are completely erased from the observation equation. By doing this all time dependent correlations are removed, and it becomes impossible to model the time dependent stochastic process which each independent parameter actually has. This can be seen as a problem, but it gives some advantages as well. One of them is that the double differences becomes independent at each epoch without any time correlations and when several epochs are used together in an adjustment one can use the assumption with no correlation between the epochs as in Eq.(34). This assumption is correct if all the other site dependent parameters, like the ionosphere, troposphere, multipath and antenna parameters, are completely removed in the same manner as the time parameters. However, even if very accurate deterministic models are used to eliminate the site dependent influence of each parameter in the observation equation, there will still be some influence left since the physical conditions vary at each receiver position. This means that the assumption in Eq. (34) will be incorrect, since the correlations between the epochs are incorrectly modelled, and a loss of information is unavoidable. It should be noted that if the receivers are placed within a few kilometres from each other and at the same level of height, then the influence of the remaining ionosphere and the troposphere parameters will become very small and insignificant. A problem with the double differencing procedure is also that some observations will be lost, because the observations that are measured to

satellites that are only visible at one receiver will be lost. Another problem with the differencing process is the complexity of rearranging the covariance matrix, especially in the multipoint situation, when the number of observations is changing at the receivers from epoch to epoch. This procedure is, according to Beutler et al. (1987), quite time consuming.

In the undifferenced approach are all unknown parameters in the observation equations are estimated each epoch with a Kalman filter. Models are used to remove the deterministic part of each parameter and the remaining part is assumed to be stochastic and estimated each epoch in a state vector by the filter. It is important, in this approach, to model the time correlation of each parameter correctly so it represents the true stochastic nature of the estimated parameters. This is one of the main challenges with the undifferenced approach. A true benefit with the undifferenced approach is that all observations can be used. There are no limitations as in the other approach where the same observations have to be done at the receivers. One of the most important advantages with the multipoint solution is that observations from several receivers can be used simultaneously and easily without any complicated correlations as is the case of double differences. Since one of the goals with this project is to use several reference receivers in a multipoint solution and considering the benefits of the undifferenced approach we continue to study how a general model for this approach can be formed. This is done in the following chapter.

It should be mentioned that the Kalman filter approach can also be used in the double differenced approach, but it is much harder to determine the time correlation for the unknown parameters since they are a combination of four observations.

3 The Model

There are several different methods which can be used to estimate parameters in real-time i.e. the Kalman-filter and sequential least squares adjustment. Both these methods are based on the same algorithm but the Kalman-filter gives the possibility for each parameter to dynamically change in time, which not the sequential least squares adjustment do. This is the reason to why the Kalman-filter has become so popular within surveying applications. Jansson (1998) i.e. used the Kalman-filter to improve the precision in real-time kinematic positioning.

This chapter starts with an explanation of the discrete Kalman-filter algorithm and we continue with an explanation of each of the additional error parameters. In the last section of this chapter the complete state space model for undifferenced positioning with GPS is summarised.

3.1 The Kalman filter

GPS-receivers can be programmed to perform observations in discrete time intervals (epochs). The observations can be seen as a sample of a continuous time process. The complete set of observations at an epoch k can in linearised matrix notation be written as

$$\mathbf{L}_k = \mathbf{H}_k \mathbf{X}_k + \boldsymbol{\varepsilon}_k \tag{35}$$

where the vector $\mathbf{L}_k$ contains the observations, $\mathbf{H}_k$ is the design matrix, which relates the unknowns in the state vector $\mathbf{X}_k$ to the observations, and $\boldsymbol{\varepsilon}_k$ is the observation errors. Which parameters that are found in the state vector for each GPS receiver depends on if the receiver is a reference or a rover receiver. More about how each parameter in the state vector is modelled is found in Section 3.2. Common for all the parameters in the state vector is that they all have some kind of correlation in time, i.e. in other words they each represent a dynamic process which can be linearly represented by a first order differential equation (the state space model):

$$\dot{\mathbf{x}}(t) = \mathbf{F}(t)\mathbf{x}(t) + \mathbf{G}(t)\mathbf{u}(t) \tag{36}$$

where $\mathbf{x}$ is a state vector, $\dot{\mathbf{x}}$ its time derivate, $\mathbf{F}$ is the system dynamic matrix, $\mathbf{G}$ is the coefficient matrix of the random forcing function $\mathbf{u}$, which elements are white noise. Without any further information, the parameters in the state vector would follow the path described by their differential equations. But, if observations are available (related to the parameters in the state vector) the state variables can be updated. This is the basic idea behind the Kalman filter and to make it "fit to use", one must convert it from a time continuous process into a discrete process.

The discrete Kalman filter is a recursive algorithm that can be described in two steps. The first is a prediction step, where the state vector and its covariance matrix are predicted from one epoch (k) into the next (k+1). In the second step, the predicted parameters are blended with the observations in epoch (k+1) in a least squares manner. The following derivation of the discrete Kalman filter is only an overview a complete derivation is given by Brown and Hwang (1997).

3.1.1 The prediction step

The prediction step is based on the homogeneous solution of the differential Eq.(36), which can be written as

$$\hat{\mathbf{x}}_{k+1}^{-} = \mathbf{T}_{k+1,k}\hat{\mathbf{x}}_k + \underbrace{\int_k^{k+1} \mathbf{T}_{k+1,\tau}\mathbf{G}_\tau \mathbf{u}_\tau \mathrm{d}\tau}_{\mathbf{w}_k} \tag{37}$$

where $\hat{\mathbf{x}}_k$ is the state vector at epoch k and $\hat{\mathbf{x}}_{k+1}^{-}$ the predicted state vector at epoch k+1. Matrices with the superscript "^" denote estimated values and "-"denotes predicted parameters. $\mathbf{T}_{k+1,k}$ is the transmission matrix from epoch k to k+1 and $\mathbf{u}$ the forcing function. The integration at the end of Eq.(37) is the driven response, which is the integrated noise during the time interval between two epochs $\mathrm{d}\tau$. It contains the total change in the transmission matrix, coefficient matrix and the forcing function, in the continuous case. In the discrete case this integration is summarised in the matrix $\mathbf{w}_k$, which contains the total integrated value of the system noise in the predicting procedure. $\mathbf{w}_k$ is the parameter that constitute the difference between the Kalman-filter and the sequential least squares adjustment. In the sequential least square adjustment is $\mathbf{w}_k$ equal to zero for all parameters.

The following assumptions are done concerning the correlations in observations and the state vector parameters in the Kalman-filter algorithm:

- All observations are uncorrelated within a epoch.
- All parameters in the state vectors are uncorrelated both within one epoch and in time.
- There is no correlation between the driven noise of the process and the observations.

Some comments to these assumptions are necessary. The fact that all observations are uncorrelated within an epoch is a quite usual assumption in least squares adjustments since it is very difficult to derive the correlation but the between epoch assumption is directly contradictory with the earlier description of the undifferenced approach. But

the assumption holds, since the correlation between the epochs is modelled by the differential equations. The second assumption, that the parameters in the state vector are uncorrelated, makes it easy to predict a state vector from one epoch to the next, with Eq.(37), since the matrix $\mathbf{w}_k$ then becomes random noise with zero mean, and it has no influence on the prediction at all.

Along with the estimated state vector belongs a covariance matrix. This is also transformed from one epoch to the next with the following equation

$$\mathbf{Q}^{-}_{x,k+1} = \mathbf{T}_{k+1,k}\mathbf{Q}_{x,k}\mathbf{T}^{T}_{k+1,k} + \mathbf{Q}_k \tag{38}$$

where $\mathbf{Q}_{x,k}$ and $\mathbf{Q}^{-}_{x,k+1}$ are the covariance matrix at epoch k and the predicted covariance matrix for epoch k+1. $\mathbf{Q}_k$ is the covariance matrix of the system noise, and $\mathbf{T}$ is the same transmission matrix as in Eq.(37). The transmission matrix can be formed by solving the following differential equation.

$$\dot{\mathbf{T}}_{k+1,k} = \mathbf{F}_k\mathbf{T}_{k+1,k} \tag{39}$$

with the following starting condition $\mathbf{T}_{k,k} = \mathbf{I}$. If the transmission matrix is considered as constant during the time of interest, the differential equation has the solution of an exponential function of the transmission matrix, which can be expressed in Taylor-series as

$$\mathbf{T}_k = e^{\mathbf{F}\Delta t} = \mathbf{I} + \mathbf{F}\Delta t + \frac{(\mathbf{F}\Delta t)^2}{2!} + \frac{(\mathbf{F}\Delta t)^3}{3!} + \ldots \tag{40}$$

Where Δt is introduced as the fix time interval between two epochs. The exponential function implies that the correlation in time between the parameters in two state vectors is reducing exponentially.

The covariance matrix $\mathbf{Q}_k$ of the system noise $\mathbf{w}_k$, can be expressed as:

$$\begin{aligned}
&\mathbf{Q}_k = \mathrm{E}\left[\mathbf{w}_k\mathbf{w}_k^{T}\right] = \\
&\mathrm{E}\left[\int_k^{k+1}\int_k^{k+1}\mathbf{T}(k+1,s)\mathbf{G}(s)\mathbf{u}(s)\mathbf{u}^{T}(t)\mathbf{G}^{T}(t)\mathbf{T}^{T}(k+1,t)\,dt\,ds\right] = \\
&\int_k^{k+1}\int_k^{k+1}\mathbf{T}(k+1,s)\mathbf{G}(s)\mathbf{E}\left[\mathbf{u}(s)\mathbf{u}^{T}(t)\right]\mathbf{G}^{T}(t)\mathbf{T}^{T}(k+1,t)\,dt\,ds
\end{aligned} \tag{41}$$

where

$$\mathrm{E}\left[\mathbf{u}(s)\mathbf{u}^{T}(t)\right] = \mathbf{Q} \tag{42}$$

Q is a diagonal matrix containing power spectral densities (PSD) of the process forcing function **u**. Using equation (40), the solution of the integral (41) can be approximated by following expansion, Farrell and Barth(1999, p. 86).

$$\begin{aligned}\mathbf{Q}_k &= \mathrm{E}\left\{\mathbf{w}_k\mathbf{w}_k^T\right\} \approx \mathbf{Q}_G\Delta t + \left(\mathbf{F}\mathbf{Q}_G + \mathbf{Q}_G\mathbf{F}^T\right)\frac{\Delta t^2}{2} + \\ &+\left[\mathbf{F}^2\mathbf{Q}_G + 2\mathbf{F}\mathbf{Q}_G\mathbf{F}^T + \mathbf{Q}_G\left(\mathbf{F}^T\right)^2\right]\frac{\Delta t^3}{6} + \\ &+\left[\mathbf{F}^3\mathbf{Q}_G + 3\mathbf{F}\mathbf{Q}_G\left(\mathbf{F}^T\right)^2 + 3\mathbf{F}^2\mathbf{Q}_G\mathbf{F}^T + \mathbf{Q}_G\left(\mathbf{F}^T\right)^3\right]\frac{\Delta t^4}{24} + \ldots\end{aligned} \tag{43}$$

where

$$\mathbf{Q}_G = \mathbf{G}\mathbf{Q}\mathbf{G}^T \tag{44}$$

The power spectral density functions actually express how much the variance of each parameter in the state vectors can change from one epoch to the next.

3.1.2 The filtering step

After the prediction step follows the filtering step, also called the update step by Sjöberg (2005), where the predicted parameters $\hat{\mathbf{x}}_{k+1}^-$, from the previous epoch, are updated with the optimal combination of the difference between the observations $\tilde{\mathbf{L}}_{k+1}$ and a "set of observations" that are generated with the predicted parameters $\hat{\mathbf{x}}_{k+1}^-$. The generated observations are created by using the direct functional relationship $\mathbf{h}_{k+1}(\hat{\mathbf{x}}_{k+1}^-)$ described by the observation equations in Eqs.(13) and (14), which are presented slightly modified in Chapter 4 . The superscript "~" is introduced to indicate measured values. The general equation for this procedure is given by:

$$\hat{\mathbf{x}}_{k+1} = \hat{\mathbf{x}}_{k+1}^- + \mathbf{K}_{k+1}\left[\tilde{\mathbf{L}}_{k+1} - \mathbf{h}_{k+1}(\hat{\mathbf{x}}_{k+1}^-)\right] \tag{45}$$

A blending matrix $\mathbf{K}_{k+1}$, also called the Kalman gain matrix, is introduced in the equation. This is derived from the theory of recursive parameter estimations where no correlations between the state vectors in the epochs are expected.

$$\mathbf{K}_{k+1} = \mathbf{Q}_{x,k+1}^-\mathbf{H}_{k+1}^T\left[\mathbf{R}_{k+1} + \mathbf{H}_{k+1}\mathbf{Q}_{x,k+1}^-\mathbf{H}_{k+1}^T\right]^{-1} \tag{46}$$

Where $\mathbf{R}_{k+1}$ is the prior variance-covariance matrix of the observation noise ε_k in Eq.(35). Koch (1999 p.177) describes how this matrix can be derived so it will not be done here. He also derives the updating procedure of the covariance matrix

$$\mathbf{Q}_{x,k+1} = \left[\mathbf{I} - \mathbf{K}_{k+1}\mathbf{H}_{k+1}\right]\mathbf{Q}_{x,k+1}^- \tag{47}$$

which includes the predicted covariance matrix $\mathbf{Q}^{-}_{x,k+1}$, see also Sjöberg (2005 Sect. 12.1).

3.1.3 Summarising of the Kalman filter

The Kalman filter can be summarised in the following steps. The first step is an initialisation step. This is needed since the dynamics of the state vector parameters are described with first order differential equations. In the second step the state vector and its covariance matrix are propagated from the previous epoch to the current by the use of transition matrices. In the third step is the Kalman gain matrix determined and the fourth along with the fifth step conclude the algorithm by updating of the predicted state vector and its covariance matrix into the current epoch.

1. Initialisation:

$$\hat{\mathbf{x}}^{-}_{0} = \mathrm{E}[\mathbf{x}_0], \quad \mathbf{Q}^{-}_{x0} = \mathrm{var}[\mathbf{x}^{-}_{0}] \tag{48}$$

2. Time propagation

$$\hat{\mathbf{x}}^{-}_{k+1} = \mathbf{T}_{k+1,k}\hat{\mathbf{x}}_k, \quad \mathbf{Q}^{-}_{x,k+1} = \mathbf{T}_{k+1,k}\mathbf{Q}_{x,k}\mathbf{T}^{T}_{k+1,k} + \mathbf{Q}_k \tag{49}$$

3. Gain calculation

$$\mathbf{K}_{k+1} = \mathbf{Q}^{-}_{x,k+1}\mathbf{H}^{T}_{k+1}\left[\mathbf{R}_{k+1} + \mathbf{H}_{k+1}\mathbf{Q}^{-}_{x,k+1}\mathbf{H}^{T}_{k+1}\right]^{-1} \tag{50}$$

4. Measurement update

$$\hat{\mathbf{x}}_{k+1} = \hat{\mathbf{x}}^{-}_{k+1} + \mathbf{K}_{k+1}\left[\tilde{\mathbf{L}}_{k+1} - \mathbf{h}_{k+1}(\hat{\mathbf{x}}^{-}_{k+1})\right] \tag{51}$$

5. Covariance update

$$\mathbf{Q}_{x,k+1} = \left[\mathbf{I} - \mathbf{K}_{k+1}\mathbf{H}_{k+1}\right]\mathbf{Q}^{-}_{x,k+1} \tag{52}$$

The Kalman filter is an iterative procedure, once started with an initialisation in step 1 it will continue with a loop through step 2 to 5 during each observation epoch.

3.2 Parameter modelling

The deterministic and stochastic models are described in this section for all the unknown parameters in the observation equations. The deterministic models are used to remove the deterministic part of each unknown parameter, and the stochastic models describe the stochastic nature of the remaining difference between the true value and the deterministic model. In the observation equations all known values are moved to the left side of the equal sign. The deterministic values are assumed to be known values and therefore moved to the left side in the observation equations. The updated observation equations are presented in Section 3.3. The presentation of unknown parameters starts with position and velocity and thereafter follows each of the other

parameters covering; the receiver clocks, the atmospheric delays, multipath and finally the common errors.

3.2.1 Position and velocity

Both for relative and single point positioning, it is necessary to compute the geometric distance $\rho_A^s(t_A)$, which is given by the following equation:

$$\rho_A^s(t_A) = \sqrt{\left(X^s - X_{A,e}\right)^2 + \left(Y^s - Y_{A,e}\right)^2 + \left(Z^s - Z_A\right)^2} \tag{53}$$

where $\left(X^s, Y^s, Z^s\right)$ are coordinates of satellite s at emission time t_G^s and $X_{A,e}$ and $Y_{A,e}$ are receiver coordinates corrected for the Earth rotation during the signal travel time Δt^s:

$$\begin{cases} X_{A,e} = X_A - \omega_e Y_A \Delta t^s \\ Y_{A,e} = Y_A + \omega_e X_A \Delta t^s \end{cases} \tag{54}$$

To be able to use standard linear least squares adjustment, Eq. (53) has to be linearised:

$$\rho_k^p(t_k) = \rho_{k0}^p(t_k) + \frac{\partial \rho_{k0}^p(t_k)}{\partial X_{k0}} \Delta X + \frac{\partial \rho_{k0}^p(t_k)}{\partial Y_{k0}} \Delta Y + \frac{\partial \rho_{k0}^p(t_k)}{\partial Z_{k0}} \Delta Z + \text{HOT} \tag{55}$$

where $\Delta X, \Delta Y$ and ΔZ are the difference between approximate coordinates $X_{A,0}$, $Y_{A,0}$, $Z_{A,0}$ and the true coordinates and the respectively derivatives are:

$$\begin{aligned} \frac{\partial \rho_{A0}^s(t_A)}{\partial X_{A0}} &= a_X = -\frac{X^s - X_{A0} + Y_{A0}\omega_e \Delta t - X_{A0}\omega_e^2 \Delta t^2}{\rho_{A0}^s} \\ \frac{\partial \rho_{A0}^s(t_A)}{\partial Y_{A0}} &= a_Y = -\frac{Y^s - Y_{A0} - X_{A0}\omega_e \Delta t - Y_{A0}\omega_e^2 \Delta t^2}{\rho_{A0}^s} \\ \frac{\partial \rho_{A0}^s(t_k)}{\partial Z_{A0}} &= a_Z = -\frac{Z^s - Z_{A0}}{\rho_{A0}^s} \end{aligned} \tag{56}$$

also based on the approximate coordinates.

For the monitoring applications, it is reasonable to assume that the points are moving slowly. Therefore, this motion can be kinematically modelled as constant velocity model (PV model). In the case of the position-velocity model we assume that the GPS antenna is moving with a constant velocity and that the velocity vector is changing randomly, i.e. the velocity is modelled as a random-walk process. This yields state vector for one receiver A:

$$\mathbf{X}_{PV,A} = \begin{bmatrix} \mathbf{X}_A & \mathbf{v}_A \end{bmatrix} = \begin{bmatrix} X_A & Y_A & Z_A & v_{XA} & v_{YA} & v_{ZA} \end{bmatrix}^T \tag{57}$$

with the dynamic model:

$$\begin{aligned}\dot{\mathbf{X}}_A &= \mathbf{v}_A \\ \dot{\mathbf{v}}_A &= \mathbf{0} + \mathbf{u}_a\end{aligned} \tag{58}$$

and the covariance matrix

$$\mathrm{E}\left[\mathbf{u}_a(s)\mathbf{u}_a^T(t)\right] = \mathbf{Q}_a = \begin{bmatrix} q_{aX} & 0 & 0 \\ 0 & q_{aY} & 0 \\ 0 & 0 & q_{aZ} \end{bmatrix} \tag{59}$$

where q is noise spectral amplitude. The unit of q is $\left(\mathrm{m/s^2}\sqrt{\mathrm{Hz}}\right)^2$.

The dynamic matrix $\mathbf{F}_{PV,A}$ for the PV model together with the coefficient matrix $\mathbf{G}_{PV,A}$ and the random forcing function $\mathbf{u}_{a,A}$ are:

$$\mathbf{F}_{PV,A} = \begin{bmatrix} 0 & 0 & 0 & 1 & 0 & 0 \\ 0 & 0 & 0 & 0 & 1 & 0 \\ 0 & 0 & 0 & 0 & 0 & 1 \\ 0 & 0 & 0 & 0 & 0 & 0 \\ 0 & 0 & 0 & 0 & 0 & 0 \\ 0 & 0 & 0 & 0 & 0 & 0 \end{bmatrix}, \quad \mathbf{G}_{PV,A} = \begin{bmatrix} 0 & 0 & 0 \\ 0 & 0 & 0 \\ 0 & 0 & 0 \\ 1 & 0 & 0 \\ 0 & 1 & 0 \\ 0 & 0 & 1 \end{bmatrix}, \quad \mathbf{u}_{a,A} = \begin{bmatrix} u_{ax} \\ u_{ay} \\ u_{az} \end{bmatrix} \tag{60}$$

Please note, that we estimates position and velocity only for rover receivers since these receivers are assumed to be in motion. The coordinates at the reference receivers are held fixed. There should always be at least one reference receiver in the network.

Since, in the case of our PV-model, $\mathbf{F}^n = \mathbf{0}, \quad n \geq 2$, the process noise covariance matrix will become exactly:

$$\mathbf{Q}_k = \mathbf{Q}_G \Delta t + \left(\mathbf{F}\mathbf{Q}_G + \mathbf{Q}_G\mathbf{F}^T\right)\frac{\Delta t^2}{2} + \mathbf{F}\mathbf{Q}_G\mathbf{F}^T\frac{\Delta t^3}{3} \tag{61}$$

$$\mathbf{Q}_{k,A} = \begin{bmatrix} \frac{q_{aX}\Delta t^3}{3} & 0 & 0 & \frac{q_{aX}\Delta t^2}{2} & 0 & 0 \\ 0 & \frac{q_{aY}\Delta t^3}{3} & 0 & 0 & \frac{q_{aY}\Delta t^2}{2} & 0 \\ 0 & 0 & \frac{q_{aZ}\Delta t^3}{3} & 0 & 0 & \frac{q_{az}\Delta t^2}{2} \\ \frac{q_{aX}\Delta t^2}{2} & 0 & 0 & q_{aX}\Delta t & 0 & 0 \\ 0 & \frac{q_{aY}\Delta t^2}{2} & 0 & 0 & q_{aY}\Delta t & 0 \\ 0 & 0 & \frac{q_{az}\Delta t^2}{2} & 0 & 0 & q_{aZ}\Delta t \end{bmatrix} \tag{62}$$

and the transition matrix for the position and the velocity is given by:

$$\mathbf{T}_{PV,A} = \mathbf{I} + \mathbf{F}_{PV,A}\Delta t = \begin{bmatrix} 1 & 0 & 0 & \Delta t & 0 & 0 \\ 0 & 1 & 0 & 0 & \Delta t & 0 \\ 0 & 0 & 1 & 0 & 0 & \Delta t \\ 0 & 0 & 0 & 1 & 0 & 0 \\ 0 & 0 & 0 & 0 & 1 & 0 \\ 0 & 0 & 0 & 0 & 0 & 1 \end{bmatrix} \tag{63}$$

where Δt is the time period between two epoch.

3.2.2 Receiver clock

The nominal time t_A in a receiver A is related to true GPS time as described in Eq. (2). The clock delay δt_A is not constant in time, it develops as the integral of the frequency error of the clock oscillator. The total clock delay can be described as a bias $\delta t_{b,A}$ plus a drift parameter $\delta t_{dr,A}$.

$$\delta t_A = \delta t_{b,A} + \Delta t \delta t_{dr,A} \tag{64}$$

How the bias and drift values varying in time depends on the receiver design. Trimble, for example, does not correct the clocks until the drift offset is 1 millisecond. Leica, on the other hand, corrects the receiver clocks of their receivers instantly each epoch. To cover all types of receivers we solve this problem in two steps. First in each epoch a combined bias/drift value is estimated for the total receiver clock delay. This is done with the observations within in the epoch in a single point positioning algorithm using the linear model for point positioning with code ranges, described by Hoffmann-Wellenhof et al. (2001, p.257-259). This algorithm is designed for positioning, where

both the coordinates and the receiver clock are unknown, which is the case at the rover stations. A small modification is introduced at the reference station where the coordinates are known from the beginning and the only remaining unknown parameter is the combined value of the bias/drift of the receiver clock. This value is treated from now on as a known parameter and moved to the right side of the observation equations. The estimated value does not remove the complete clock bias and drift, and the remaining part is estimated in the Kalman filter. Witchayangkoon (2000) recommends to model this part as a random walk process, which gives a slightly better result than modelling it as a white noise process. The dynamic model of the remaining receiver clock error δt_A is modelled with the following differential equation:

$$\dot{\delta t}_A = u_{\delta t,A} \tag{65}$$

which is written at the general form as in Eq.(36), with the following dynamic matrix:

$$\mathbf{F}_{\delta t,A} = \mathbf{0} \tag{66}$$

and the coefficient matrix $\mathbf{G}_{\delta t,A}$:

$$\mathbf{G}_{\delta t,A} = \mathbf{I} \tag{67}$$

The process noise vector for the remaining clock error is given by:

$$\mathbf{u}_{\delta t,A} = u^T_{\delta t,A} \tag{68}$$

We model the process noise $u_{\delta t,A}$ as white noise with the covariance matrix

$$\mathbf{Q}_{\delta t,A} = E\left[\mathbf{u}_{\delta t,A}(t)\mathbf{u}^T_{\delta t,A}(t)\right] = q_{\delta t,A} \tag{69}$$

The noise spectral amplitude amplitudes $q_{\delta t,A}$ can be computed using Alan variance parameter h_0, (Brown and Hwang 1992):

$$q_{\delta t,A} = 2h_0 \tag{70}$$

The numerical value of the bias part of the Alan variance parameters for a typical crystal clock used in the GPS receiver is:

$$h_0 = 2\times 10^{-19}\,\mathrm{sec}^2/\mathrm{s} \tag{71}$$

Since the parameter is modelled as a random walk process, the transition matrix becomes an identity matrix since the dynamic matrix in Eq.(66) is zero:

$$\mathbf{T}_{\delta t,A} = \mathbf{I} \tag{72}$$

Inserting the coefficient matrix $\mathbf{G}_{\delta t,A}$, the covariance matrix $\mathbf{Q}_{\delta t,A}$ and the dynamic matrix $\mathbf{F}_{\delta t,A}$ into Eq. (43) we get the process noise covariance matrix

$$Q_{k,\delta t,A} = q_{\delta t,A}\Delta t \tag{73}$$

The equations above are developed for a single frequency receiver. If a dual frequency receiver is used where both frequencies are steered by the same clock, there can be a small difference between L_1 and L_2 channels due to hardware delays ($\delta t_{o,A}$). We model this difference as a constant offset in clock correction applied to L_1 and L_2:

$$\delta t_{A,L2} = \delta t_{A,L1} + \delta t_{o,A} \tag{74}$$

The offset $\delta t_{o,A}$ is modelled as a random constant for which the process forcing function is zero and the dynamic process of the offset can be described by the following differential equation:

$$\dot{\delta t}_{o,A} = u_{o,A} = 0 \tag{75}$$

The dynamic matrix $\mathbf{F}_{\delta to}$ will only contain zeros since the constant offset do not change during the time between the epochs. Coefficient matrix $\mathbf{G}_{\delta to}$ and the dynamic matrix $\mathbf{T}_{\delta to}$ are both identity matrices as:

$$\mathbf{G}_{\delta to} = \mathbf{T}_{\delta to} = \mathbf{I} \tag{76}$$

Since the dynamic matrix $\mathbf{F}_{\delta to}$ only contains zeros and the forcing random noise $u_{o,A}$ is zero, the process noise covariance matrix will also become zeros:

$$\mathbf{Q}_{k,\delta to} = \mathbf{0} \tag{77}$$

when Eq.(43) is used.

3.2.3 The Atmospheric delays

The GPS-satellites are transmitting signals at an approximate altitude of approximately 20200 km above mean sea level. All the signals that reach a receiver placed on earth have passed the atmosphere and have been affected by it. The atmosphere is usually, in GPS-related topics, divided in two parts, an ionized and a non ionized part, according to the presents of charged particles. The ionized part is normally called the ionosphere and the nonionized the troposphere. The naming is a rather rough generalisation since each name is just the name of one of many layers with the same influence on the passing signals i.e. the ionized part that we call the ionosphere normally contains of both the ionosphere and the protonosphere, but since both of them has the same influence on the passed signals they are gathered under one name.

Subsequent sections give a general description of how the atmosphere influences passing signals and how they are modelled in our Kalman filter.

3.2.3.1 Ionospheric delay

The ionized part of the atmosphere starts at an approximate height of 80 km above sea level. Ionization in the atmosphere is caused by UV and X-radiation from the sun. All gas molecules that are exposed for the radiation are heated and electrons are liberated from them in a process called photo-ionization. Both the ionized molecules and the electrons are charged particles which influence the propagations of radio waves but it is mainly the electrons that influence the radio. The ionization rate depends on the density of the gas and intensity of radiation. At low altitudes, where the gas is denser, the charged particles will be recombined rapidly into neutral molecules. Therefore is this part of the atmosphere almost free from ionized molecules and called the neutral atmosphere or troposphere. On higher altitudes, where the gas has a lower density, the time before a collision with another particle is increased. Thus, the gas will be full of charged particles which influence the passing signals. The amount of charged particles will increase with higher altitude up to approximately 350 – 400 km where it starts to decrease. This is mainly because that the density of the gas becomes so low at this altitude that even if the ionization of the molecules are more or less total the amount of charged particles are so low that it will not influence a passing signal. The total amount of electrons in the atmosphere is usually measured in total electron content (TEC) which represents the number of electrons along the signal path from the satellite to the receiver with the size of one square metre.

The radiation depends also on factors as the geomagnetic latitude, time of day, ionospheric storms. The earth magnetic field of the earth influences incoming radiation. The amount of electrons in the atmosphere is higher in the polar areas and at the equator than at latitudes in between them. This implies that the position on earth is one essential factor. The time of day is another factor that influences the radiation. Directly at sunrise starts the ionization process in the atmosphere and it continues to increase until approximately 14:00 local time according to Klobuchar (1987), then it starts to fade until the next sunrise. The radiation does not only have a diurnal variation it also has a long time variation. UV radiation from the sun is changing with regular pattern which coincide with the number of sunspots. The fluctuation has a period of 11 years and the last maxima were found during 2002.

Besides the factors that directly influence the presence of particles due to photo-ionisation the Sun ejects solar winds which are streams of high-energy particles. These winds affects the magnetic field of the earth and indirectly also the ionosphere. Sometimes, arises massive explosions on the surface of the Sun, Coronal Mass Ejections, which causes fluctuations of the geomagnetic field and quick changes in the

ionosphere, also called ionospheric storms. These storms are quite difficult to predict but luckily they are rare of occurrence.

The ionosphere does not influence the code and phase observations in the same manner, code observations are advanced and the phase observations are delayed. Further, phase observations are delayed differently according to their frequency. E.g. Leick (2004, pp. 215-219), describes the concept of group and phase propagation through the ionosphere and points out that the ionosphere influences the higher frequencies less than lower. Following his derivation one can also see that the code advance and phase delay is equal in size but with opposite sign.

There are some methods which can be used to remove or at least reduce the ionospherical influence. Klobuchar (2001) compares the efficiency of some of them. The result is summarised in Table 2.

Table 2. Summary of the efficiency of different deterministic ionospherical models, Klobuchar (2001)

Efficiency	Type of approach
0%	No model
50%	Ionospheric Correction Model Algorithm (ICA)
75%	State of the art ionospheric models like the International Reference Ionosphere (IRI)
90%	Use Wide Area Augmentation System (WAAS) ionospheric corrections
99%	Use dual-frequency receivers

In the first approach the ionospherical delay ignored totally. The size of an unmodelled ionospheric error can be at the size of 20-30 metres. The ICA model is designed by Klobuchar (1987) and it corrects approximately 50% of the ionospheric delay by estimating eight parameters. These parameters are included in the navigation message and available in real-time. More advanced models like IRI uses hundreds of parameters to estimate the ionospheric delay and they manage to model approximately 75% of the delay. A problem with this model according to Klobuchar (2001) is that it does not use any real-time data and they are therefore not appropriate for real-time applications. There are systems which estimate the ionospheric delay in near real-time, like the Wide Area Augmentation System (WAAS) in the USA and European Geostationary Navigation Overlay Service (EGNOS). In these systems are real-time observations, from a reference network of permanent GPS receivers, used to determine the

ionosphere delay among many other parameters. The corrections are distributed from geostationary satellites, thus to use these systems one must have receivers that are prepared to receive the signals and the satellites must be visible from the receiver position. The approach, which according to Klobuchar (2001) gives the best result, is to use dual frequency receivers. Observations from two frequencies can be used to eliminate 99% of the ionospherical delay.

3.2.3.1.1 Deterministic mode

We are using the ICA model, Klobuchar (1987), as deterministic model for the ionospheric delay. The main reason for this choice is that its parameters, are distributed in the navigation message in real-time. So is also the EGNOS parameters but they are only transmitted from the geostationary satellites and the coverage of these satellites are rather limited in the Nordic countries.

The transmitted ICA parameters describe the diurnal curve of the ionosphere which is consisting of a cosine and a constant part. The cosine part representing the daytime variations and the constant part the night. Both amplitude and period of the cosine part is varying depending on the position on earth. ICA parameters are computed based on the output from an empirical model that describes the world-wide ionospheric behaviour. Each 10 day are the parameters updated in normal conditions but if the solar flux value changes largely during a five day period then are the parameters updated more frequently.

The input parameters in this algorithm will be given here, the complete derivation can be found in Klobuchar (1987) and it is also described in ICD-GPS-200C (1999), the interface control document that describes the broadcasted messages. Beware the numerical example given in the former paper, does not give the right result, verified by correspondence with the author. The general ICA algorithm can be summarised as

$$\Delta I_{ICA} = f\left(\phi, \lambda, El, Az, IP\right) \tag{78}$$

where

ΔI_{ICA}	Ionospherical delay
ϕ_A	Geodetic latitude
λ_A	Geodetic longitude
El	Elevation angle to the satellite
Az	Azimuth to the satellite
IP	The 8 distributed Ionospheric Parameters

A typical example of how the ionospheric delay is changing diurnal, calculated by the ICA model, is presented in Figure 5.

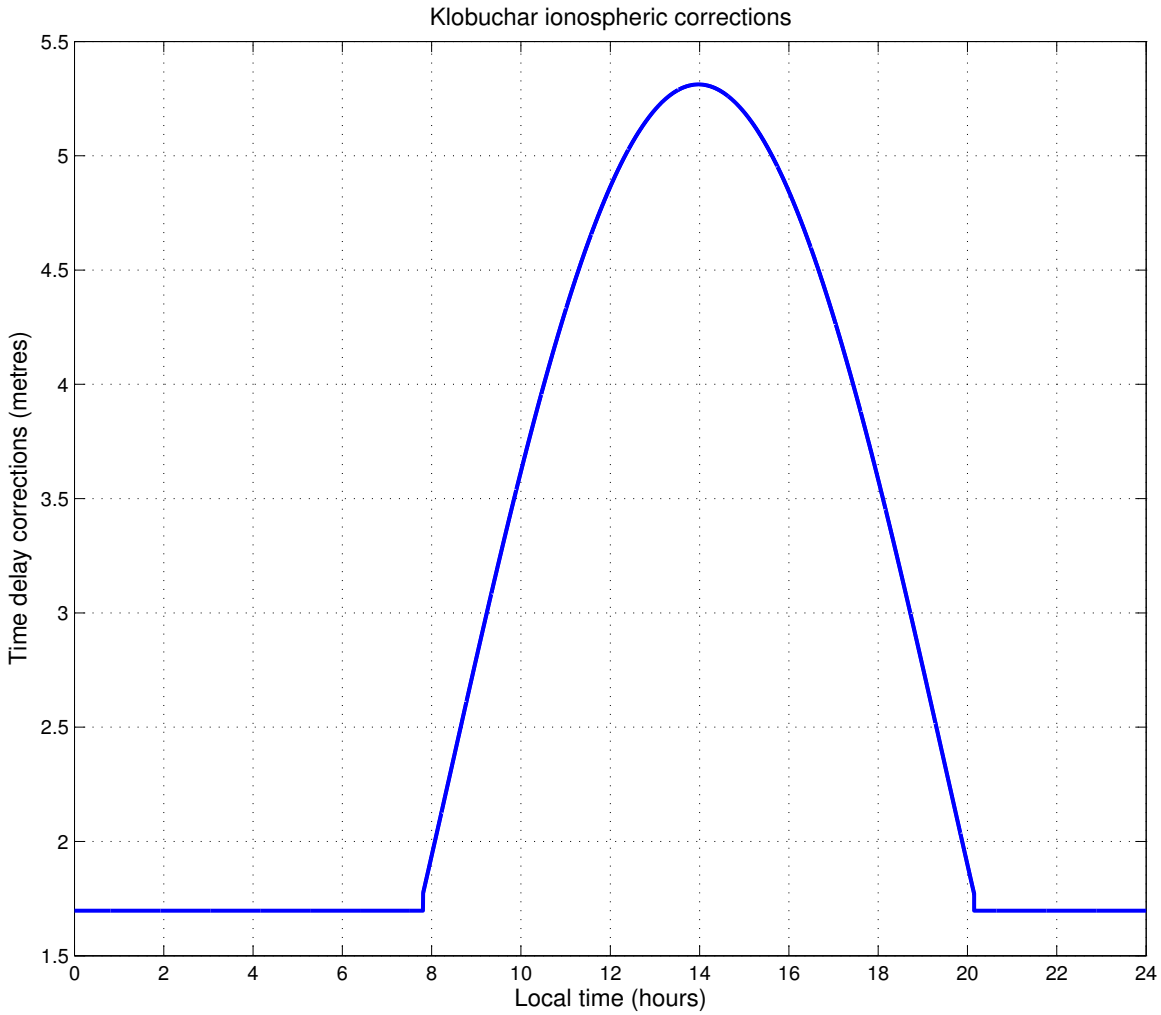

Figure 5. Klobuchar correction model (ICA) calculated for a user position (lat: 58, long: 12), to a satellite at elevation angle 40 deg and azimuth 210 deg.

3.2.3.1.2 Parameter modelling

When the values from the deterministic model is removed from the observations, we estimate the remaining parts of the ionosphere by creating one parameter for each observation, I_A^s , at the reference stations. These parameters are not constant in time and therefore they are being modelled as random walk processes with the following dynamic equation:

$$\dot{I}_A^s = u_{I,A} \tag{79}$$

It is not possible to estimate the ionosphere delay at the rover stations since the coordinates are unknown. Instead we use the estimated ionospheres at the reference

stations and interpolate the ionospheric influence at the rover stations. The inverse distance between the rover and the reference stations are used as the weights in the interpolation algorithm as described in the following equation with several reference stations (A, B,…) and rover station C.

$$I^s_{i,C}(t) = \frac{d^{-1}_{AC} I^s_A(t) + d^{-1}_{BC} I^s_B(t) + \ldots}{d^{-1}_{AC} + d^{-1}_{BC} + \ldots} \tag{80}$$

The subscript i indicates that this parameters is interpolated from several stations.

Matrixes $\mathbf{F}_I$, $\mathbf{T}_I$, $\mathbf{Q}_I$ and $\mathbf{G}_I$ for two reference and one roving station will be of size $(2 \cdot \text{nsat}) \times (2 \cdot \text{nsat})$, where nsat is the number of satellites (s = 1, 2,…, nsat), because there are $(2 \cdot \text{nsat})$ parameters to be estimated, namely I^s_A and I^s_B. (Provided that all receivers measure the same set of satellites). The subscript indicates that the matrices belongs to the ionospheric delays:

$$\mathbf{F}_I = \mathbf{0} \tag{81}$$

The $\mathbf{T}_I$ and $\mathbf{G}_I$ matrices are identity matrices and the process noise covariance matrix are given by

$$\mathbf{Q}_{k,I} = \Delta t \cdot \text{diag}(q_I, q_I, \ldots) \tag{82}$$

where we assume that noise parameters q_I are the same for all reference and rover stations.

3.2.3.2 Tropospheric refraction

The troposphere is a nondispersive media and has completely different properties than the ionosphere. It is found below the ionosphere, up to a height of approximately 50 km above mean sea level, and is one of the limiting error sources in GPS-positioning according to Mendes and Langley (1994). The troposphere influences all GPS-frequencies in the same way and for that reason the size of its influence on a passing signal is directly related to the travelling distance trough the tropospheric layer. Tropospheric refraction is directly related to the amount of water that is mixed in the air. Temperature is one factor that influences the amount of water that can be moisturised in the air. Air with higher temperatures can hold more water vapour than air with lower temperatures. When the maximum of vaporised water is reach at a certain temperature one call this saturated air. Unsaturated air will always strive for full saturation, and when an unsaturated air meets a saturated they both will mix and diffuse in direction to the lower part reach full saturation. Further when the temperature is dropped in a saturated air the surplus will condensate until the saturation value is reach at the new temperature. The condensate will be transformed as rain, snow or hail

depending on the temperature and fall downwards towards the ground and will reach the ground if it does not reach another unsaturated air layer. The temperature and so also the amount of moisturised air changes both temporally and spatially, consequently becomes the troposphere quite unpredictable. What is known is that the temperature is lower at higher altitudes which results in a higher tropospheric influence at lower altitudes.

To visualise how a signal is influenced one can divide the troposphere into an infinity amount of thin horizontal layers each with its own refractive index n. According to Snell's law, a ray of light that is passing from one refractive index to another will change direction caused by the change of refraction. The path is bending when it passes through the troposphere. Further, the signal velocity will also change when the signal passes through layers with different refractive indexes. The velocity will be reduced in air layers with higher refractive indexes.

The bending of the signal path usually is modelled by a mapping function m which gives the relation between a zenith delay and slant delay at different elevation angles. Equation (83) is an example of how a mapping function m is used to map the zenith tropospheric delay (ZTD) to the slant delay T_A^s between receiver A and a satellite s which is found at elevation angle e_A^s above the horizon.

$$T_A^s(t) = ZTD(t) \cdot m(e_A^s) \tag{83}$$

To describe the time delay in the troposphere we return to the example with the horizontal thin layers and follow a signal through them along the zenith direction. Since the zenith direction is perpendicular to the horizontal layers, the incoming signal will not be bended, thus the only influence on the signal is caused by the delay. The total zenith tropospheric delay, T, can be expressed as an integral

$$ZTD = \int_h^\infty n(s)\,ds - \int_h^\infty ds = \int_h^\infty \left(n(s) - 1\right) ds = 10^{-6} \int_h^\infty N(s)\,ds \tag{84}$$

where s is the distance, $n(s)$ the refraction, both integrated over the zenith distance from height h to ∞. $N(s)$ the refractivity, is normally introduced as a replacement of $\left(n(s) - 1\right)$ in Eq.(84), scaled 10^6 times because the refractive index is very close to unity.

Since the neutral atmosphere consists of both dry air and water vapour, the refractivity can be separated into two parts, one which contain the influence of the dry part N_d and the other which contain the wet N_w, first suggested by Hopfield (1969).

$$N = N_d + N_w \tag{85}$$

Approximately 90 % of the tropospheric refraction is represented in the dry part of the atmosphere and the remaining 10% from the wet part. The problem however is that the wet part is very unpredictable. The size of the dry part is approximately 2.4 meters at main sea level and 0-0.4 metres for the wet part. Thayer (1974) introduced a model to determine the refractivity given as

$$N = \underbrace{k_1 \frac{p_d}{T} Z_d^{-1}}_{N_d} + \underbrace{k_2 \frac{p_w}{T} Z_w^{-1} + k_3 \frac{p_w}{T^2} Z_w^{-1}}_{N_w} \tag{86}$$

which is related to partial pressure of dry air p_d and wet vapour air p_w, with the corresponding compressibility factors Z_d^{-1} and Z_w^{-1}, the absolute temperature T given in Kelvin. k_1, k_2 and k_3 are empirically determined physical constants. The first two terms in Eq.(86) are related to the induced polarisation if air and water vapour molecules respectively. The third term depends is related to the permanent dipole moment of the water vapour molecules.

Davis et al. (1985) propose an alternative division of the refractive index. Their idea is to split the refraction into a hydrostatic and a nonhydrostatic part instead of a dry and a wet. They did this by dividing the dry part in Eq.(86) as follow:

$$\begin{aligned} N &= k_1 \frac{p_d}{T} Z_d^{-1} + k_2 \frac{p_w}{T} Z_w^{-1} + k_3 \frac{p_w}{T^2} Z_w^{-1} \\ &= k_1 \frac{p_d}{T} Z_d^{-1} + k_1 \frac{p_w}{T} Z_d^{-1} - k_1 \frac{p_w}{T} Z_d^{-1} + k_2 \frac{p_w}{T} Z_w^{-1} + k_3 \frac{p_w}{T^2} Z_w^{-1} \\ &= \underbrace{k_1 \frac{p}{T} Z_d^{-1}}_{N_h} + \underbrace{(k_2 - k_1) \frac{p_w}{T} Z_w^{-1} + k_3 \frac{p_w}{T^2} Z_w^{-1}}_{N_w} \end{aligned} \tag{87}$$

The difference from the previous refraction model is that the first part now has the refractivity of an ideal gas in hydrostatic equilibrium and easy to determine with high precision by directly measuring the total pressure p ($p = p_d + p_w$) at the observation site, instead of the partial pressure as in the previous model.

The total slant delay between receiver A and satellite s in Eq. (83) can be rewritten for a hydrostatic and a wet part

$$T_A^s(t) = T_{h,A}(t) \cdot m_h(e_A^s) + T_{w,A}(t) \cdot m_w(e_A^s) \tag{88}$$

where e_A^s is elevation angle of satellite s as viewed from station A. Subscript h denotes hydrostatic and w wet part of the troposphere.

In the subsequent sections the a priori model for the tropospheric corrections is described. Thereafter, the dynamic parameter models are described and finally the mapping functions.

3.2.3.2.1 A priori models

There are several models derived of the tropospheric delay during the years. Most famous models are derived by Hopfield (1969) and Saastamoinen (1972). Both the models take metrological data from the surface at the observation site into account. A problem with the metrological observations is that they are not a good representation of the total troposphere since they are influenced by surface layer biases which are introduced by micro-metrological effects. There are a priori models for both the hydrostatical and the wet part of the troposphere that only uses a limiting amount of metrological observations. A typical example of this for the hydrostatical delay is given by Davis et al. (1985):

$$T_{hd} = 0.0022768\left(\frac{P_0}{1-0.00266\cos(2\varphi)-0.00027H}\right) \tag{89}$$

Where P_0 is the total atmospheric pressure at the centre of antenna at the observation site, φ the geometric site latitude and H the height above mean sea level in kilometres. The uncertainties of this expression are according to the authors somewhere between 0.5 and 20 millimetres per 1000 bar which is slightly better than Saastamoinen's model which by the other hand gives a result on the millimetre level according to Mendes and Langley (1999) where this model where compared with radiosonde observations during a year at 50 stations placed all around the world. The denominator in Eq.(89) is always close to unity (for reasonable weights) independent of the values of φ and H it is always close to unity. This means that the main influence on the tropospheric delay is left to the atmospheric pressure which is changing according to the observation height.

The wet zenith delay has a more random nature since it varies according to the amount of water vapour in the air. Both Hopfield (1969) and Saastamoinen (1973A), (1973B) and (1973C), derive models for the wet part of the tropospheric delay. Both models where compared with several other models by Mendes and Langley (1999) to find a model that was useful for aircraft applications where metrological observations is rather difficult to perform. They used radiosonde observations to study the r.m.s. scatter of the models and they found that the size of the scatter where about 5 cm. They presented in the same paper an alternative slightly improved model of the zenith wet troposphere

$$T_{wd} = 0.0122 + 0.00943p_w \tag{90}$$

This model where originally derived for aircraft applications where accurate observations of the wet partial pressure is rather difficult to determine. Instead they use data from form some standard model as the International Organisation for Standardisation Reference Atmospheres for Aerospace where values can be interpolated according to position and time of year. This model show the same result as the old models at low latitudes but about 1.6 times better at middle and high. And since it does not use any metrological data it is preferable in our applications.

As mentioned before, we do no metrological observations at the observation site. To determine the deterministic part of the troposphere we use standard values for the metrological observations. In table 3 the metrological values that we use are listed, the values represent metrological observations at mean sea level.

Table 3. Metrological standard values

Air pressure	1013.25 hpa
Temperature	$+20°$ C
Relative humidity	50%

3.2.3.2.2 Mapping function

Mapping functions are used to map the zenith delay to the actual elevation angle to the satellite. Most of them are derived empirically by adopting equations to radiosonde observations. The mapping functions can be separated into groups by studying their input parameters. Some models use parameters from surface metrology measured on site location, like Ifadis (1986), others are based on geometrical parameters, like Niell (1996) and there are those, which are based on a combination of both geometrical and atmospheric parameters like Marini (1972). The atmospheric parameters makes the model more “difficult to use” while the pressure component is proved to be “weak”, Ifadis (2000). Therefore we have chosen to use the Niell mapping function since it is based only on geometrical parameters of the observation site and the date of year and no metrological observations are needed. Several authors like Ifadis (2000), Davis et al. (1985) and Mendes and Langley (1994) show that the Niell mapping function is very attractive since it can be applied at elevation angles down to 3 degrees above the horizon.

In Niell mapping function is the same equation Eq.(91) used to determine both the hydrostatic and wet mapping function with slightly different parameters.

$$m(\varepsilon) = \frac{1 + \dfrac{a}{1 + \dfrac{b}{1 + c}}}{\sin\varepsilon + \dfrac{a}{\sin\varepsilon + \dfrac{b}{\sin\varepsilon + c}}} + h_{[km]} \left(\frac{1}{\sin\varepsilon} - \frac{1 + \dfrac{a_h}{1 + \dfrac{b_h}{1 + c_h}}}{\sin\varepsilon + \dfrac{a_h}{\sin\varepsilon + \dfrac{b_h}{\sin\varepsilon + c_h}}} \right) \tag{91}$$

where a, b and c are determined from the following general equation:

$$a(\varphi, DOY) = \tilde{a} - a_p \cos\left(2\pi \frac{DOY - DOY_0}{365.25} \right) \tag{92}$$

In Eqs. (91) and (92) φ is the latitude, ε is satellite elevation angle above the horizon at the observation site, DOY is day of the year and h is the height above sea level in kilometres.

The parameters a_h, b_h and c_h are all empirically determined by adopting the equation to real radiosonde data measured at 25 stations spread all over the northern hemisphere. The values for each parameter can be found in appendix A.

3.2.3.2.3 Parameter modelling

The total deterministic tropospheric delay is determined with equation (88) and is subtracted from the observations. The hydrostatic a priori parameter determined by using Davis and Mendes zenith models for the hydrostatic and wet tropospheric delays. The deterministic zenith delay values are mapped to the corresponding slant delay using Neill mapping functions. Remaining unmodelled part of the tropospheric delay is now treated as a wet delay, mainly since the wet models are more unpredictable than the hydrostatic. At each reference station is the zenith tropospheric parameter modelled as a random walk procedure. The dynamic equation that is used for the wet delay $T_{w,A}$ at reference stations reads:

$$\dot{T}_{w,A} = u_{T,A} \tag{93}$$

where the subscript w indicates that it is a wet delay and A represents the receiver name. The random part at the rover stations is determined by interpolation each epoch, just as for the ionosphere.

$$T_{wi,C}(t) = \frac{d_{AC}^{-1} T_A(t) + d_{BC}^{-1} T_B(t) + \ldots}{d_{AC}^{-1} + d_{BC}^{-1} + \ldots} \tag{94}$$

where d_{AC} corresponds the distance between the receivers A and C. The subscript i represent, as before, an interpolated parameter. Interpolated values are then mapped in to the correct elevation angle with the wet part of Niell mapping function.

The dynamic matrix $\mathbf{F}_T$ for the zenith troposphere contains only zeros since it is modelled as a random walk procedure, which means that no dynamic change are introduced during the time between the epochs:

$$\mathbf{F}_T = \mathbf{0} \tag{95}$$

The state vector contains the estimated parameters for the reference stations, in this case station A and B:

$$\mathbf{X}_T = \begin{bmatrix} T_{h,A} & T_{h,B} \end{bmatrix}^T \tag{96}$$

$\mathbf{G}_T$ and transition matrix $\mathbf{T}_T$ will be identity matrix. The process noise covariance matrix are given by

$$\mathbf{Q}_{k,T} = \Delta t \cdot \mathrm{diag}(q_T, q_T, \ldots) \tag{97}$$

It is reasonable to assume, that the noise parameters q_T are the same for all stations and all satellites.

3.2.4 Receiver antenna models and multipath

All observations that are measured with a GPS-receiver are related to the phase centres of the used antenna. The phase centres does not necessarily coincide with the physical centre of the antenna. It is changing with the frequency of the incoming signal, with the elevation angle, azimuth direction to the satellite and the local environment around the antenna. To overcome this problem are the GPS-antennas calibrated. Calibration can be done in both in absolute and relative mode. Wübbena et al. (1996) describes absolute calibration which GEO++ performs and Madler (2002) describes the relative calibration procedure that the National Geodetic Survey (NGS) USA uses. According to Madler (2002) errors up to 10 cm can be introduced to the estimated coordinates if the antenna corrections are ignored. The general trend right now is that one use absolute calibrated antennas in GPS-survey when high accuracy is wanted. The main difference between absolute and relative calibrations is that in the absolute calibrations the corrections are determined in both elevation and azimuth direction of the antenna and in the relative calibration only the elevation dependent corrections are determined. However we have implemented the NGS-antenna corrections in lack of calibrated antennas.

An error parameter that also is dependent of the frequency, used antenna and elevation angle is the multipath. Multipath occurs when the signal bounces before it reaches the antenna. How the multipath influence can be reduced is discussed in the following sections, but before this is done are the NGS-parameters described together with an

algorithm that modifies the parameters so they can be used on an antenna orientated in an arbitrary direction.

3.2.4.1 NGS antenna parameters

The NGS antenna calibration procedure is based on relative observations at two points placed only a few metres from each other. At one of the points a permanent reference antenna is mounted and on the other, the antenna is placed which is to be calibrated. Both antennas are orientated to the magnetic north. The calibration procedure is divided into two steps: in the first step the antenna reference point (ARP) is determined, which is the constant offset between the physical and phase centre of the antenna, in each direction (North, East and Up). The phase centres for the L1 and L2 channels do not coincide so one set of offset parameters are determined for each frequency.

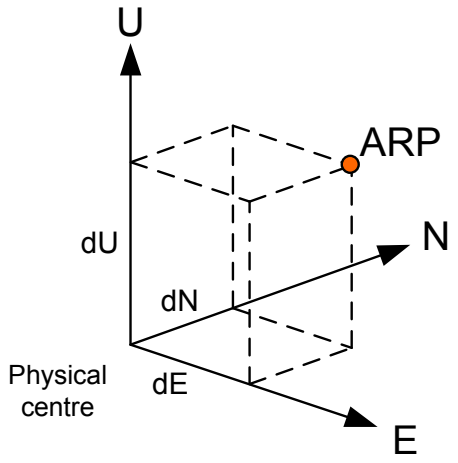

Figure 6. The phase centre of an antenna does not always coincide with the physical centre. NGS determines the offsets to the antenna reference point ARP.

In the second step the phase centre variations (PCV) are determined. These values are necessary since the phase centre is changing with the elevation angles to the satellite. NGS determines PCV values for elevation angels, from 10 to 90 degrees, with a step of 5 degrees, for both satellite frequencies (L1 and L2). The result from the calibrations is summarised in a set of parameters. A template of these parameters is found in Table 4. The template starts with a header with a description of the tested antenna, how many different antennas that are used to determine the parameters and the date of the parameters. Thereafter follows the parameters for the L1 frequency, with one row with the ARP offsets and two rows with the elevation depending errors. After these rows follows the same set of parameters for the second frequency L2.

Table 4. Template for the NGS calibration parameters

```
ANTENNA ID        DESCRIPTION                    DATA SOURCE (# OF TESTS) YR/MO/DY

 [north]  [ east]  [  up ]                                    | L1 Offset (mm)
 [90]  [85]  [80]  [75]  [70]  [65]  [60]  [55]  [50]  [45]  | L1 Phase at
 [40]  [35]  [30]  [25]  [20]  [15]  [10]  [ 5]  [ 0]        | Elevation (mm)
 [north]  [ east]  [  up ]                                    | L2 Offset (mm)
 [90]  [85]  [80]  [75]  [70]  [65]  [60]  [55]  [50]  [45]  | L2 Phase at
 [40]  [35]  [30]  [25]  [20]  [15]  [10]  [ 5]  [ 0]        | Elevation (mm)
```

A calibrated antenna has a complete set of values in the template. These values are used to determine distance corrections at different azimuths and elevation angles. Linear interpolation is used for values between the tabulated values. Eq. (98) is used to determine the corrections in a certain direction $\mathrm{APC}_{\alpha,\varepsilon}$

$$\mathrm{APC}_{\alpha,\varepsilon} = \Delta_{\mathrm{Hor}} - \Delta_{\mathrm{PCV}} \tag{98}$$

where

$$\Delta_{\mathrm{Hor}} = \left(\mathrm{N}\cos\alpha + \mathrm{E}\sin\alpha\right)\cos\varepsilon \tag{99}$$

$$\Delta_{\mathrm{PCV}} = \text{ Interpolated value} \tag{100}$$

α is the azimuth and ε is the elevation angle of the satellite, N and E are the North and East components respectively.

3.2.4.2 Modification of the NGS antenna parameters

The NGS antenna parameters are determined for antennas that are oriented towards the magnetic north but this is not always the case. In engineering applications the antennas are often mounted on a 5/8 inch bolt. If the thread on the bolt is not orientated so the antenna ends orientated towards the magnetic north some type of algorithm is needed to modify the antenna parameters so they are oriented towards the magnetic north. This can be done with an additional correction to the horizontal parameters in the antenna model. Eq.(99) is then rewritten as

$$\Delta_{\mathrm{Hor}} = \left[\mathrm{N}\cos\left(\alpha + \beta_{\mathrm{cor}}\right) + \mathrm{E}\sin\left(\alpha + \beta_{\mathrm{cor}}\right)\right]\cos\left(\varepsilon\right) \tag{101}$$

where β_{cor} is the additional horizontal correction, for which a value could be attained by using a simple compass. This additional correction changes ARP to the new azimuth as can then be seen in Figure 7. The maximal horizontal displacement of the ARP is found when β_{cor} is 180 degrees. In this case the sign of the horizontal ARP components has changed into the opposite.

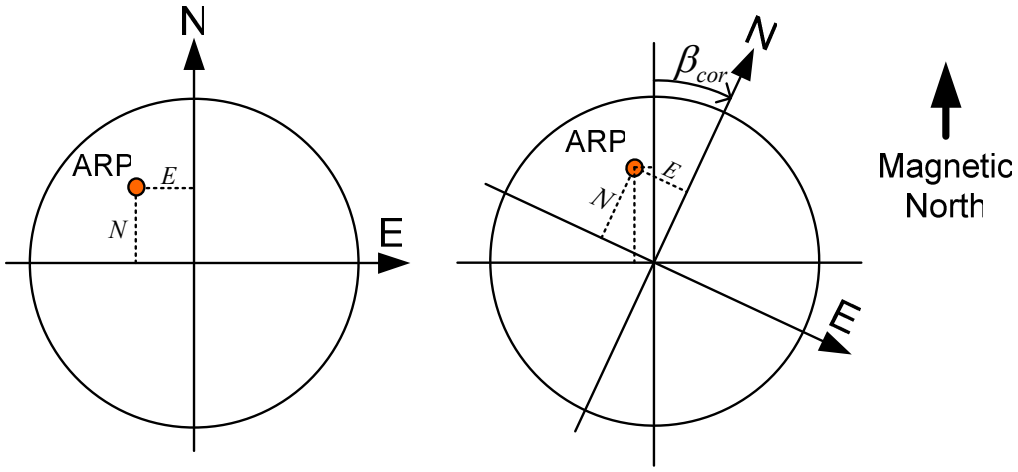

Figure 7. The ARP position changes when antenna is orientated in another direction. The worst case occurs when the antenna is orientated to south instead of the correct direction, to north. In this case the horizontal ARP values change sign.

The direction of the maximum error and the size of the error can be found by differentiation of Eq. (101)according to the sum of the angles $(\alpha+\beta_{cor})$.

$$\frac{\partial\Delta_{Hor}}{\partial(\alpha+\beta_{cor})}=\left[-N\sin(\alpha+\beta_{cor})+E\cos(\alpha+\beta_{cor})\right]\cos(\varepsilon) \tag{102}$$

Setting Eq. (102) to zero we get

$$\tan(\alpha+\beta_{cor})=\left(\frac{E}{N}\right) \tag{103}$$

The maximum size of the horizontal error can be fund by using the second derivate Eq.(101) as,

$$\Delta_{HorMax}(\varepsilon)=\frac{\partial^2\Delta_{Hor}}{\partial^2(\alpha+\beta_{cor})}=\left[-N\cos(\alpha+\beta_{cor})-E\sin(\alpha+\beta_{cor})\right]\cos(\varepsilon) \tag{104}$$

Rewriting Eq.(104) by transforming some sine and cosine expressions into tangent

$$\Delta_{HorMax}(\varepsilon)=\left[\frac{N}{\sqrt{1^2+\tan(\alpha+\beta_{cor})^2}}+\frac{E\tan(\alpha+\beta_{cor})}{\sqrt{1^2+\tan(\alpha+\beta_{cor})^2}}\right]\cos(\varepsilon) \tag{105}$$

$$=\left[\frac{N}{\sqrt{1+\left(\frac{E}{N}\right)^2}}+\frac{E\left(\frac{E}{N}\right)}{\sqrt{1+\left(\frac{E}{N}\right)^2}}\right]\cos(\varepsilon) \tag{106}$$

$$= \left[N\sqrt{1+\left(\frac{E}{N}\right)^2} \right] \cos(\varepsilon) \tag{107}$$

and we finally get an expression of the maximum size of the horizontal errors Δ_{HorMax} at different elevation angles

$$\Delta_{HorMax}(\varepsilon) = \left(\sqrt{N^2 + E^2}\right)\cos(\varepsilon) \tag{108}$$

In Figure 8 an example is given of how large the distance error will become at different elevation angles if the NGS-parameters are used on an incorrect orientated antenna. The worst case is introduced in the figure when the antenna is orientated 180 degrees.

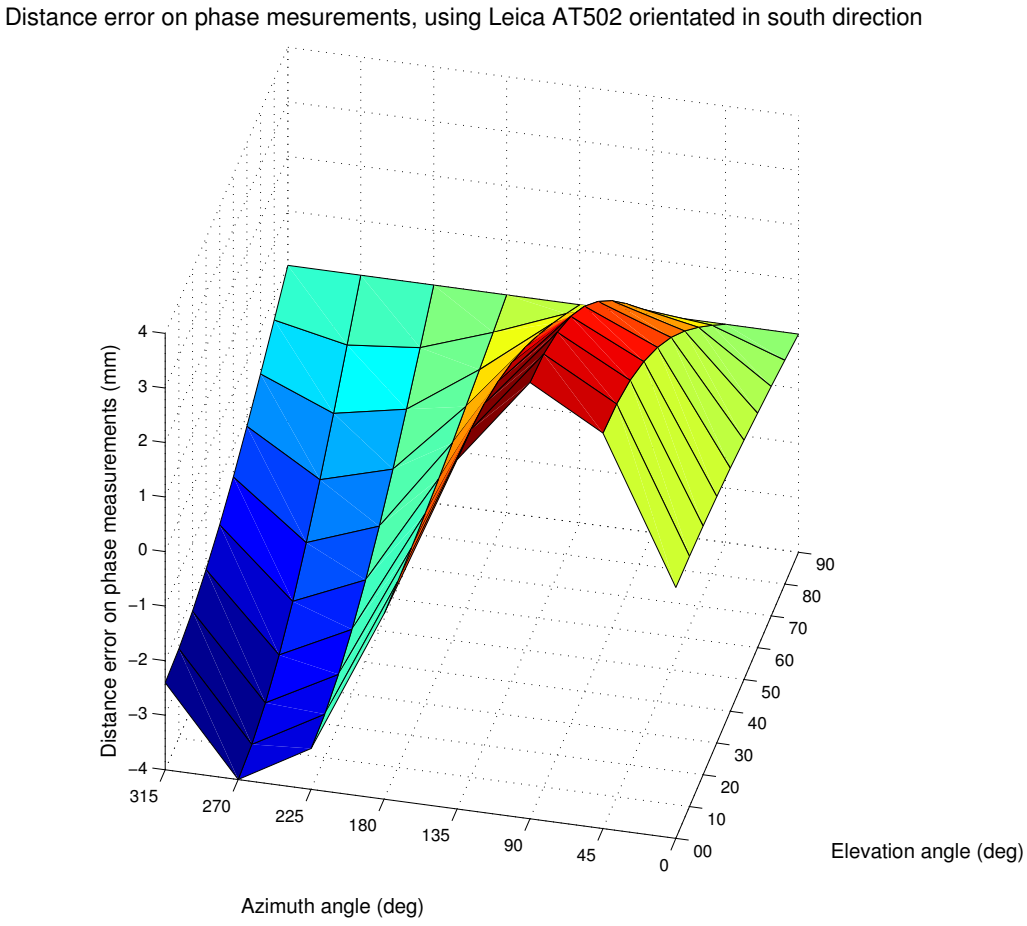

Figure 8. Distance error involved in L1, when the NGS antenna model is used on an incorrect rotated antenna (Leica AT 502). The minimum errors are found in zenith, which corresponds the straight line at elevation angle 90 degrees and the maximum errors are found at elevation angle 0 degrees and at azimuth 85.7 ± 180 degrees.

3.2.4.3 Multipath

The GPS measurements are corrected for the phase centre variation with the use of the NGS-antenna models as described in the previous section. These corrections have different sizes depending on the azimuth and elevation angle for the incoming signal. Besides the influence of the antenna, there is another error source, multipath, that also is varying with the same factors. The combination of multipath and the remaining part that are left of the influence of the antenna phase centre bias can be treated as one parameter MPA for each station-satellite combination. The MPA effect is periodical and it repeat itself in the case of static antenna, as the satellite constellation repeats in one sidereal day (ca 23h 56min). This fact can be used if long observation series (more than 24 hours) are available. If we do not estimate MPA, then this effect directly affects the solution and its periodicity can be seen on the residuals. No stochastic process can describe the real MPA perfectly. If we try to estimate MPA by modelling it as a stochastic process, the residuals will contain the unmodelled part of MPA. These residuals can be stored in a look-up table for each satellite and its azimuth and the next day they can be used as "observed" MPA. The values in the table can be updated (re-estimated) every day as a weighted mean from the previous and currently estimated value. The initial values in the look-up table of the MPA parameters can be set to 0, with a certain standard error (for example 1 cm for phase and 5 cm for code MPA). The idea is that the MPA parameters will be computed with fixed ambiguities after the measurement update in equation (51) as residuals:

$$\mathrm{MPA}_{k+1} = \tilde{\mathbf{L}}_{k+1} - \mathbf{h}_{k+1}(\hat{\mathbf{x}}_{k+1}) \tag{109}$$

Where $\tilde{\mathbf{L}}_{k+1}$ is a vector with the observations that is modified with all the deterministic parameters described in this chapter and $\mathbf{h}_{k+1}(\hat{\mathbf{x}}_{k+1})$ is a function which uses the estimated parameter in the actual epoch (k+1) to determine estimated observations in the actual epoch. We do not use the traditional least square approach for determine the residuals that are given by Fan (2003, p94):

$$\hat{\boldsymbol{\varepsilon}} = \tilde{\mathbf{L}}_{k+1} - \mathbf{H}\hat{\mathbf{x}}_{k+1} \tag{110}$$

Where $\hat{\boldsymbol{\varepsilon}}$ is the residuals and matrix $\mathbf{H}$ is the design matrix, which contains linearized components. We know the direct relation between the estimated parameters in $\hat{\mathbf{x}}_{k+1}$ so the estimated observations can be calculated directly by function $\mathbf{h}_{k+1}(\hat{\mathbf{x}}_{k+1})$, which are based on a slightly modified version of the code and phase observation equations, described in Eqs.(140) and (141).

These residuals are stored until the next day when they are added as known parameters on the left side of the observation equations. This algorithm is not yet implemented in our deformation monitoring software it is left for further work.

3.2.5 Common errors

If the distance between two receivers is short one can assume that the signal slopes from one satellite to both receivers are close to parallel. All errors that influences the distance towards the satellite and that not are covered by the other error sources, introduced earlier in this section are modelled as common errors. Among these common errors are the following errors and phenomena included; the satellite positional error, the residual satellite clock error and tide earth. The satellite positional error and the satellite clock residuals are exactly what the parameter says and needs no further description. Tide earth is a geodynamical phenomenon where gravitational forces in the solar system, especially the moon, make the surface of the earth moving. The size of the earth tide may reach as much as 0.5 meters according to Fan (2001). If the receivers are placed near each other the size of the influence of the geodynamical phenomenon will become the same at both stations and thereby the error can treated as a common error.

All the common parameters are modelled together in a random walk process, which can be described with the following dynamic equation.

$$\dot{o}^s = u_o \tag{111}$$

where u_o is the forcing function for the common errors. The subscript o indicates common errors. The dynamic matrix for a random walk process is:

$$\mathbf{F}_o = \mathbf{0} \tag{112}$$

The transition and design matrixes will be identity matrixes:

$$\mathbf{T}_o = \mathbf{G}_o = \mathbf{I} \tag{113}$$

and the process noise covariance matrix for the common errors are given by

$$\mathbf{Q}_{k,o} = \Delta t \cdot \mathrm{diag}(q_o, q_o, q_o, ...) \tag{114}$$

3.3 Updated observation equations and observation weighting

The observation equations given in Eq. (13) and (14) will now be modified on the known side with the a priori values. Different observation equations are also derived separately for reference and rover stations since the number of unknown parameters are not the same. Position and velocity are only estimated at the rover stations since the reference stations are assumed to be fixed. This concerns also the atmospheric parameters, since they are interpolated from the values at the reference stations at the rover stations.

3.3.1 Updated observation equations at the reference stations

The code observation equations for reference stations A are given by:

$$\begin{aligned} & P^S_{A,L1}(t_A) - \rho^S_A(t_A) + c\left(\delta t^S - T^S_{GD}\right) - MPA^S_{A,L1,P}(t) \\ & -I^S_{d,A}(t) - T^S_{d,A}(t) - APC_{\alpha,\varepsilon}(t) - \left(-\dot{\rho}^S_A(t_A) + c\right)\delta t_{A,L1} = \\ & \delta t_{dr,A} + I^S_A(t) + T_{w,A}(t) + o^S + \varepsilon_{L1,P} \end{aligned} \tag{115}$$

and

$$\begin{aligned} & P^S_{A,L2}(t_A) - \rho^S_A(t_A) + c\left(\delta t^S - \frac{f_1^2}{f_2^2}T^S_{GD}\right) - MPA^S_{A,L2,P}(t) \\ & -\frac{f_1^2}{f_2^2}I^S_{d,A}(t) - T^S_{d,A}(t) - APC_{\alpha,\varepsilon}(t) - \left(-\dot{\rho}^S_A(t_A) + c\right)\delta t_{A,L1} = \\ & \delta t_{dr,A} + \left(-\dot{\rho}^S_A(t_A) + c\right)\delta t_{o,A} + \frac{f_1^2}{f_2^2}I^S_A(t) + T_{w,A}(t) + o^S + \varepsilon_{L2,P} \end{aligned} \tag{116}$$

where on the left side of the observation equation we find the known values as the pseudorange observation $P^S_{A,L1}$, ρ^S_A the true geometric distance, which is known at the reference stations, δt^S the group delay, T^S_{GD} is the additional clock delay correction which is used on code observations, MPA^S_A the multipath delay, $I^S_{d,A}$ the deterministic ionosphere, $T^S_{d,A}$ the deterministic troposphere, $APC_{\alpha,\varepsilon}$ the antenna phase centre corrections and finally the bias part of the receiver clock $\delta t_{A,L1}$.

On the right side the unknown parameters are found as the drift error in the receiver clock $\delta t_{dr,A}$, the clock offset between the frequencies $\delta t_{o,A}$ that occur in the dual frequency mode , the remaining part of the ionosphere I^S_A and the remaining wet part of the troposphere $T_{w,A}$, the common errors are found in o^S, and, finally, the observation noise ε_P. The constant c is the speed of light in vacuum. Subscript L1 and L2 corresponds to the actual frequency, subscript d indicated a priori deterministic models derived in the previous sections. The observation equation for the code observations on the L2 frequency contains the same known parameters, but they are related to the L2 frequency. Some of the terms are the same and can be connected between the frequencies by a scale factor $\left(f_1^2/f_2^2\right)$.

The analogous phase observation equations at a reference receiver are given by:

$$\begin{aligned} & \Phi^S_{A,L1}(t_A) - \rho^S_{k0}(t_A) + c\delta t^S - MPA^S_{A,L1,\Phi}(t) \\ & +I^S_{d,A}(t) - T^S_{d,A}(t) - APC_{\alpha,\varepsilon}(t) - \left(-\dot{\rho}^S_A(t_A) + c\right)\delta t_{A,L1} = \\ & \delta t_{dr,A} + \lambda_{L1}N^S_{A,L1} - I^S_A(t) + T_{w,A}(t) + o^S + \varepsilon_{L1,\Phi} \end{aligned} \tag{117}$$

and

$$\begin{aligned}&\Phi^S_{A,L2}(t_A)-\rho^S_{k0}(t_A)+c\delta t^S-MPA^S_{A,L2,\Phi}(t)\\&+I^S_{d,A}(t)-T^S_{d,A}(t)-APC_{\alpha,\varepsilon}(t)-\left(-\dot\rho^S_A(t_A)+c\right)\delta t_{A,L2}=\\&\delta t_{dr,A}+\lambda_{L1}N^S_{A,L2}-I^S_A(t)+T_{w,A}(t)+o^S+\varepsilon_{L2,\Phi}\end{aligned}\qquad(118)$$

The phase observations are given by Φ^S_A and the additional parameter N is introduced as the unknown ambiguities and λ represents the wavelengths on the L1 and L2 frequency.

3.3.2 Updated observation equations at the rover stations

The corresponding equations at the rover station C becomes for the code observations:

$$\begin{aligned}&P^S_{C,L1}(t_C)-\rho^S_{C0}(t_C)+c\left(\delta t^S-T^S_{GD}\right)-MPA^S_{C,L1,P}(t)\\&-I^S_{d,C}(t)-T^S_{d,C}(t)-I^S_{i,C}(t)-T^S_{wi,C}(t)-APC_{\alpha,\varepsilon}(t)-\left(-\dot\rho^S_C(t_C)+c\right)\delta t_{C,L1}=\\&a_X\Delta X+a_Y\Delta Y+a_Z\Delta Z+\delta t_{dr,C}+o^S+\varepsilon_{L1,P}\end{aligned}\qquad(119)$$

and

$$\begin{aligned}&P^S_{C,L2}(t_C)-\rho^S_{C0}(t_C)+c\left(\delta t^S-\frac{f_1^2}{f_2^2}T^S_{GD}\right)-MPA^S_{C,L2,P}(t)\\&-\frac{f_1^2}{f_2^2}I^S_{d,C}(t)-\frac{f_1^2}{f_2^2}I^S_{i,C}(t)-T^S_{wi,C}(t)-APC_{\alpha,\varepsilon}-\left(-\dot\rho^S_C(t_C)+c\right)\delta t_{C,L1}=\\&a_X\Delta X+a_Y\Delta Y+a_Z\Delta Z+\delta t_{dr,C}+\left(-\dot\rho^S_C(t_C)+c\right)\delta t_{o,C}+o^S+\varepsilon_{L2,P}\end{aligned}\qquad(120)$$

And for the phase observations

$$\begin{aligned}&\Phi^S_{C,L1}(t_C)-\rho^S_{C0}(t_C)+c\delta t^S-MPA^S_{C,L1,\Phi}(t)\\&-I^S_{d,C}(t)-T^S_{d,C}(t)-I^S_{i,C}(t)-T^S_{wi,C}(t)-APC_{\alpha,\varepsilon}(t)-\left(-\dot\rho^S_C(t_C)+c\right)\delta t_{C,L1}=\\&a_X\Delta X+a_Y\Delta Y+a_Z\Delta Z+\delta t_{dr,C}+\lambda_{L1}N^S_{A,L1}+o^S+\varepsilon_{L1,\Phi}\end{aligned}\qquad(121)$$

and

$$\begin{aligned}&\Phi^S_{C,L2}(t_C)-\rho^S_{C0}(t_C)+c\delta t^S-MPA^S_{C,L2,\Phi}(t)\\&-\frac{f_1^2}{f_2^2}I^S_{d,C}(t)-T^S_{d,C}(t)-\frac{f_1^2}{f_2^2}I^S_{i,C}(t)-T^S_{wi,C}(t)-APC_{\alpha,\varepsilon}-\left(-\dot\rho^s_A(t_A)+c\right)\delta t_{C,L2}=\\&a_X\Delta X+a_Y\Delta Y+a_Z\Delta Z+\delta t_{dr,C}+\left(-\dot\rho^S_C(t_C)+c\right)\delta t_{o,C}+\lambda_{L2}N^S_{C,L2}+o^S+\varepsilon_{L2,\Phi}\end{aligned}\qquad(122)$$

In the updated observation equations (119) to (122) some new parameters are introduced. ρ_{k0}^{p} are the geometric distance between the satellite and a set of a priori approximate coordinates. These coordinates are needed since the observation equation is linearised and the true coordinates are unknown. New approximate coordinates are used each epoch based on the estimation in the previous epoch. The interpolated ionospheric and tropospheric delay is also introduced at the rover station as known parameters. On the unknown side of the observation equations are the coordinate deviations from the a priori coordinates estimated. Subscript d denotes as before the deterministic part, subscript i is introduced as the interpolated value, at the rover stations, of the ionosphere and the troposphere.

3.3.3 Observation weighting

In positioning with undifferenced observations, based on a Kalman filter, correct stochastic and functional models are needed both for the time dynamic process and for the observations. The functional and stochastic models for the dynamic process in the Kalman-filter are described in Section 3.1. Here, in this section we study different weighting schemes for the observations. The observations are assumed to be uncorrelated, thus the covariances for each observation is placed on the diagonal in the covariance matrix **R**. Typical factors that influence the GPS observation noise level is the receiver dependent noise, diffraction and multipath. Since these parameters vary during time, new weights are needed each epoch.

The receiver dependent noise is related to the accuracy in the correlation procedure, which is performed in a GPS-receiver. In the correlation procedure the correlation is maximised between the receiver generated signal and the observed signal. The correlation can not become 100%, since the incoming signal is contaminated with noise. A rule of thumb says that the noise level of the signal is about 1% of the signal wavelength (Seeber, 1993 p.310). This implies that a phase observation would have the noise level of approximately 2 millimetres, the wavelength is about 0.2 metres, and about 3 metres for the code observations where the wavelength is 300 metres.

Beside the system dependent noise there are other noise sources like diffraction that occurs when something blocks the true signal path between a satellite and a receiver but the signal still arrives to, and is recorded by the receiver, and multipath occurs when the signal bounces before it reaches the antenna. There are some similarities and some differences between diffraction and multipath that are useful to have in mind. Wanninger et al. (1999) summarises these in Table 5.

Table 5. Comparison: Diffraction and Multipath effects (Wanninger et al., 1999)

	Diffraction Effects	**Multipath Effects**
Common features	• Depends on local environment of receiving antenna • Repeats with identical satellite constellations and unchanged environment • No mitigation by relative positioning • The effects on coordinate estimation is reduced with increase of observation time (static observations) • In kinematic mode rapid changes of diffraction effects: mitigation by filtering	
Differences	• No line-of-sight, only diffracted signal are received • Independent of signal frequency: geometry free linear combination are not affected • Maximum error; in the order of decimetres • Signal strength reduced	• Superposition of direct and reflected (indirect) signals • Frequency dependent: detected in the geometry free combination • Maximum error $\lambda_i/4$ • Fluctuation in the signal strength

3.3.3.1 Weighting methods

The simplest method that can be used in observation weighting is to apply equal weights to all observations of the same type. A problem with this method is that it does not treat fact that the noise level is increased at lower elevation angles. The normal method to avoid this is to remove all observations to satellites that are visible below a certain elevation angle. The drawback of this approach is that the number of satellites becomes less which results in a poorer satellite geometry that also influences the positioning accuracy negatively.

To avoid this, more sophisticated weighting methods have been developed. These methods use mainly two different quality indicators: elevation angle and signal-to-noise ration (SNR). All the factors (diffraction, multipath and receiver dependent noise) are influenced by the elevation angle according to Collins and Langley (1999). This makes

the elevation angle a good quality indicator which can be used for observation weighting. The other quality indicator, SNR, can be derived directly from each observation. The SNR is usually represented by the carrier-to-noise ratio (C/No) which is a normalised SNR value and represents the ratio of the power level of the signal carrier to the noise power in a one Hertz bandwidth. C/No values have a specific place in observation files given in RINEX-format.

There are several different weighting models based on the above mentioned quality indicators. More or less all of them are based on least squares fitting of some kind of function onto double difference residuals. To determine reliable values of the unknown coefficients is a large set of observations needed with observations spread over the complete range of values for the actual quality indicator.

For example, Jin and de Jong (1996) uses double difference residuals when they create a model of the weights with Eq.(123) that describes the relation between the double difference residuals $\hat{\varepsilon}_{DD}$ and the elevation angle E:

$$\hat{\varepsilon}_{DD} = a_0 + a_1 \cdot e^{\left(-\frac{E}{E_0}\right)} \tag{123}$$

where a_0, a_1 and E_0 are coefficients that are depending on instrument brand and the observation type. With a large set of observations the coefficients can be estimated. The observation weights are determined by entering the current elevation angle E for the observation into Eq.(123). By squaring the result we get the a prior variance factor for the observation, which is placed in the a prior variance-covariance matrix **R**. This matrix is used to provide the observations with correct weights in Eq.(46).

An alternative approach that also uses the elevation angle is presented by Wieser and Gaggl (2005):

$$\hat{\varepsilon}_E^2 = \frac{a_0^2}{\sin^2 E} \tag{124}$$

where E is the elevation angle and a_0 a coefficient that are estimated empirically with the double difference residuals as mentioned before. In this equation one directly get the a priori variance factor that are placed into the variance-covariance matrix **R**.

Hartinger and Brunner (1999) have derived a method that they call the sigma-e which is based on a similar equation but instead of the elevation angle they use the C/No values.

$$\hat{\varepsilon}_\varepsilon^2 = a_0 + a_1 \cdot 10^{\left(-\frac{C/No}{10}\right)} \tag{125}$$

the coefficient a_0 is not presented in this paper; it is introduced by the same authors one year later, in Brunner et al. (2000). Again, this is a model that directly give the a priori variance factors that can directly be placed into the variance-covariance matrix.

A comparative study of these models is done by Satirapod and Wang (2000) and they concluded that the weighting procedure based on C/No gives the best result. They also studied the C/No values from several receivers connected to the same antenna and they concluded the C/No values is receiver dependent but they show a similar pattern. This implies that one set of weighting coefficients are necessary for each receiver to determine the correct weights.

The weighting model presented by Hartinger and Brunner (1999) shows a very good performance it reduces the residuals of the baseline component approximately 40 % according to their result. The research group within Engineering surveying and Metrology at the University of Graz have developed several improvements to the sigma-e model. Sigma-Δ where introduced Brunner et al. (2000) which is also based on the C/No values and sigma-F by Wieser and Brunner (2000) which is based on fuzzy algebra. The authors show that both these methods improve the result compared with the sigma-e method.

To study how the performance is influenced when different weighting models are applied some tests will be presented in Section 6.3.3.

3.4 Complete model

Now when actual deterministic and dynamic models for the introduced parameters, we can summarise the matrices in the Kalman filter algorithm, described in Section 3.1.3. If we start with the time propagation matrix **T** we get the following matrix

$$\mathbf{T} = \begin{bmatrix} \mathbf{T}_{PV} & \mathbf{0} & \mathbf{0} & \mathbf{0} & \mathbf{0} & \mathbf{0} & \mathbf{0} \\ \mathbf{0} & \mathbf{T}_{\delta t} & \mathbf{0} & \mathbf{0} & \mathbf{0} & \mathbf{0} & \mathbf{0} \\ \mathbf{0} & \mathbf{0} & \mathbf{T}_{T} & \mathbf{0} & \mathbf{0} & \mathbf{0} & \mathbf{0} \\ \mathbf{0} & \mathbf{0} & \mathbf{0} & \mathbf{T}_{I} & \mathbf{0} & \mathbf{0} & \mathbf{0} \\ \mathbf{0} & \mathbf{0} & \mathbf{0} & \mathbf{0} & \mathbf{T}_{MPA} & \mathbf{0} & \mathbf{0} \\ \mathbf{0} & \mathbf{0} & \mathbf{0} & \mathbf{0} & \mathbf{0} & \mathbf{T}_{o} & \mathbf{0} \\ \mathbf{0} & \mathbf{0} & \mathbf{0} & \mathbf{0} & \mathbf{0} & \mathbf{0} & \mathbf{T}_{AMB} \end{bmatrix} \tag{126}$$

where a time propagation matrix is introduced for each unknown parameter in the model. Following the same procedure, the complete matrix of the dynamic model **F**:

$$\mathbf{F} = \begin{bmatrix} \mathbf{F}_{PV} & \mathbf{0} & \mathbf{0} & \mathbf{0} & \mathbf{0} & \mathbf{0} & \mathbf{0} \\ \mathbf{0} & \mathbf{F}_{\delta t} & \mathbf{0} & \mathbf{0} & \mathbf{0} & \mathbf{0} & \mathbf{0} \\ \mathbf{0} & \mathbf{0} & \mathbf{F}_{T} & \mathbf{0} & \mathbf{0} & \mathbf{0} & \mathbf{0} \\ \mathbf{0} & \mathbf{0} & \mathbf{0} & \mathbf{F}_{I} & \mathbf{0} & \mathbf{0} & \mathbf{0} \\ \mathbf{0} & \mathbf{0} & \mathbf{0} & \mathbf{0} & \mathbf{F}_{MPA} & \mathbf{0} & \mathbf{0} \\ \mathbf{0} & \mathbf{0} & \mathbf{0} & \mathbf{0} & \mathbf{0} & \mathbf{F}_{o} & \mathbf{0} \\ \mathbf{0} & \mathbf{0} & \mathbf{0} & \mathbf{0} & \mathbf{0} & \mathbf{0} & \mathbf{F}_{AMB} \end{bmatrix} \tag{127}$$

The forcing functions **u** is given by;

$$\mathbf{u} = \begin{bmatrix} \mathbf{u}_{a} & \mathbf{u}_{\delta t} & \mathbf{u}_{T} & \mathbf{u}_{I} & \mathbf{u}_{MPA} & \mathbf{u}_{o} \end{bmatrix}^{T} \tag{128}$$

and the design matrix of the forcing functions as G:

$$\mathbf{G} = \begin{bmatrix} \mathbf{G}_{PV} & \mathbf{0} & \mathbf{0} & \mathbf{0} & \mathbf{0} & \mathbf{0} \\ \mathbf{0} & \mathbf{G}_{\delta t} & \mathbf{0} & \mathbf{0} & \mathbf{0} & \mathbf{0} \\ \mathbf{0} & \mathbf{0} & \mathbf{G}_{T} & \mathbf{0} & \mathbf{0} & \mathbf{0} \\ \mathbf{0} & \mathbf{0} & \mathbf{0} & \mathbf{G}_{I} & \mathbf{0} & \mathbf{0} \\ \mathbf{0} & \mathbf{0} & \mathbf{0} & \mathbf{0} & \mathbf{G}_{MPA} & \mathbf{0} \\ \mathbf{0} & \mathbf{0} & \mathbf{0} & \mathbf{0} & \mathbf{0} & \mathbf{G}_{o} \\ \mathbf{0} & \mathbf{0} & \mathbf{0} & \mathbf{0} & \mathbf{0} & \mathbf{0} \end{bmatrix} \tag{129}$$

The state vector is given by the following matrix:

$$\mathbf{x} = \begin{bmatrix} \mathbf{X}_{PV} & \mathbf{X}_{\delta t} & \mathbf{X}_{T} & \mathbf{X}_{I} & \mathbf{X}_{MPA} & \mathbf{X}_{o} & \mathbf{X}_{AMB} \end{bmatrix}^{T} \tag{130}$$

The modified observations are placed in a vector; each element in this vector contains the observations at stations A, B, C and so on:

$$\tilde{\mathbf{L}} = \begin{bmatrix} \tilde{\mathbf{L}}_{A}^{T} & \tilde{\mathbf{L}}_{B}^{T} & \tilde{\mathbf{L}}_{C}^{T} & \ldots \end{bmatrix}^{T} \tag{131}$$

Together with the observations belongs a matrix **R** with the prior variance-covariance values for each observation:

$$\mathbf{R} = \begin{bmatrix} \mathbf{R}_{A} & 0 & 0 & \\ 0 & \mathbf{R}_{B} & 0 & \\ 0 & 0 & \mathbf{R}_{C} & \\ & & & \ddots \end{bmatrix} \tag{132}$$

Since no correlation is assumed between the observations, this matrix becomes a diagonal matrix.

4 Details of Implementation

The purpose with the software that we develop is to determine deformations in real time. We are in a phase of development and have for the evaluation purposes developed a post processing software so we can calculate the same dataset over and over again to evaluate different settings. The software is developed in object orientated Matlab code since Matlab has a lot of build in functions for matrix calculations and result presentation. The disadvantage with Matlab is the computational speed which directly makes it impossible to run the program in real-time applications especially when the computation load becomes high. In our program this scenario occurs when the number of receiver is high and if there are many satellites tracked by the receivers.

The overview of the complete algorithm is summarised in Figure 14. The algorithm starts at the top of the figure with an initialisation procedure. After this the Kalman filter algorithm follows, which is repeated each epoch until all epochs are processed. The result, estimates of the unknown parameters in the state vector, is stored each epoch in a result file.

The initialisation procedure contains three steps; first an initialisation file is read, which includes the start values of the unknown parameters in the state vector, filenames of observation, satellite orbit and NGS-antenna parameter files, the total content of the initialisation file is given in Section 4.2. In the second step these files are read and stored in the computer memory as variables. The satellite orbits are given in Receiver INdependent EXchange format (RINEX) if the orbits are broadcasted in the navigation message or in SP3 format in the case of precise orbits. The content in these files are slightly different and therefore is a module developed to generate “standard orbits”, presented by Horemuž and Andersson (2006), and it will be discussed in Section 4.1. In the final step of the initialisation is the Kalman filter initialised with start values from the initialisation file, $\hat{\mathbf{x}}_0^-$ and $\mathbf{Q}_{x0}^-$ are filled in. When these three steps are completed, the post processing program is initialised and ready to start.

Before the Kalman filter is started, the first common epoch in the observation files is found, which makes it possible to use observation files with different start and stop epochs. The Kalman filter procedure starts in step 1 with reading the standard orbits for the current epoch and thereafter the observations from all the observation files. The observations are used to fill in the observation matrix **L,** the related design matrix **H**, the variance-covariance matrix **R** and to add and remove states in the state vector that belongs to satellites that are new or lost in the current epoch. When the sizes of all matrices are adjusted cycle slip detection algorithms are implemented. If a cycle slip is detected to a satellite the ambiguity value reinitialised with new values is calculated by

the cycle slip algorithm. More about the cycle slip detection is found in Section 4.4. After the cycle slip detection algorithm follows the Kalman filter prediction and updating. The last step of the filter loop is ambiguity fixing, which is entered if the filter has passed a certain number of epochs. The ambiguity fixing is based on the lambda method developed at the University of Delft and is described in Section 4.5. At the end of a loop in the Kalman filter the updated unknown parameters in the state vector are presented with their standard errors.

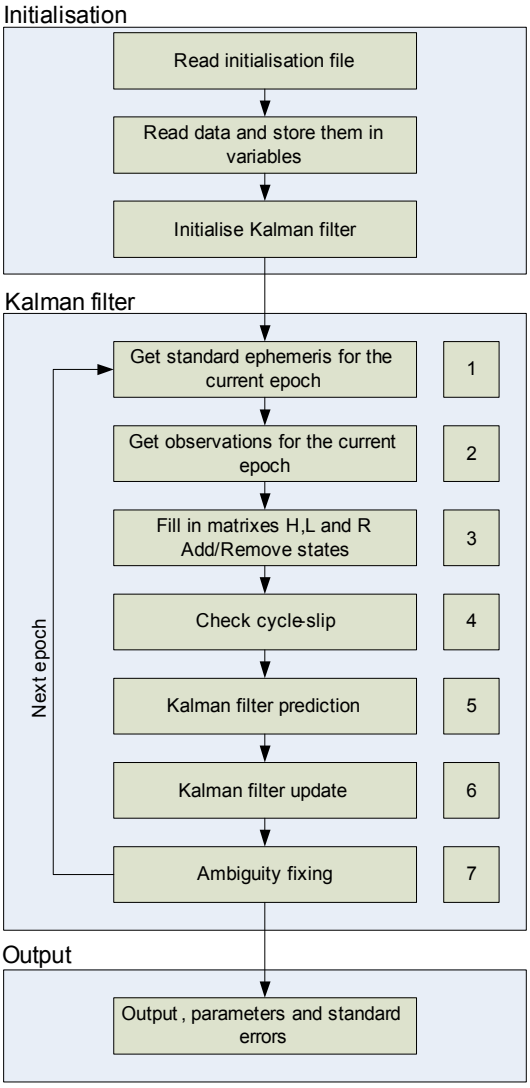

Figure 9. Flowchart of the complete post processing Kalman filter algorithm

4.1 Read data files and generate ephemerides polynomial coefficients

Some input information is needed in both the real-time and the post processing algorithms before the Kalman-filter can run. The real-time algorithms acquire that the

observations and broadcast observations be in real-time, but input values are needed about the antenna parameters, precise orbits and start values for the Kalman-filter estimates. In the post processing algorithms that we are using all observations are accessible before the algorithm is run. This section starts with an explanation about the input formats that we using for the observations, ephemerides, antenna parameters. The final part describes how we develop a general algorithm to calculate the satellite coordinates for both precise and broadcast ephemerides.

4.1.1 Observation and orbit parameters in RINEX format

The post processing program reads observations and orbital parameters defined in RINEX format v2.10. The data format is developed at the University of Bern and presented by Gurnter (2001). Separate file types are generated for observations and the navigation message.

The observation file contains a header which includes information about the observation station, as point number, initial coordinates, height readings, antenna type and so on this is the field protocol for the instrument. After the file heading follows the observation data from each epoch as code pseudorange, phase and Doppler observations. The type of observations that are available is depending on the used instrument.

The navigation file starts as well as the observation file with a header. In the header of the navigation file the parameters for the Klobuchar ionospheric model are found together with time correction parameters for the satellite clock. After the header, follows broadcasted parameters ephemerides for each GPS satellite which is a set of six parameters that describe the Kepler ellipse, three secular correction terms and six periodic correction terms. All the parameters in the broadcast navigation message is determined at the Master Control Station of GPS and are updated each second hour. The accuracy of the coordinates in the broadcast ephemerides are 160 centimetres (cm) and the time is given with an accuracy of less then 7 nanoseconds (ns) according to IGS (The International GNSS service). The satellite coordinates are determined each observation epoch with the algorithm described in by the document IDG-GPS-200C (1999).

4.1.2 Precise ephemerides

The precise ephemerides are calculated at IGS (International GNSS Service) and contain satellite coordinates with a sample interval of 15 minutes. The accuracy of these coordinates are depending on the type of precise ephemerides that are used. Ultra-Rapid precise orbits are a set of real-time predicted parameters that has a coordinate

accuracy of 10 cm and clock accuracy of approximately 5 ns. This product is available trough the internet at the IGS web site and is updated each four hours. NGS offer also other datasets of the ephemerides as the final orbits that has a slightly better accuracy, less than 5 cm in the coordinates and less then 0.1 ns of the satellite clock. Satellite coordinates at an epoch t are determined by interpolation techniques like Lagrange interpolation.

4.1.3 NGS antenna files

For each receiver antenna file NGS antenna parameters are read in the format that is specified by Table 4. The offset parameters in these models are given in a north, east and up system and are transformed from the local coordinate system into WGS 84 and are applied directly to the calculated coordinates. The elevation dependent corrections on the other hand are applied directly to the observations.

4.1.4 Generate standard ephemerides polynomial coefficients

The broadcast ephemerides are represented by a set of Kepler orbit parameters with correction terms and the precise orbits are given by satellite coordinates with a sample interval of 15 minutes. The broadcast ephemerides are updated approximately every 2 hours, and the predicted precise ephemerides are updated each 24 hours. The final precise ephemerides are not available in real-time, they are determined in a post processing procedure which uses observations from several days to calculate the orbits. The accuracy in the broadcast ephemerides is about 3 metres and 0.05 metre for the final post-processed coordinates.

When broadcasted parameters are used to calculate the satellite coordinates, the standard algorithms are used, as described in document ICD-GPS-200C. In the case when precise ephemerides are used then are the satellite coordinates determined by interpolation in the tabular coordinates.

Instead of using two different algorithms to determine the satellite coordinates, we have developed a general algorithm that is independent of the ephemerides input type implying that, both precise and broadcasted ephemerides can be used. The basic idea with the algorithm is to interpolate satellite coordinates, for a given epoch, from a set of polynomial coefficients that describes the satellite orbits. The polynomial coefficients form what we call the standard orbits. These are determined by fitting a polynomial of a certain degree, in a least squares sense, to satellite coordinates that are given in fixed intervals. The polynomial we use is given by:

$$p(t) = a_1 t^n + a_2 t^{n-1} + \ldots + a_n t + a_{n+1} \tag{133}$$

in which t is the time in seconds from the beginning of the time interval and a_n is the polynomial coefficients of order n. The time interval we use is 15 minutes, just as in precise orbits, and we call it tabular orbits. Broadcasted ephemerides are transformed into tabular orbits simply by calculating the satellite coordinates and clock corrections by the standard algorithm at the wanted time interval. The general real-time satellite calculation algorithm is given in Figure 10.

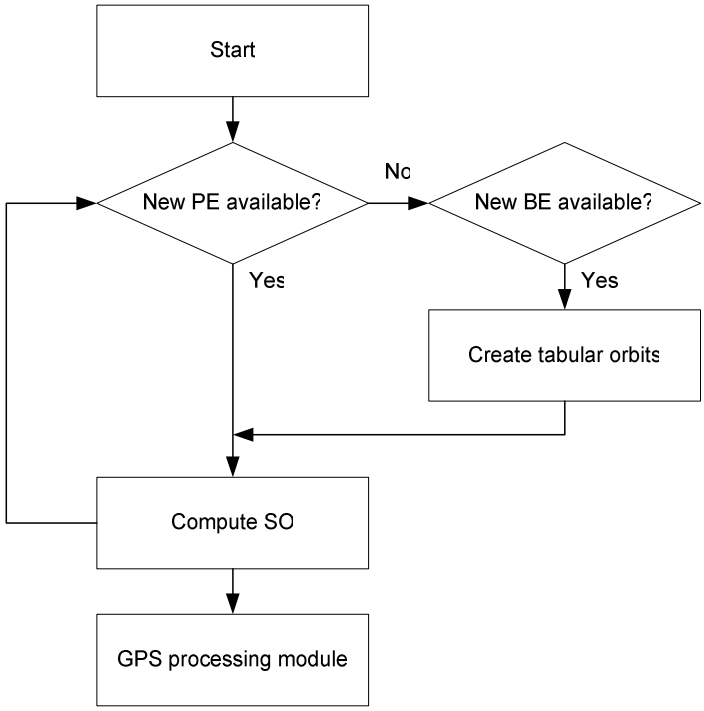

Figure 10. General flowchart for calculating satellite positions

When the algorithm is started the first thing that is done is to check if precise ephemerides (PE) are available. If the answer is yes, then the algorithm directly starts to calculate the standard orbits and if it is no then are the broadcasted ephemerides used instead, where an extra step is needed to create the standard orbits.

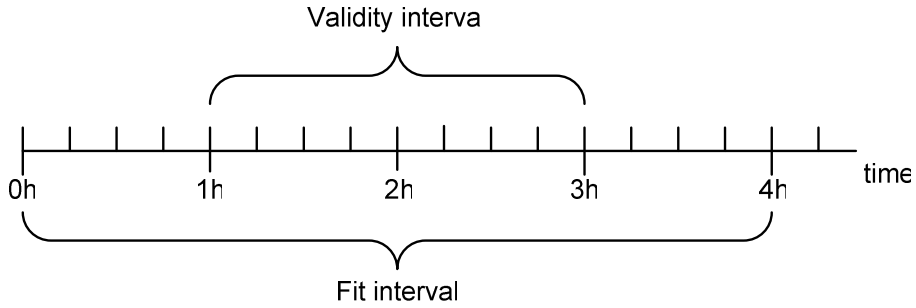

Figure 11. Fit and validity intervals

If a polynomial is fit to equidistant data, oscillations can occur at the beginning and the end of the interval. This is a known problem in numerical analyses where these oscillations are called Runge's Phenomenon (RP). To avoid RP the first and last part of the fit interval are removed and the remaining part is named the validity interval. In Figure 11 are validity interval and the fit interval shown for a 4 hour fit interval and a 2 hour validity interval.

A typical example of RP can be seen in Figure 12, where the difference between interpolated coordinates is compared with coordinates that are calculated with the direct formulas. The oscillations are obvious at the start and end of the 3 hour interval.

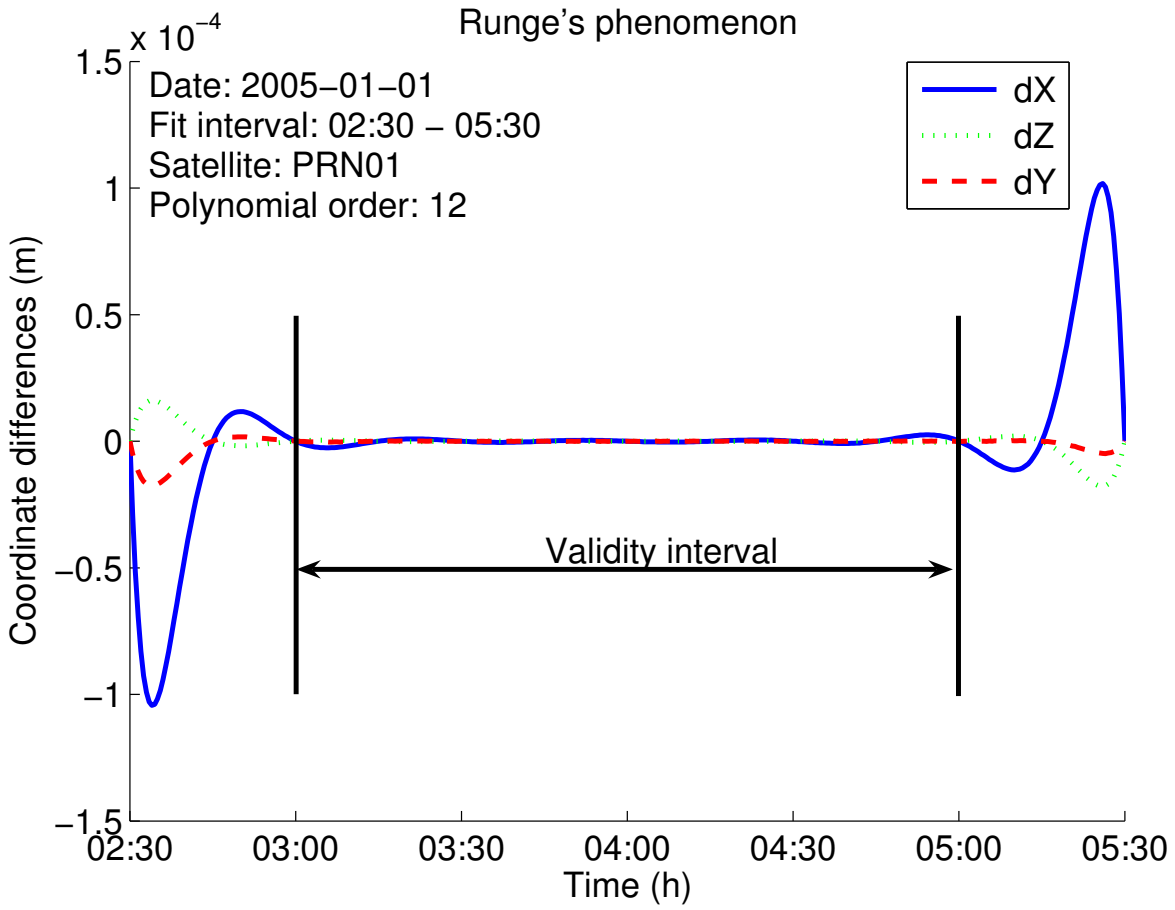

Figure 12. Runge's phenomenon on a 3 hour fit interval

A new set of standard orbits are calculated as soon as time has reached the end of the validity interval or if new ephemerides parameters are found.

The performance of this algorithm is studied in Horemuz and Andersson(2006) and they found that optimal performance is obtained when a 4 hour fit interval is used together with a 2 hour validity interval and a maximum polynomial order is used, which in this case is 16.

4.2 Start values of unknown parameters

Start values for each parameter in the state vector are given in the ini-file, together with values of their standard deviations and power spectral densities. Here follows an explanation of the start values and their standard deviation of each of the parameters.

The start coordinates are taken from the header of the observation files. These coordinates represents a navigated solution and are given in the global reference system WGS84. The standard deviations of the coordinates are given in the local coordinate system at the observation site $\sigma_N = \sigma_E = 10\text{m}$ and $\sigma_U = 20\text{m}$. There is no power spectral density function needed for the coordinates in a position-velocity model applied in the Kalman filter. To use the standard deviations they must be transformed from the local coordinate system into WGS 84. The transformation is done with the same algorithms that are used for the antenna model.

Initial value for the velocity is set to zero $(V_N = V_E = V_U = 0\,\text{m/s})$, and the standard error is set to $\sigma_N = \sigma_E = \sigma_U = 0.001\text{m/s}$. The power spectral density value describes the maximum change rate of the velocity, and it is set to 1 mm/ sqrt(sec), which is a rather exact value, but if the filter fast should converge towards correct coordinates we use this value. See the result in Section 6.1.1.

The receiver clock bias and drift is determined each epoch in a single point positioning procedure and subtracted from the observations. The start value for the remaining clock error is set to zero at all receivers and the accuracy is limited to the accuracy of the estimation in the single point positioning. The remaining error is estimated with a random walk process.

The ionosphere bias is estimated when dual frequency observations are measured at the reference stations. The deterministic part is determined and removed with the Klobuchar ionospherical model which removes approximately 50 % of the ionospheric model. The remaining part is estimated with start value 0 and a standard deviation of 5 meters. The standard deviation of the start value is doubled in the case where no ionospherical parameters are found in the header of the navigation message.

The deterministic model for the hydrostatic and wet part of the troposphere, modelled by Davis (1985) and Mendes and Langley (1999), gives a very good value of the total zenith tropospheric delay if the total air pressure and the wet pressure is known at the observation site. By using these models it is possible to assume that the start value of the zenith delay becomes zero. Accuracy of the observations is very high if the total and wet air pressure is measured at the observation site, approximately 5 centimetres. But since no metrological observations are made must the accuracy be adjusted up a bit. We have decided to upgrade the standard deviation value 10 times to 50 cm.

Initially the ambiguities are estimated with a geometry-free solution, which is explained more in detail in Section 4.4.3. The standard deviation of the estimated ambiguities for the geometry free solution is in that section derived to approximately 10 cycles (under good conditions). It should be noted that the correlation between the estimated values in the geometry free solution is very high and therefore we have decided to increase the standard deviation to 20 cycles.

The final start value is for the errors that are common for all receivers under the assumption that the receivers are placed relatively close to each other (a few kilometres). Initial values can be computed using Eq.(13), after receiver clock computation, or they can be estimated together with clock error on reference stations.

4.3 Fill in matrices L, H, R and Add/Remove states

When the Kalman filter is initialised and standard orbits for the satellites are found and the observations read for the current epoch, it is time to fill in the observation matrix **L**, the design matrix **H** and the corresponding weight matrix **R**. The sizes of these matrices are directly related to the number of receivers, the number of satellites and the number of frequencies that are observed. To describe the sizes of the matrices let us denote:

n_{REF} - number of reference stations
n_{ROV} - number of roving stations
n_{REC} - number of receivers

$$n_{REC} = n_{REF} + n_{ROV} \tag{134}$$

$n_{A,s}$ - number of observed satellites on station A
$n_{A,P1}$ - number of P_1 observations on station A
$n_{A,P2}$ - number of P_2 observations on station A
$n_{A,L1}$ - number of L_1 observations on station A
$n_{A,L2}$ - number of L_2 observations on station A
$n_{A,obs}$ - number of observations on station A

$$n_{A,obs} = n_{A,P1} + n_{A,P2} + n_{A,L1} + n_{A,L2} \tag{135}$$

n_{obs} - number of observations on all stations

$$n_{obs} = n_{A,obs} + n_{B,obs} + \ldots + n_{Z,obs} \tag{136}$$

$n_{obs,L1}$ - number of L_1 observations
n_{TI} - number of tropospheric parameters; (is equal to number of ionospheric parameters)

$$n_T = n_{REF} + n_{obs,L1} \tag{137}$$

The ordering of observations is per station, i.e. first shown are the reference stations with all observed satellites and then follow all roving stations. The observation vector for Z receivers as:

$$\underset{n_{obs}\times 1}{\tilde{\mathbf{L}}} = \begin{bmatrix} \underset{n_{A,obs}\times 1}{\tilde{\mathbf{L}}_A^T} & \underset{n_{B,obs}\times 1}{\tilde{\mathbf{L}}_B^T} & \dots & \underset{n_{Z,obs}\times 1}{\tilde{\mathbf{L}}_Z^T} \end{bmatrix}^T \tag{138}$$

where A, B,…,Z are the receivers. The observation vector for station A to the z satellites are given by:

$$\tilde{\mathbf{L}}_A = \begin{bmatrix} \tilde{\mathbf{L}}_A^{a\,T} & \tilde{\mathbf{L}}_A^{b\,T} & \dots & \tilde{\mathbf{L}}_A^{z\,T} \end{bmatrix}^T \tag{139}$$

where each element is a matrix containing the actual observations modified with the deterministic parameters

$$\tilde{\mathbf{L}}_A^s = \begin{bmatrix} P_{A,L1}^s(t_A) + c\left(\delta t^s - T_{GD}^s\right) - MPA_{A,L1,P}^s - I_{d,A}^s - T_{d,A}^s - APC_{\alpha,\varepsilon} \\ P_{A,L2}^s(t_A) + c\left(\delta t^s - \frac{f_1^2}{f_2^2}T_{GD}^s\right) - MPA_{A,L2,P}^s - \frac{f_1^2}{f_2^2}I_{A,d}^s - T_{d,A}^s - APC_{\alpha,\varepsilon} \\ \Phi_{A,L1}^s(t_A) + c\delta t^s - MPA_{A,L1,\Phi}^s + I_{A,d}^s - T_{d,A}^s - APC_{\alpha,\varepsilon} \\ \Phi_{A,L2}^s(t_A) + c\delta t^s - MPA_{A,L2,\Phi}^s + \frac{f_1^2}{f_2^2}I_{A,d}^s - T_{d,A}^s - APC_{\alpha,\varepsilon} \end{bmatrix} \tag{140}$$

Predicted observations are calculated by the direct functional relationship between the predicted parameters in the state vector and the observations $\mathbf{h}_k(\hat{\mathbf{x}}_k^-)$:

$$\mathbf{h}(\hat{\mathbf{x}}^-) = \begin{bmatrix} \rho_A^{s\,-}(t_A) + \left(-\dot{\rho}_A^s + c\right)\delta t_{A,L1}^- + I_A^{s\,-} + T_A^{s\,-} + o^{s^-} \\ \rho_A^{s\,-}(t_A) + \left(-\dot{\rho}_A^s + c\right)\delta t_{A,L2}^- + \frac{f_1^2}{f_2^2}I_A^{s\,-} + T_A^{s\,-} + o^{s^-} \\ \rho_A^{s\,-}(t_A) + \left(-\dot{\rho}_A^s + c\right)\delta t_{A,L1}^- - I_A^{s\,-} + T_A^{s\,-} + \lambda_{L1}N_{A,L1}^{s^-} + o^{s^-} \\ \rho_A^{s\,-}(t_A) + \left(-\dot{\rho}_A^s + c\right)\delta t_{A,L2}^- - \frac{f_1^2}{f_2^2}I_A^{s\,-} + T_A^{s\,-} + \lambda_{L2}N_{A,L2}^{s^-} + o^{s^-} \end{bmatrix} \tag{141}$$

Take i.e. $\rho_A^{s\,-}(t_A)$, which is calculated with Eq.(53) in the predicted coordinates and the satellite coordinates at time t_A. Another parameter that needs a further explanation is $\dot{\rho}$ which is the orthogonal projection of the satellite velocity vector onto the vector between the GPS-antenna and the satellite $\boldsymbol{\rho}$. The velocity vector of the satellite $\mathbf{v}^e$ is expressed in e-frame (earth frame), obtained from standard orbits as the first derivative of the polynomial. $\dot{\rho}$ is orthogonal projection of $\mathbf{v}^e$ onto $\boldsymbol{\rho}$:

$$\dot{\rho} = \left|\mathbf{v}^e\right| \cos\alpha \tag{142}$$

where α is angle between $\mathbf{v}^e$ and $\boldsymbol{\rho}$, which is the scalar product of the vectors calculated as (Råde and Westergren 1998, p78):

$$\cos\alpha = \frac{\boldsymbol{\rho}\mathbf{v}^e}{\left|\boldsymbol{\rho}\right|\left|\mathbf{v}^e\right|} \tag{143}$$

Inserting Eq.(142) to Eq.(143) we get the orthogonal projection:

$$\dot{\rho} = \frac{\boldsymbol{\rho}\mathbf{v}^e}{\left|\boldsymbol{\rho}\right|} \tag{144}$$

Continuing with the design matrix **H** for two stations and one satellite:

$$\underset{n_{obs}\times n_{par}}{\mathbf{H}} = \left[\underset{n_{obs}\times 6}{\mathbf{H}_{PV}} \quad \underset{n_{obs}\times 3n_{REC}}{\mathbf{H}_{\delta t}} \quad \underset{n_{obs}\times n_{TI}}{\mathbf{H}_{T}} \quad \underset{n_{obs}\times n_{TI}}{\mathbf{H}_{I}} \quad \underset{n_{obs}\times 1}{\mathbf{H}_{o}} \quad \underset{n_{obs}\times n_{obs,\Phi}}{\mathbf{H}_{AMB}}\right] \tag{145}$$

where each of the components in the design matrix will be given in the following equations for a reference station A, a rover station B and one satellite. Starting with the design matrix for the position velocity

$$\mathbf{H}_{PV} = \begin{bmatrix}\mathbf{H}_{A,PV}\\ \mathbf{H}_{B,PV}\end{bmatrix} = \begin{bmatrix} 0 & 0 & 0 & 0 & 0 & 0\\ 0 & 0 & 0 & 0 & 0 & 0\\ 0 & 0 & 0 & 0 & 0 & 0\\ 0 & 0 & 0 & 0 & 0 & 0\\ a_x & a_y & a_z & 0 & 0 & 0\\ a_x & a_y & a_z & 0 & 0 & 0\\ a_x & a_y & a_z & 0 & 0 & 0\\ a_x & a_y & a_z & 0 & 0 & 0 \end{bmatrix} \tag{146}$$

thereafter follows the design matrix for the receiver clocks:

$$\mathbf{H}_{\delta t} = \begin{bmatrix} \mathbf{H}_{A,\delta t} \\ \mathbf{H}_{B,\delta t} \end{bmatrix} = \begin{bmatrix} \frac{-\dot{\rho}_A^s(t_A)+c}{c} & 0 & 0 & 0 \\ \frac{-\dot{\rho}_A^s(t_A)+c}{c} & \frac{-\dot{\rho}_A^s(t_A)+c}{c} & 0 & 0 \\ \frac{-\dot{\rho}_A^s(t_A)+c}{c} & 0 & 0 & 0 \\ \frac{-\dot{\rho}_A^s(t_A)+c}{c} & \frac{-\dot{\rho}_A^s(t_A)+c}{c} & 0 & 0 \\ 0 & 0 & \frac{-\dot{\rho}_A^s(t_A)+c}{c} & 0 \\ 0 & 0 & \frac{-\dot{\rho}_A^s(t_A)+c}{c} & \frac{-\dot{\rho}_A^s(t_A)+c}{c} \\ 0 & 0 & \frac{-\dot{\rho}_A^s(t_A)+c}{c} & 0 \\ 0 & 0 & \frac{-\dot{\rho}_A^s(t_A)+c}{c} & \frac{-\dot{\rho}_A^s(t_A)+c}{c} \end{bmatrix} \quad (147)$$

The order of clock parameters depends on the clock error δt_A and offset between L1 and L2 $\delta t_{o,A}$.

The design matrix for the tropospheric delay is given by:

$$\mathbf{H}_T = \begin{bmatrix} \mathbf{H}_{A,T} & \mathbf{H}_{B,T} \end{bmatrix}^T = \begin{bmatrix} m_h(e_A^s) & m_h(e_A^s) & m_h(e_A^s) & m_h(e_A^s) & \frac{d^{-1}}{\sum d^{-1}} & \frac{d^{-1}}{\sum d^{-1}} & \frac{d^{-1}}{\sum d^{-1}} & \frac{d^{-1}}{\sum d^{-1}} \\ 0 & 0 & 0 & 0 & 1 & 1 & 1 & 1 \end{bmatrix}^T \quad (148)$$

where d are the distances between the stations. In the case the number of receivers are two, $d^{-1}/\sum d^{-1} = 1$, but not if there are more reference stations.

The design matrix for the ionosphere is given as:

$$\mathbf{H}_I = \begin{bmatrix} \mathbf{H}_{A,I} \\ \mathbf{H}_{B,I} \end{bmatrix} \quad (149)$$

where

$$\mathbf{H}_{A,I} = \begin{bmatrix} 1 & \frac{f_1^2}{f_2^2} & -1 & \frac{f_1^2}{f_2^2} & 0 & 0 & 0 & 0 \\ 0 & 0 & 0 & 0 & 1 & \frac{f_1^2}{f_2^2} & -1 & -\frac{f_1^2}{f_2^2} \\ 0 & 0 & 0 & 0 & 0 & 0 & 0 & 0 \\ 0 & 0 & 0 & 0 & 0 & 0 & 0 & 0 \end{bmatrix}^T \tag{150}$$

$$\mathbf{H}_{B,I} = \begin{bmatrix} 1 & \frac{f_1^2}{f_2^2} & -1 & -\frac{f_1^2}{f_2^2} & 0 & 0 & 0 & 0 \\ 0 & 0 & 0 & 0 & 1 & \frac{f_1^2}{f_2^2} & -1 & -\frac{f_1^2}{f_2^2} \\ 1 & \frac{f_1^2}{f_2^2} & -1 & -\frac{f_1^2}{f_2^2} & 0 & 0 & 0 & 0 \\ 0 & 0 & 0 & 0 & 1 & \frac{f_1^2}{f_2^2} & -1 & -\frac{f_1^2}{f_2^2} \end{bmatrix}^T \tag{151}$$

And finally the design matrix for the common errors and the ambiguities:

$$\begin{bmatrix} \mathbf{H}_o & \mathbf{H}_{AMB} \end{bmatrix} = \begin{bmatrix} 1 & 0 & 0 & 0 & 0 & 0 \\ 1 & 0 & 0 & 0 & 0 & 0 \\ 1 & 0 & \lambda_1 & 0 & 0 & 0 \\ 1 & 0 & 0 & \lambda_2 & 0 & 0 \\ 0 & 1 & 0 & 0 & 0 & 0 \\ 0 & 1 & 0 & 0 & 0 & 0 \\ 0 & 1 & 0 & 0 & \lambda_1 & 0 \\ 0 & 1 & 0 & 0 & 0 & \lambda_2 \end{bmatrix} \tag{152}$$

4.4 Cycle slip detection

When a GPS receiver is observing in phase mode, it records the fractional phase difference between the incoming phase and the generated phase observation and counts the phase shifts when the fractional phase switches from 2π to 0. This is continued from that the instrument observation is started until it is stopped. If, by some reason, the signal between the receiver and satellite is lost the integer counter has to start over again, which causes a jump in the continuous count of phase shifts. These jumps are called cycle slips and they need to be detected to determine accurate positions. Sjöberg (2005, p.74) summarizes the reasons that cycle slips occur:

- An obstacle disturbance of the ray path
- Too low signal-to-noise ratio (e.g. as a result of multi-path, ionosphere bias, large receiver accelerations, ect.)
- Failure of the satellite oscillator

All high precision GPS-based processes are sensitive to cycle slips and we need to determine new start values to the filter both in the case when the ambiguities are fixed and when they are unfixed. As explained earlier start values are determined with a geometry-free solution.

The general procedure to detect the cycle slip is to study a time series of some kind of combination of observation that are less sensitive to disturbances than the raw observations. As can be seen in the observation equations, there are many sources that disturb the observations. In the following sections some observation combinations are presented which are used in our software to detect cycle slips.

4.4.1 Single frequency phase / code combinations

A combination of code and phase observations can be used to detect cycle slips in the case where only observations are measured on one frequency. The difference between the code and phase observation $R^S_{A,i,I}$ results in a value that is strongly related to the ionosphere and the ambiguities. This can be seen on the right side of Eq. (153).

$$R^S_A(t) = P^S_A(t) - \Phi^S_A(t) = 2I^S_A(t) - \lambda N^S_A + cT_{GD} + \delta_R + \varepsilon^S_{A,R} \tag{153}$$

where the new parameters on the right side of the equal sign are, δ_R that contains the multipath and $\varepsilon^S_{A,R}$ the measuring noise on the phase and code observations. The difference between the values of $R^S_{A,i,I}$ at epoch t and epoch $t = t + 1$ will become very small if the time between the epochs is short and if no cycle slips occurs during the time between the epochs. This conclusion can be drawn with the knowledge that the ionosphere and the multipath usually change very slowly in time and that the group delay is constant. The problem with this method is, according to Hoffmann-Wellenhof et al. (2001, p.208), that the noise level range of ±5 cycles, mainly caused by the noise level of the code measurements.

4.4.2 Dual frequency phase combinations

Cycle slip detection can be performed by differencing the phase observations of the two frequencies L1 and L2 as follows:

$$\Phi^s_A = \Phi^s_{A,L2}(t) - \Phi^s_{A,L1}(t) = \lambda_{L2} N^s_{A,L2} - \lambda_{L1} N^s_{A,L1} + \left(1 - \frac{f_1^2}{f_2^2}\right) I^s_A(t) + \delta_\Phi + \varepsilon_\Phi \tag{154}$$

where δ_Φ and ε_Φ is as above the multipath and the observation noise for the phase combination. The accuracy in the phase observations are higher than for the code observations so this method is a better method than the single frequency combination presented in the previous section. Based on the rule of thumb about the noise level introduced in Section 3.3.3 it is according to Hoffmann-Wellenhof et al. (2001, p.211) possible to determine cycle slips jumps up to ± 4 cycles when comparing the differences calculated at two subsequent epochs. The remaining problem with this method is to determine on which of the frequencies a cycle slip occurs.

4.4.3 Geometry free solution

The final approach that we are using in our software to detect cycle slips is the geometry-free solution, which is used when both types of observations is made on the L1 and L2 frequencies, here described as Leick (2004, p.244). In this approach, all observations are combined into a solution which given in matrix notation becomes:

$$\begin{bmatrix} P_1 - cT_{GD} \\ P_2 - \alpha_f cT_{GD} \\ \Phi_1 \\ \Phi_2 \end{bmatrix} = \begin{bmatrix} 1 & 1 & 0 & 0 \\ 1 & \alpha_f & 0 & 0 \\ 1 & -1 & \lambda_1 & 0 \\ 1 & -\alpha_f & 0 & \lambda_2 \end{bmatrix} \begin{bmatrix} \rho + \Delta \\ I_{1,P} \\ N_1 \\ N_2 \end{bmatrix} + \begin{bmatrix} \delta_{1,P} \\ \delta_{2,P} \\ \delta_{1,\Phi} \\ \delta_{2,\Phi} \end{bmatrix} + \begin{bmatrix} \varepsilon_{1,P} \\ \varepsilon_{2,P} \\ \varepsilon_{1,\Phi} \\ \varepsilon_{2,\Phi} \end{bmatrix} \tag{155}$$

where Δ is a parameter which includes the clock errors, and the tropospheric error and the scale factor between the L1 and L2 frequency $\alpha_f = (f_1/f_2)^2$. This equation system can be written in matrix notations as follows:

$$\mathbf{L} = \mathbf{AX} + \boldsymbol{\delta} + \boldsymbol{\varepsilon} \tag{156}$$

where **A** is the design matrix, completely independent of the receiver-satellite geometry, therefore this solution is called the geometry-free solution. $\boldsymbol{\delta}$ and $\boldsymbol{\varepsilon}$ are as before the multipath and the measuring noise vector and if they are ignored a solution to the equation system becomes

$$\mathbf{X} = \mathbf{A}^{-1}\mathbf{L} \tag{157}$$

where all the estimated parameters in **X** except for the ambiguities are time dependent. The ambiguities remain constants until a cycle slip occur. Leick (2004, p.245), show that there is a high correlation between the parameters in **X** and to solve this problem one can use an additional matrix **Z** that de-correlates the parameters as follows:

$$\mathbf{z} = \mathbf{Zx} \tag{158}$$

where **Z** is

$$\mathbf{Z} = \begin{bmatrix} 1 & 0 & 0 & 0 \\ 0 & 1 & 0 & 0 \\ 0 & 0 & 1 & -1 \\ 0 & 0 & 1 & 0 \end{bmatrix} \tag{159}$$

The new parameters which are estimated after the transformation are

$$\mathbf{z} = \begin{bmatrix} \rho + \Delta & I_{1,P} & N_W = N_1 - N_2 & N_1 \end{bmatrix}^T \tag{160}$$

The new parameter N_W is the wide-lane ambiguity which has a standard deviation of 0.25 cycles of L_W according to Sjöberg (2005, p.85) and is therefore a very good indicator of a cycle slip, but then again it is difficult to determine on which frequency the cycle slip occur since the wide lane ambiguity is a combination of the ambiguities on L1 and L2.

4.4.4 Implementation of cycle slip detection

All the presented parameters, that are introduced in the previous sections, to detect cycle slips, are implemented in our software. During a calculation, if one of these values exceeds three times their standard deviation a cycle slip is flagged and eventual fixed ambiguities are released. It should be noted that all the used standard deviations are based on the assumed noise level in the signal that are introduced in Section 3.3.3. Additional error sources influences the standard deviation and the possibility to detect cycle slips when real observations are used. Investigations how to improve this algorithm is a subject for future research.

4.5 Phase ambiguity fixing

To reach high accuracy positions using phase observations it is necessary to determine the unknown ambiguities N which are present on the left side in the observation equations. Many different ambiguity fixing methods have been developed during the years, among them the Fast Ambiguity Resolution Approach (FARA) by Frei and Beutler (1990), the Least-Squares AMBiguity Decorrelation Adjustment (LAMBDA) by Teunissen (1994) and the "KTH-method" presented by Sjöberg (1997), (1998A), (1998B), (1999), Sjöberg and Horemuz (1999) and Horemuz and Sjöberg (2002). The goal with all of them is to find the optimal combination of fixed set of phase ambiguities ($\mathbf{x}$) that minimize the residual between the fix and the float phase ambiguities ($\hat{\mathbf{x}}$):

$$\min = \left(\hat{\mathbf{x}} - \mathbf{x}\right)^T \mathbf{Q}_{\hat{\mathbf{x}}}^{-1} \left(\hat{\mathbf{x}} - \mathbf{x}\right) \tag{161}$$

where $\mathbf{Q}_{\hat{\mathbf{x}}}$ is the covariance matrix of the float solution. Several different candidate solutions are tested by changing the fixed values in the vector **x**.

One of the most successful methods is the Lambda method developed at Delft University of technology and introduced by Teunnisen (1994) and described by Jonge and Tiberius (1996). The LAMBDA-method has become a de facto standard within GPS surveying since it gives a good result and is time efficient. The time efficiency depends mainly on the low number of candidates of the fix solution that the method produces.

The input variables to the Lambda-method are the float solution of the ambiguities that are estimated in a least squares estimation and the corresponding covariance matrix. The Lambda-method consists of three essential steps: in the first step the covariance matrix of the float solution is decorrelated to reduce the search space. In the second steo all possible candidates are determined and in the final are the ambiguities fixed.

We use a Matlab algorithm for the Lambda method that is developed by Joosten (2001). The input parameters that we use in the Lambda method are the ambiguity parameters in the state vector $\mathbf{X}_k^-$ and the corresponding part of the covariance matrix $\mathbf{Q}_X$. The algorithm returns two alternative solutions of the ambiguities, the best and the second best solution. To check the strength of the solution we check the ratio between the best and second best solution from Eq.(161) as:

$$\frac{\min_{\text{2nd best}}}{\min_{\text{best}}} > 3 \tag{162}$$

where $\min_{\text{2nd best}}$ and $\min_{\text{best}}$ are the quadratic form of the second best and the best solution. If the ratio between the solutions fulfil the condition in Eq.(162), the ambiguities are fixed, otherwise they are kept unfixed until the next epoch where a new ambiguity fixing algorithm is performed.

4.6 Output parameters, standard errors

The main purpose with the software we develops is to detect deformations. To optimize its performance we have designed the software so that it is easy to change its parameters. The parameters and the start values are set in an ini-file, which content are discussed in Section 4.2. Several output parameters are stored at each epoch when the software is run. The following parameters are stored at each epoch and receiver

- All parameters in the state vector **X** stored together with their covariance matrix (the standard deviation for each parameter are determined by taking the square root of the diagonal elements in the cofactor matrix $\mathbf{Q}_X$).

- the cycle slip detection parameters for single frequency combination, iono-free combination and the geometry-free combination.
- The quality indicators that can be used for observation weighting: elevation angle and C/No value
- The residuals for each observation type calculated as $\mathbf{v} = \tilde{\mathbf{L}} - \mathbf{h}(\hat{\mathbf{x}})$

5 The simulator

We have developed a simulator that generates GPS observations with the main purpose to improve the debugging procedure and to allow the study of the processing performance of the deformation monitoring software in a controlled environment. With the simulator, it is possible to generate controlled observations between satellites and any point that represents the receiver position. By known observations we mean that all parameters in the observation equation are considered as known since their values and their stochastic process is chosen in the simulation procedure.

The simulator is developed in Matlab, and it includes two steps: initialisation and simulation. In the initialisation all settings are defined for the simulation. A detailed description of the initialisation is found in Section 5.2.1. After the initialisation follows the simulation loop, where observations at each GPS receiver are generated, epoch by epoch. During each epoch the deterministic and the stochastic parts are generated for each parameter that influences the GPS observations, of the observation equations. As output from the simulator are RINEX-files with one file for each receiver.

In the following sections the stochastic processes are described together with the parameters that are generated in each of them, and thereafter the simulation loop is described more in detail.

5.1 Stochastic processes

In the simulator the same deterministic models are used as in the Kalman filter algorithm described in the previous sections, and their stochastic parts are generated with the same type of stochastic processes as are modelled in the Kalman filter. We use three different types of stochastic models in the simulator: white noise, random walk and Gauss-Markov processes. In the white noise process no correlations are introduced between the epochs, implying that the autocorrelation function is zero and the stochastic properties of each white noise variable can be given by:

$$\delta_{v,k} = n_{RND,k} \cdot \sigma_v \tag{163}$$

where $\delta_{v,k}$ is the noise at epoch k, $n_{RND,k}$ is a normally distributed random value calculated at each epoch k and σ_v is the standard deviation of the parameter v, which is modelled as a white noise process. Two parameters are modelled as white noise processes: the observation errors and the orbital errors.

Both the random walk and the Gauss-Markov processes are continuous in time, and the time correlation between the epochs is introduced. Starting with the random walk process, which have the following stochastic model

$$\delta_{v,k} = \delta_{v,k-1} + n_{RND,k} \cdot \sigma_v \tag{164}$$

where $\delta_{v,k}$ as before is the noise in epoch k, $\delta_{v,k-1}$ is the noise calculated in the previous epoch and the random part is determined as white noise, like in Eq.(163). The stochastic parts of the ionosphere and the troposphere are generated with this model.

The Gauss-Markov process is a little more complicated than the random walk model. It has an exponential autocorrelation function, which means that the correlation is reducing with time. To calculate the noise level at an epoch k one can use the following relation

$$\delta_k = e^{-(\beta \cdot \Delta t)} \delta_{v,k-1} + W_k \tag{165}$$

Where β is a constant, Δt is the time between the epochs and W_k is a white sequence distributed as follows

$$W_k = N\left(0, \sigma_v^2 \left(1 - e^{-2\beta\Delta t}\right)\right) \tag{166}$$

The noise value can be determined each epoch as

$$\delta_{k,i} = e^{-(\beta \cdot \Delta t)} \delta_{v,k-1} + \left(\sigma_v \sqrt{\left(1 - e^{-2\beta\Delta t}\right)}\right) n_{RND,k} \tag{167}$$

The only parameter that is estimated with a Gauss-Markov process is the multipath.

Besides the parameters that are generated with stochastic models as described above, some parameters are assumed to be static in time in the simulator. We assume that this holds for the positions, velocity, phase ambiguities and the clock errors in the satellites and the receiver. If these values are changed they are changed by a known value. As an example, deformations can be simulated by changing the coordinates from one epoch to the next. The same procedure can be followed to generate cycle slips. How all parameters are treated in the simulator is summarised in Table 6.

Table 6. This table describes how different unknown parameters are modelled in the simulator

Parameter	**Deterministic part**	**Stochastic model**
Position	Static	No
Velocity	Static	No
Ambiguities	Static	No
Receiver clock error	Static	No

Table 6, cont.

Satellite clock error	In the Broadcast ephemerides	No
Observation errors	No	White noise
Common errors	No	White noise
Ionosphere	Klobuchar eq(78)	Random walk
Troposphere, zenith value	Modelled with eqs.(89) and (90)	Random walk
Multipath	No	Gauss-Markov process

Besides the models for the unknown parameters that are summarised in Table 6, there are also corrections for antenna phase centre variations added to the simulated observations.

5.2 The flow in the simulator

The simulator starts with an initialization, which is followed by a simulation loop, where the observations between satellites and receivers are generated. The output from the simulator is RINEX files that contain the simulated observations. The flowchart of the simulator can be found in Figure 13.

5.2.1 Initialisation of the simulator

The simulation is controlled by a setup-file which is read as the first step of the simulator initialisation procedure. All parameters that can be controlled in the simulation is set here like, filenames, start time, number of epochs to be simulated, time intervals between the epochs, coordinates of the receivers, standard deviations for each stochastic parameter and a set of switches that controls if the stochastic parameters should be included in the simulator; see Table 7.

Table 7. The setup file for the simulation software contains a set of switches that are used to control if the stochastic part of the parameters should be generated or not.

```
-----------------------------------------------------------------------
Simulation settings:
StartTime:    2005 06 01 09 30 00     yyyy mm dd hh mm ss
TimeInterval  : 2                     minutes from start to end of sim
SimWeight     : N                     (Y = Yes: N = No)
SimTypeWeight : 1                     (1:Equal 2:Elevation 3:C/No)
SimIono       : N                     (Y = Yes: N = No)
SimTrop       : N                     (Y = Yes: N = No)
SimUseAntPar  : N                     (Y = Yes: N = No)
SimMultipath  : N                     (Y = Yes: N = No)ma
SimOrbErrors  : N                     (Simulate orbit errors)
-----------------------------------------------------------------------
```

As mentioned before, there some are parameters treated as fixed values during time, such as the receiver coordinates, clock errors and the phase ambiguities. Besides the receiver coordinates, all fixed parameters are generated automatically in the simulator.

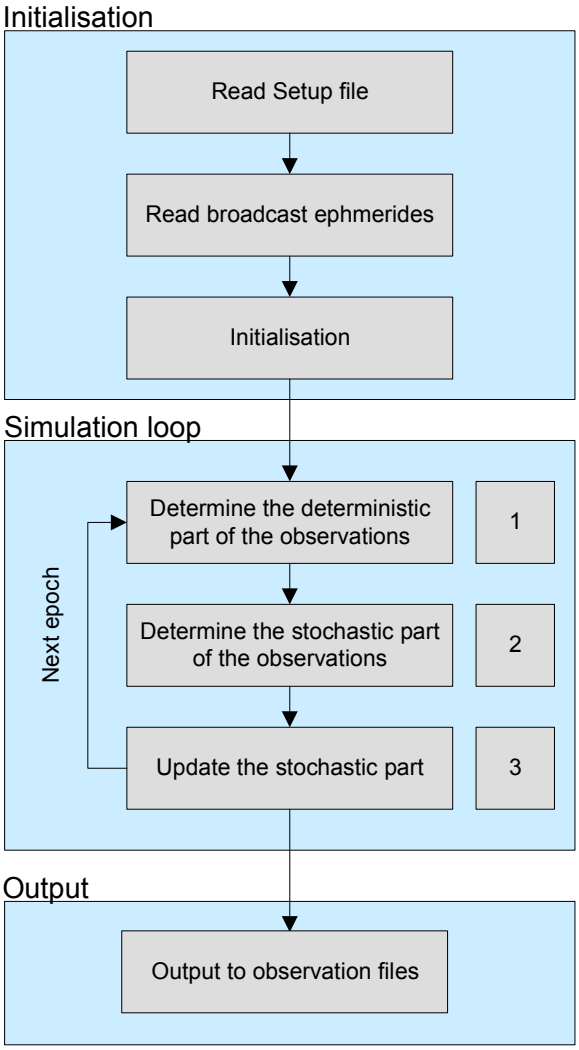

Figure 13. Flowchart of the simulator

When the setup-file is read, the initialisation continues by reading the broadcast ephemerides that are used to calculate the satellite coordinates in the simulation. This is again performed following the same procedure as in the deformation monitoring program by first determining standard orbits that are used to determine the satellite coordinates epoch by epoch.

The last step in the initialisation procedure is to generate start values for the parameters that are set to be simulated as stochastic parameters. For the pure white noise parameters, that is uncorrelated in time, and for the random walk parameters the start values are set by:

$$SV_{RW} = n_{RND,0} \cdot \sigma_{Ini} \tag{168}$$

where SV_{RW} is the generated normally distributed start value $n_{RND,0}$ and σ_{Ini} is the standard deviation for the actual parameter. Start values for the Gauss-Markov processes are represented by:

$$SV_{GM} = \left(\sigma_{Ini}\sqrt{\left(1-e^{-2\beta\Delta t}\right)}\right) n_{RND,0} \tag{169}$$

where SV_{GM} is the start value for the Gauss-Markof process.

5.2.2 Simulator loop and output

After the initialisation the simulator starts to generate observations from the initial start epoch, and it continues until the last epoch is reached. Observations are generated for each receiver to all the satellites that are available in the broadcast ephemerides file given in the initialisation. To do this we useEqs. (115) to (118) which are rewritten as follows

$$\begin{aligned} P^S_{A,L1} = {} & \rho^S_A - c\left(\delta t^S - T^S_{GD}\right) + MPA^S_{A,L1,P} + APC_{\alpha,\varepsilon} + \left(-\dot\rho^S_A + c\right)\delta t_{A,L1} + \delta t_{dr,A} \\ & + \left(I^S_A + I^S_{d,A}\right) + \left(T_{w,A} + T^S_{d,A}\right) + o^S + \varepsilon_{L1,P} \end{aligned} \tag{170}$$

$$\begin{aligned} P^S_{A,L2} = {} & \rho^S_A - c\left(\delta t^S - \frac{f_1^2}{f_2^2}T^S_{GD}\right) + MPA^S_{A,L2,P}(t) + APC_{\alpha,\varepsilon} + \left(-\dot\rho^S_A + c\right)\delta t_{A,L1} + \delta t_{dr,A} \\ & + \left(-\dot\rho^S_A + c\right)\delta t_{o,A} + \frac{f_1^2}{f_2^2}\left(I^S_A + I^S_{d,A}\right) + \left(T_{w,A} + T^S_{d,A}\right) + o^S + \varepsilon_{L2,P} \end{aligned} \tag{171}$$

$$\begin{aligned} \Phi^S_{A,L1} = {} & \rho^S_{k0} - c\delta t^S + MPA^S_{A,L1,\Phi} + APC_{\alpha,\varepsilon} + \left(-\dot\rho^S_A + c\right)\delta t_{A,L1} + \delta t_{dr,A} \\ & + \lambda_{L1}N^S_{A,L1} - \left(I^S_A + I^S_{d,A}\right) + \left(T_{w,A} + T^S_{d,A}\right) + o^S + \varepsilon_{L1,\Phi} \end{aligned} \tag{172}$$

$$\Phi^S_{A,L2} = \rho^S_{k0} - c\delta t^S + MPA^S_{A,L2,\Phi} + APC_{\alpha,\varepsilon} + \left(-\dot{\rho}^S_A + c\right)\delta t_{A,L1} + \delta t_{dr,A}$$
$$+\lambda_{L2} N^S_{A,L2} - \frac{f_1^2}{f_2^2}\left(I^S_A + I^S_{d,A}\right) + \left(T_{w,A} + T^S_{d,A}\right) + o^S + \varepsilon_{L2,\Phi} \tag{173}$$

The simulation loop contains three steps. First the deterministic and the static parameters in the equations are determined. When this performed, the stochastic parts of the parameters are determined, and finally the stochastic parameters are generated for the next epoch.

The deterministic parameters that are determined in the simulation loop are the distances between the receivers and the satellites (ρ^S_A) at the actual epoch. Satellite coordinates are determined from the standard orbits that are generated from the broadcasted ephemerides. Receiver coordinates are corrected for earth rotation during the travelling time of the signal from satellite to receiver. The satellite clock offset δt^S and the time group delay (T^S_{GD}) is obtained directly from the broadcast ephemerides. The receiver clocks ($\delta t_{A,L1}$) are assumed to be constant and with zero drift which implies that the ($\delta t_{dr,A}$) parameter is eliminated. The time offsets between the frequencies ($\delta t_{o,A}$) are also assumed to be zero, therefore this parameter also is eliminated. The ambiguities are generated as constant values, and how this is performed is described in the previous section. The deterministic parts of the zenith troposphere, $T^S_{d,A}$, is determined with Eqs. (89) and (90). The zenith values are then mapped into the actual elevation angle with Neill mapping function; Eq.(91). The deterministic part of the ionosphere $I^S_{d,A}$ is determined with the Klobuchar model; Eq.(78). When the deterministic parts of the parameters are generated the stochastic parts are generated for each parameter. How this is carried out is described in the previous section. The final step in the simulation loop is to generate the stochastic parameters for the next epoch and to place the observations into the observation files following the RINEX format given by Gurtner (2001).

6 Tests

To study the performance of the developed software for positioning and deformation monitoring, we use both simulated and real observations. The simulated observations are generated with the simulator and the true observations are collected in field with a setup that corresponds to a real deformation monitoring setting. Section 6.1 contains analyses based on simulated observations. The idea with this part is to study the performance of the software for deformation monitoring purposes and to study the influence of the antenna parameters on the estimated result. In Section 6.2 tests, where real observations are used. The observations are collected in Gothenburg during December 2005.

6.1 Tests on simulated observations

Some tests are carried out with simulated observations to study the performance of the deformation monitoring software. The main purposes with these tests are to see how the software responds on deformations and to study how the NGS-antenna parameters influence the result.

6.1.1 Deformation detection

We start with the deformation detection tests, where two observation files are generated in the simulator. The first file is generated for a reference station without any deformations, and the second file is generated as a rover with deformations. The deformations in the second observation file are simulated by simply changing the coordinates of the rover receiver from one epoch to the next. In our case the X-component of the geocentric Cartesian coordinates, given in WGS84, is changed in epoch 20 by adding 1 centimetre and in epoch 60 by adding an additional 10 centimetres. During the simulation all stochastic parameters are turned off, which means that the only errors that remain in the observations are the pure numerical errors, as the ones that occurred in the simulator when the observations were rounded to fit the RINEX-format. The simulated observations are thereafter run in the deformation monitoring software in position mode (P-mode) and position-velocity mode (PV-mode). In P-mode the positions are estimated, this corresponds to a static solution, and in PV-mode are both positions and velocities estimated which is similar to a kinematic solution.

The test starts by using the simulated observations in P-mode, which gives the result shown in Figure 14 below. In the figure the true and estimated X-coordinates are compared in WGS 84. The true coordinates are presented with a continuous line, and

the dotted line is the estimated coordinates. Looking at the continuous line, it becomes quite clear where the simulated deformations occur.

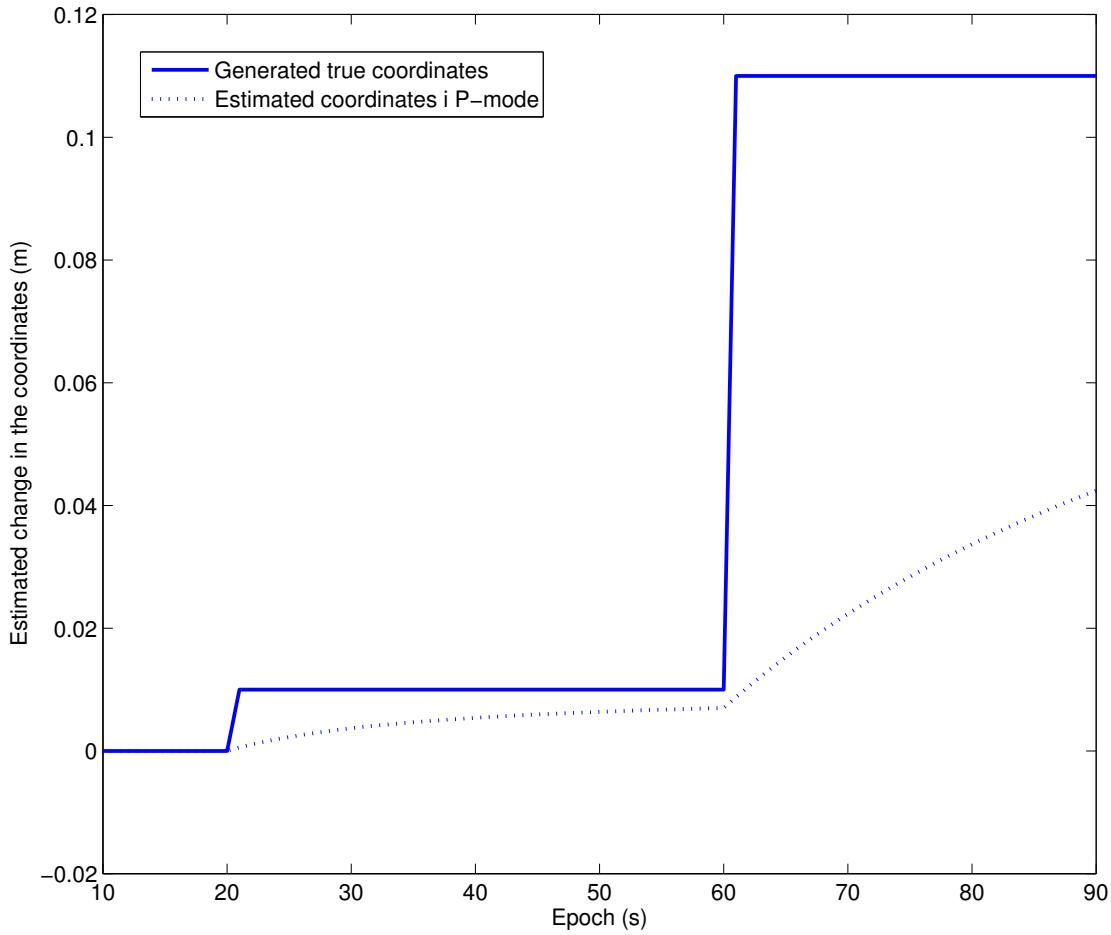

Figure 14. Estimated coordinates for from the software calculated in position mode which corresponds to traditional static calculations. The continuous line corresponds to the true simulated X-coordinates with deformations at epoch 20 and 60. The doted line corresponds to the coordinates that are estimated by the software

By studying Figure 14 it is clear that the P-mode does not give the correct coordinates when deformations occur. The solution will converge towards the correct values after some time, but it will take a lot of time.

Instead of spending more time on the P-mode, we continue with the PV-mode where the same test is carried out with different values of the PSD-values. The PSD-value describes how much the variance is allowed to change from one epoch to the following and different values are tested here to see how the coordinate and velocity estimations are changing with different PSD-values. Figure 15, shows the estimated coordinates, and in Figure 16 the velocity changes are shown.

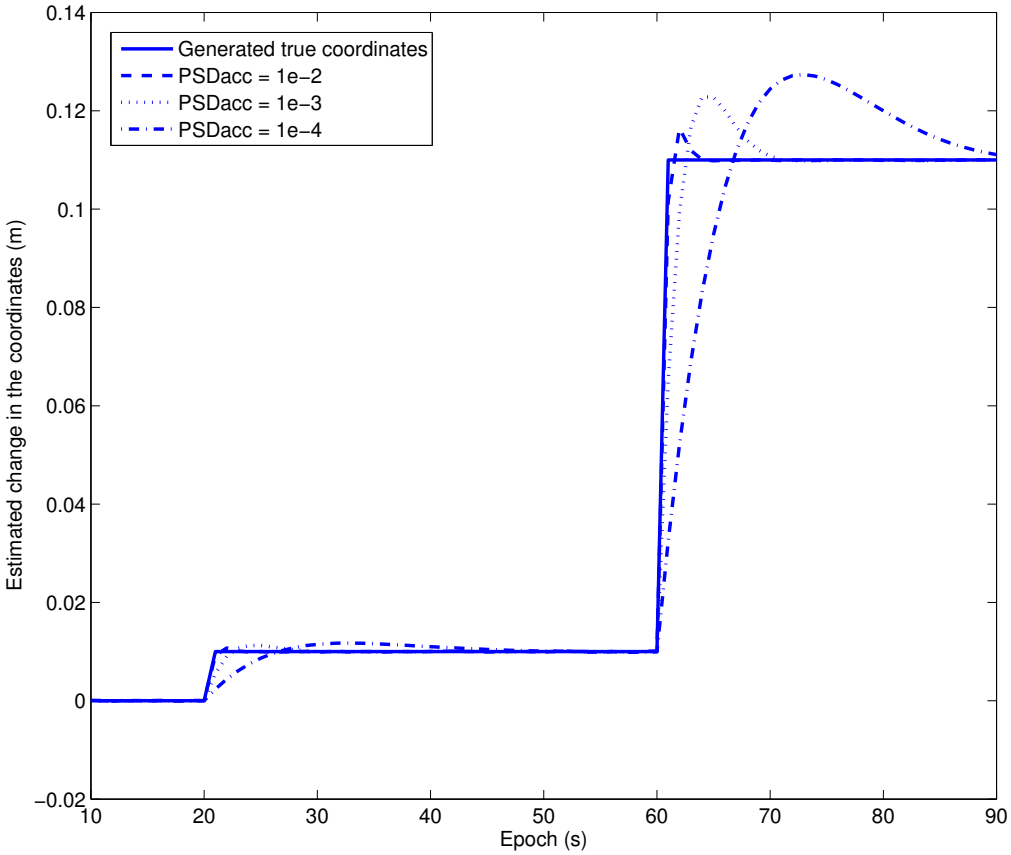

Figure 15. Deformations are simulated in epoch 20 by adding 0.01 metre to the initial coordinates and a additional 0.1 metre after 60 epochs. The true generated coordinates are given by the continuous line in the figure. The other lines represent the estimated X-coordinate, with different PSD-values of the acceleration (PSDacc), from the deformation monitoring software.

It is obvious by studying Figure 15 and 16, that the choice of PSD-value of the acceleration influences the estimation of coordinates and velocity, especially after an epoch, where a deformation occurs. With a high value of the PSD-acceleration, like PSDacc = 1e-2, the filter becomes more dynamic and the software reacts quicker on sudden deformations. This means that the size of PSD-acceleration must be set according to the expected movements of the object to be able to estimate the unknown correctly. Independent of the size of the PSD-value, the deformations can be found by studying the time series of the coordinates and the velocity. In the same epoch as the deformation occurs both the acceleration and velocity are changing as a response to the deformation. These responses can be used as deformation indicators, but exactly how this should be carried out is not analysed here, but instead this is left as an interesting subject for our further work.

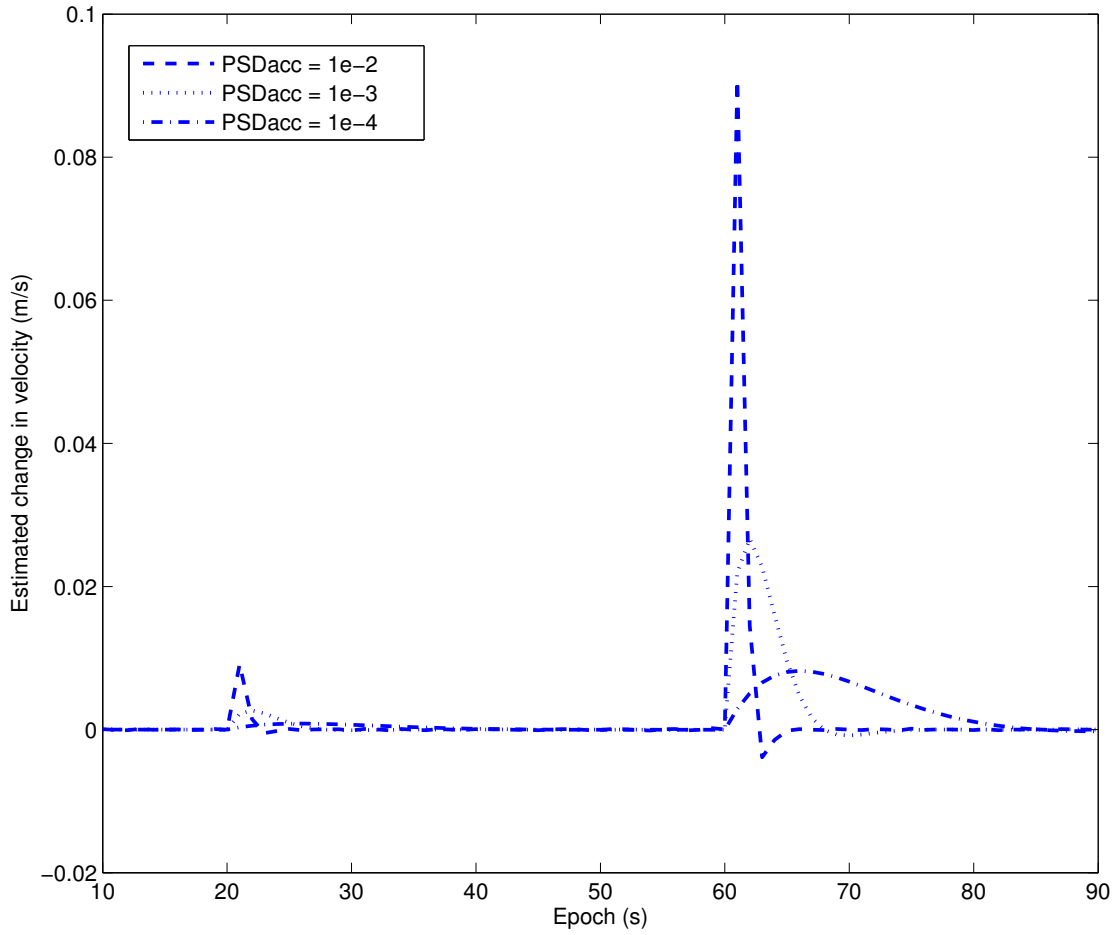

Figure 16. Velocity changes during the observation time. The simulated deformations are obvious in the velocity plot as good indicators of deformations

It must be pointed out that the observations that are used in the deformation detection test above are simulated without any observation noise. But tests where real observations are used show similar pattern, however with a higher noise level.

6.1.2 Influence of the NGS-antenna parameters

As mentioned in Section 3.2.4 we use antenna parameters determined by NGS. The calibration procedure includes determination of the antenna reference point (ARP), which corresponds to the constant offset between the physical antenna centre and the true phase centre of the antenna in the antenna coordinates system oriented towards the magnetic north, and the determination of elevation dependent error called phase centre variations (PRV). In this section we analyse how these values influence the coordinate estimation in the deformation monitoring software. The idea is to see how the estimation of the coordinates is influenced when the antenna parameters are ignored or used incorrectly. Typically a situation, where a risk that the antenna parameters are

used incorrectly, occurs when the antenna is screwed onto a tap and the antenna ends up in oriented in an arbitrary direction. If the operator of the instrument do not check the orientation of the antenna and adjust the NGS antenna parameters into the correct direction, the software will introduce new errors when it is applying corrections for the antenna since these parameters are determined for an antenna which is orientated towards north.

To analyse how the result from the deformation monitoring software behaves when the antenna parameters are used incorrectly we use simulated observations. The observations are generated for a reference receiver and a rover receiver. The antenna at the reference receiver is correctly orientated towards north while the antenna at the rover receiver is incorrectly orientated towards the south direction. The antenna parameters for the rover antenna are generated by rotating the NGS-parameters towards south. This is quite simple since the only thing one needs to do is to switch signs of the parameters that correspond to the North and East components in the parameters. These values are highlighted with italic letters in Table 8. The observation files are generated for 100 epochs for each receiver. At the reference station an Ashtech Choke ring antenna model 701946.3 is used during the simulations and at the rover station is a Leica AT302 antenna used. The main reason that Ashtech antenna is used at the reference station is that it has very stabile values of the phase centre variations at different elevations. The size of these variations is only some tenth of a millimetre. The Leica antenna on the other hand has large variation in the PRV-values with a variation from 9 to -5.5 millimetres. Further this antenna have also a large ARP offsets in the north and east component which will influence the result when the antenna is orientated.

Table 8. NGS-antenna parameters for Ashtech 701946.3 and Leica AT302 antennas. The NE-offsets for the Leica Antenna is highlighted with italic letters. The template for the antenna parameters can be found in Table 4 in Section 4.2.4.2

```
ASH701946.3          D/M element,REV.3,chokerings,GPS+GLONASS NGS (  2) 99/09/02
        .6        .8     109.8
    .0   -.1   -.2   -.2   -.1   -.1    .0    .1    .2    .2
    .2    .2    .3    .2    .2    .1    .1    .0    .0
        .7       1.4     128.4
    .0   -.2   -.3   -.3   -.3   -.3   -.3   -.3   -.2   -.2
   -.2   -.3   -.3   -.3   -.2   -.2    .0    .0    .0

LEIAT302-GP          External micropulse L1/L2 -groundplane   NGS (  7) 98/06/01
      -2.2        .3      56.7
    .0    .0    .7   2.1   3.6   5.3   6.8   8.0   8.8   9.0
   8.7   7.8   6.2   4.0   1.2  -2.0  -5.5    .0    .0
        .2      -1.7      53.6
    .0  -1.1  -1.5  -1.5  -1.1   -.6    .0    .5    .9   1.0
    .9    .5   -.1  -1.0  -2.2  -3.5  -4.8    .0    .0
```

If observations are calculated in static mode in a post processing software, the baseline would have been calculated between the physical phase centres, that are constituted by the ARP in the antennas, since this is the mean value of all observations over a long time period. In kinematic mode is the situation a different, the coordinates are here determined directly for a mean phase centre for all the observations the actual epoch. This implies that the satellite geometry influences the estimated positions if no or incorrect antenna parameters are used.

The simulated observations are used in three different calculations. In the first calculation is the correct antenna parameters used. The result from this calculation can be found in Figure 17 where the difference between the true and the estimated coordinate is presented for each epoch. The difference between the known and the estimated coordinates are very close to zero, which indicates that the antenna parameters are correctly used.

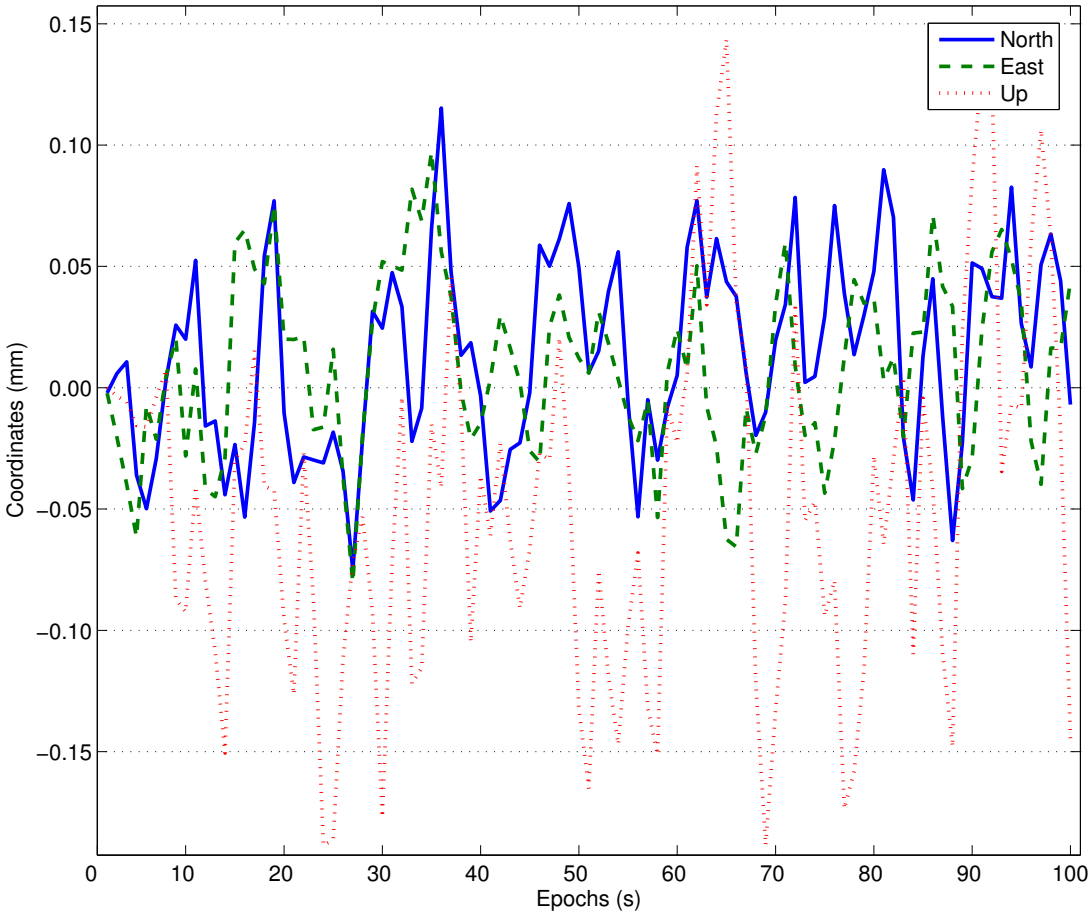

Figure 17. Results from calculations done with correct antenna parameters

In the next calculation we use antenna parameters directly from NGS without rotating them towards south as the case when the observations where generated. The result Figure 18 shows that there are some constant errors introduced on the estimated coordinates. The size of the constant errors is the double size of the horizontal ARP values of the incorrectly orientated Leica antenna, 4.4 millimetres in the North direction and 0.6 millimetres in the East direction. The result in the up direction is not influenced of the result since this component of the NGS parameters are not influenced when an antenna is rotated. The sudden jump in the coordinates at epoch 24 is related to ambiguity fixing. On the left side of the jump is the calculation done with a float solution and on the right side with fix solution.

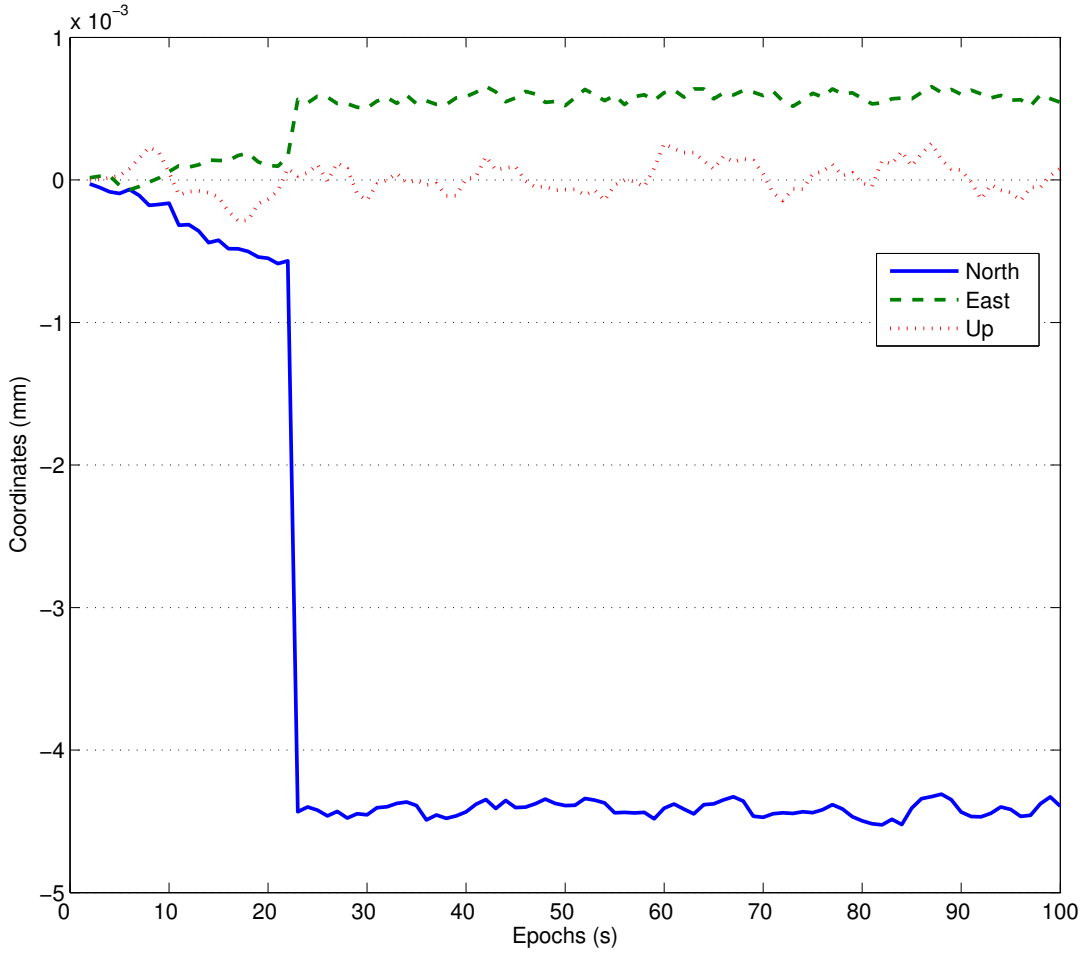

Figure 18. The result form calculations where with incorrectly orientated antenna at the rover receiver

The final calculation concerns the case where no antenna parameters are used at the rover receiver. In Figure 19 one can see the estimated coordinates as before. In this case, when no antenna model is used on the rover receiver, with an antenna orientated

south direction, the systematic error becomes much larger than in the previous cases. The change in the up direction corresponds quite well with the up parameter of the L1 frequency in the NGS parameters of the Leica antenna but the change in north and east direction is much larger than expected by looking on the North and East components of the antenna model. The size of these errors is also influenced of the PCV that are elevation dependent.

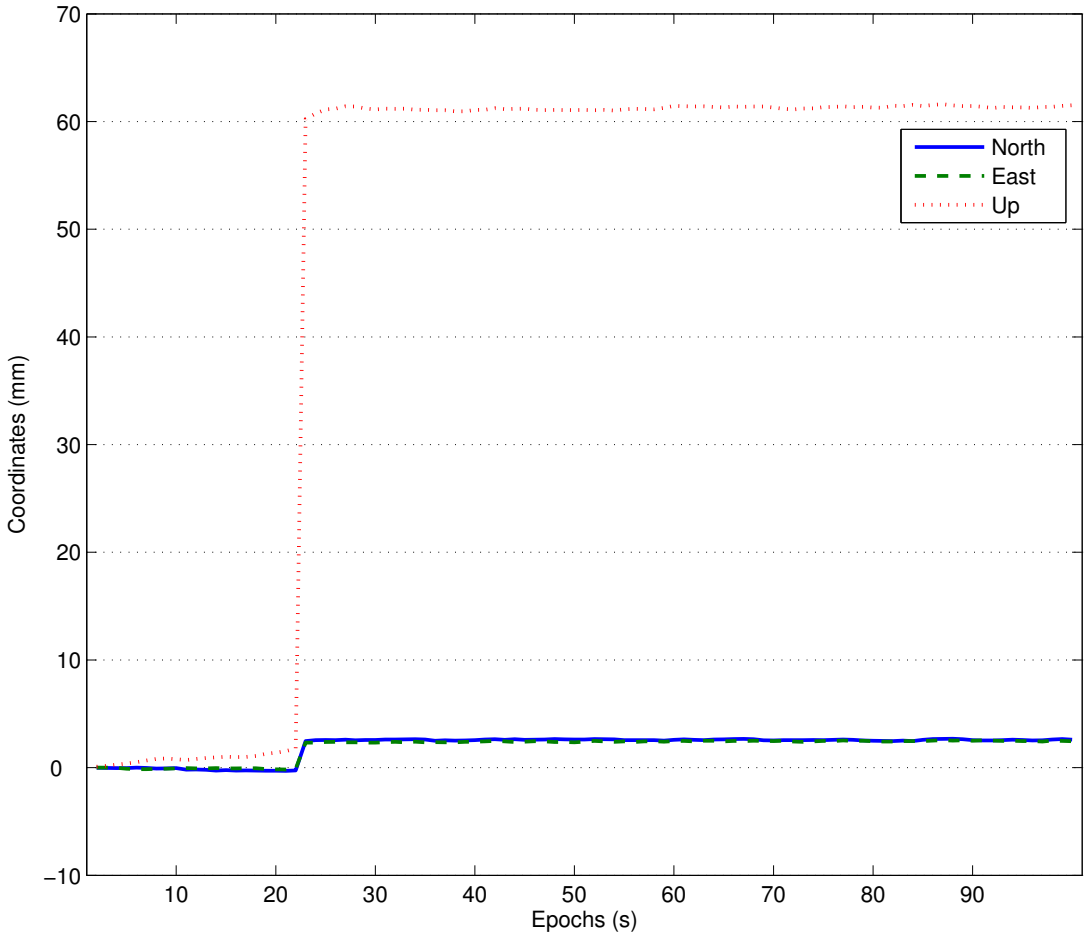

Figure 19. Result from a calculation without any antenna parameters at the rover receiver

To estimate the correct coordinates with the deformation monitoring software it is necessary to use the correct NGS-antenna parameters. Without them systematic errors introduced are with the size of several centimetres. From the result of these tests we can make the conclusion that it is better to use incorrectly oriented antenna parameters than no antenna parameters at all. If NGS-antenna parameters are used on an antenna, that are oriented in an incorrect direction the only error that will be introduced is a systematic error caused by the horizontal antenna offsets. This is true since the elevation dependent PCV corrections and the height offset are the same in all

directions, according to the NGS calibration, independent of the antenna orientation. This also means that, the only systematic error that are introduced, if incorrectly orientated antenna parameter is used during the calculations, is a horizontal offset, which do not influence the deformation monitoring performance, only the correctness of the estimated coordinates. On the other hand if no antenna parameters are used, not only the ARP offset will influence the result, the PCV corrections will also have an influence which is elevation dependent. The elevation dependency makes the estimated coordinates depending on the actual satellite configuration, which changes with time and the estimated coordinates will actually get an incorrect motion caused by the fact that no antenna parameters are used.

6.2 Tests on real observations

6.2.1 The observations

The idea with the field observations is to get a set of observations that corresponds to a possible deformation monitoring configuration where a set of reference receivers are placed a few kilometres away from the deformation site. To do this we have used two permanent reference receivers placed in Gothenburg that are established by the Swedish Road Administration, which along with the SWEPOS-network constitutes a geodetic network in the project Marieholmsförbindelsen. More information about this project can be found at the homepage of the Swedish Road Administration (www.vv.se). The Swedish National Land Survey, Lantmäteriet, is the esponsible administrator of the receivers, and it has determined the coordinates of the receivers by using observations spanning over three weeks. All observations from these reference receivers are stored in RINEX format both with an epoch interval of 1 and 15 seconds.

In total, the observations are collected with four receivers simultaneously; two of them are the permanent mounted references that are mounted on buildings. To separate them they are named HIS and BAG, which is the first three letters in the area where they are placed (Hisingsbacka and Bagaregården). The other two receivers are rover receivers, named ROV1 and ROV2. The reference receivers are Ashtech receivers used together with choke ring antennas, while the rover receivers are Trimble R7 receivers with Trimble Geodetic Zephyr antennas. The configuration of the receivers can be found in Figure 20.

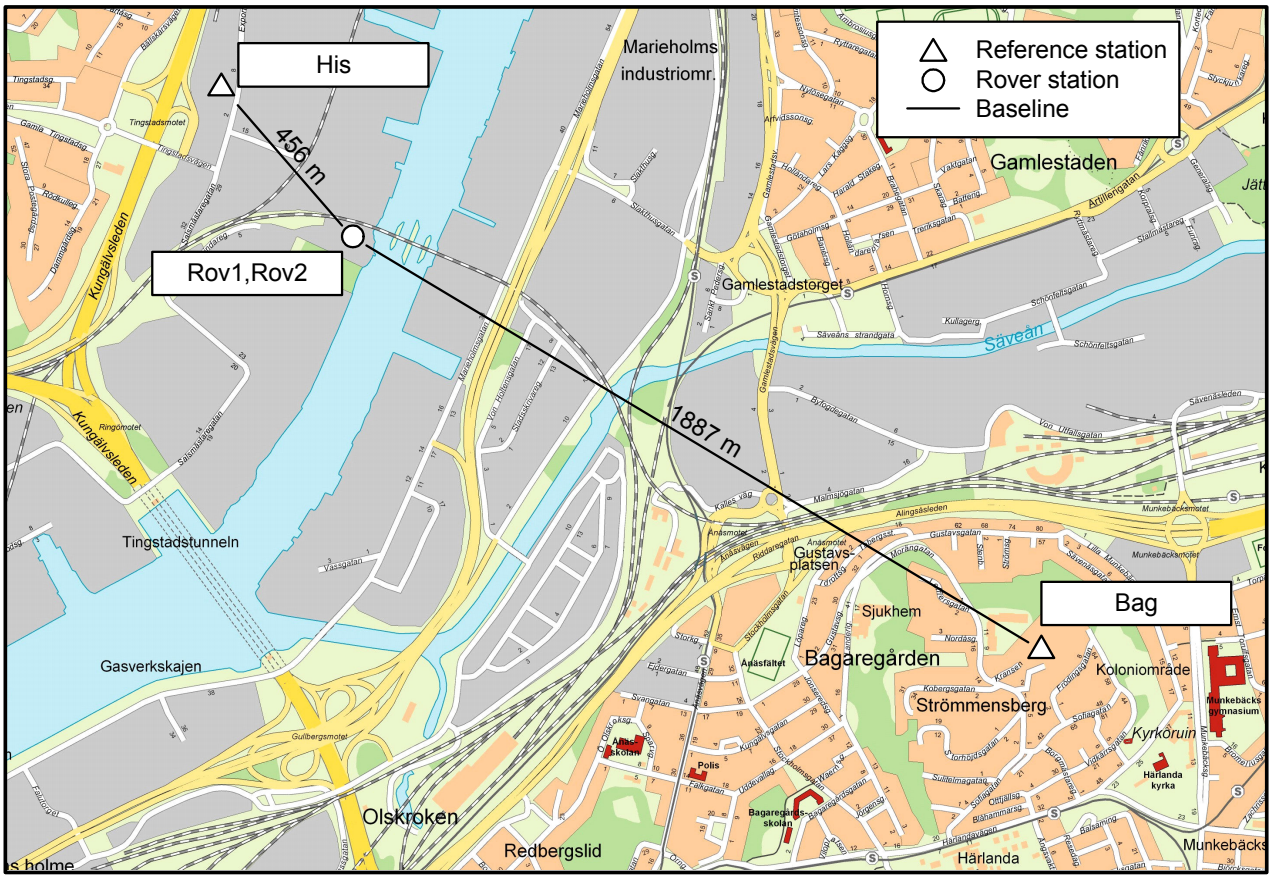

Figure 20. A map over the northern part of Gothenburg with receiver positions.

The rover receivers are placed only a few metres from each other during the tests; see Figure 21. The antenna of receiver ROV1 is held stable during all of the observations on top of a tripod while the antenna of ROV2 is used to simulate linear deformations. Its antenna is placed on top of a sliding platform, which is moved when deformations are simulated.

A compass was used to align the tripods in an approximate north-south direction. The sliding platform is oriented towards the other tripod. Finally, when the antennas are mounted on the tripods and rotated towards the geomagnetic north, the observations are started. When about 30 minutes have elapsed, the antenna on the sliding platform is moved rather fast towards the other end of the platform. On top of the sliding platform is a measuring rod, which is used to determine the true distance of motion of the antenna.

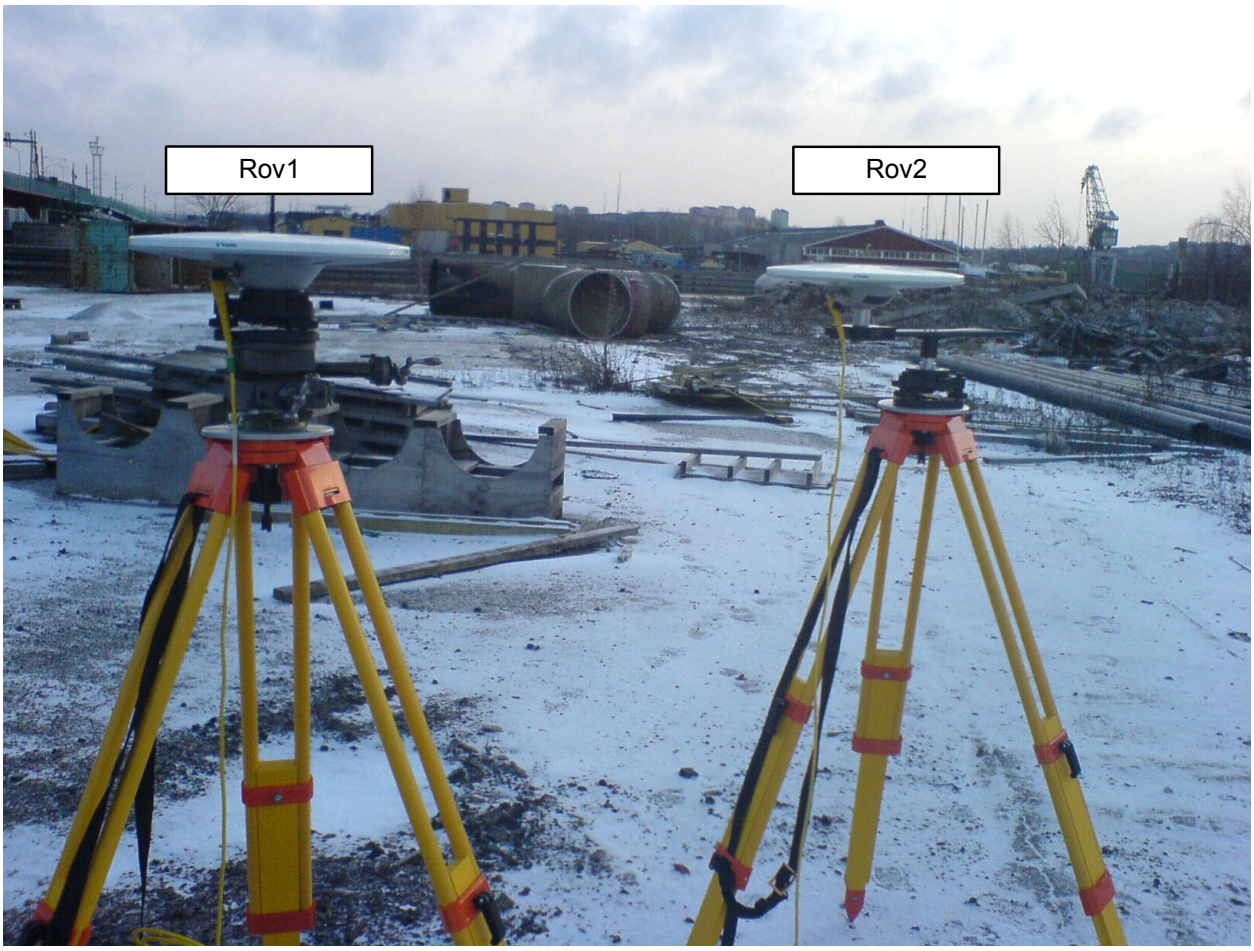

Figure 21. Picture of the rover receivers taken from west towards east.

6.3 Calculations with real observations

The idea with this section is to compare the result from conventional software, which performs calculations by combining observations in double differences, and our software, that performs the calculations with undifferenced observations. All computations are done in post-processing mode with the same observation set. The traditional software we use is Trimble Total Control (TTC) version 2.73 and SKI PRO version 3.0. A total number of four baselines are formed with the observations, each containing 600 epochs. We use the following names of the baselines: BAG-ROV1, BAG-ROV2, HIS-ROV1 and HIS-ROV2. The naming convention is simple by using the point names, first the reference station and then the rover station. Two different setups are tested, namely first static and then kinematic.

6.3.1 Static calculations

As mentioned before, ROV1 is held fix during the complete observation period, therefore we start the analyses on this dataset. The static calculations are done both in dual frequency mode and in single frequency mode. The minimum elevation angle is set to 10 degrees during the calculations. Antenna parameters are used during the

calculations and no weighting models are applied. Starting with dual frequency observations we get the results presented in Table 9 to 11. In each of the tables the coordinates of receiver ROV1 together with their standard deviations are shown.

Table 9. Estimated coordinates of point ROV1 in static mode calculated in TTC in dual frequency mode. All coordinates and standard deviations are given in WGS84

Baseline	X (m)	Y (m)	Z (m)	σ_X (mm)	σ_Y (mm)	σ_Z (mm)
HIS-ROV1	3339138.103	709216.281	5369727.785	1.1	1.0	1.4
BAG-ROV1	3339138.101	709216.280	5369727.790	1.4	1.3	1.7

Table 10. Estimated coordinates of point ROV1 in static mode calculated with Leica SKI PRO in dual frequency mode. All coordinates and standard deviations are given in WGS84

Baseline	X (m)	Y (m)	Z (m)	σ_X (mm)	σ_Y (mm)	σ_Z (mm)
HIS-ROV1	3339138.101	709216.278	5369727.785	0.1	0.1	0.1
BAG-ROV1	3339138.099	709216.277	5369727.784	0.1	0.1	0.2

Table 11. Estimated coordinates of point ROV1 in static mode calculated in undifferenced mode and with dual frequency. All coordinates and standard deviations are given in WGS84

Baseline	X (m)	Y (m)	Z (m)	σ_X (mm)	σ_Y (mm)	σ_Z (mm)
HIS-ROV1	3339138.104	709216.279	5369727.788	0.1	0.1	0.3
BAG-ROV1	3339138.109	709216.275	5369727.793	0.1	0.2	0.3

Comparing the results from the static dual frequency calculations, we can se that different softwares give different results. In general the undifferenced processing mode gives a slightly higher value on the X and Z coordinates than the commercial softwares. Exactly what this depends on can not be explained, since the commercial softwares works like black boxes. Thus, we can assume that variations in the estimated coordinates depend on, for example, that the softwares applies different weighting models to the observations or that different approach are used when modelling the troposphere. The standard deviations in SKI are generally lower than the standard deviations in our software which indicates that we do not model the deterministic and stochastic parameters as good as Leica does. In general the standard deviation is increased when the distance between the stations are increased.

The huge difference between the standard deviation in TTC and SKI (about 10 times higher) could depend on some multiplication constant but this is not confirmed with Trimble.

Table 12. Estimated coordinates of point ROV1 in static mode calculated with TTC in single frequency mode. All coordinates and standard deviations are given in WGS84

Baseline	X (m)	Y (m)	Z (m)	σ_X (mm)	σ_Y (mm)	σ_Z (mm)
HIS-ROV1	3339138.102	709216.278	5369727.785	1.4	1.3	1.6
BAG-ROV1	3339138.101	709216.278	5369727.787	1.5	1.5	1.8

Table 13. Estimated coordinates of point ROV1 in static mode calculated with Leica SKI PRO in single frequency mode. All coordinates and standard deviations are given in WGS84

Baseline	X (m)	Y (m)	Z (m)	σ_X (mm)	σ_Y (mm)	σ_Z (mm)
HIS-ROV1	3339138.101	709216.279	5369727.786	0.1	0.1	0.2
BAG-ROV1	3339138.099	709216.278	5369727.786	0.2	0.1	0.2

Table 14. Estimated coordinates of point ROV1 in static mode calculated in undifferenced mode in single frequency mode. All coordinates and standard deviations are given in WGS84

Baseline	X (m)	Y (m)	Z (m)	σ_X (mm)	σ_Y (mm)	σ_Z (mm)
HIS-ROV1	3339138.105	709216.279	5369727.788	0.2	0.1	0.3
BAG-ROV1	3339138.110	709216.275	5369727.794	0.2	0.2	0.3

For single frequency the results for the prior dual frequency calculations are repeated. The result from the undifferenced approach is slightly different than the one given by the conventional softwares. The overall standard deviations are increased, compared with the dual frequency calculations above, since fewer observations are used.
Troposphere modelling is rather complicated in the case when large height differences occur between the reference and rover stations at the receivers. Schön et al. (2005) discussed this problem and presented a solution for double difference calculations, where several reference receivers are placed at different heights around the rover stations to determine the troposphere at the rover station. In the GPS network in Gothenburg, where we performed our tests, there are quite large height differences between the reference stations and the rover station. The rover station is placed approximately 39 metres over the WGS84 ellipsoid which gives a height difference to

the reference stations of approximately 24 metres for the short baseline and 79 metres on the long baseline. To study if the height difference influences the result during the coordinate estimations we have simulated observations for two baselines. The receivers of the first baseline are placed on the same height over the ellipsoid and in the second baseline is a height difference of 100 metres used. As in the case where the influence of the antenna parameters where studied, no additional errors where added to the observations during the simulations. When calculating the baselines in TTC we found that correct coordinates where estimated when the points where placed on the same height above the ellipsoid and when a height difference where introduced the same type of offsets occur as we found in the coordinates in

Table 11 and 14, above. If the same baselines are calculated in our software, which is based on undifferenced observations, the correct coordinates are estimated. Thus, we do not use the same tropospheric algorithm as is used in TTC or Leica SKI PRO, and therefore we get other coordinates during the static calculations. This is a case that we have to study more in detail in our further development of our deformation monitoring software.

6.3.2 Kinematic calculations

Now we continue to study the result from the kinematic solution. This is done with the same datasets as in the static calculations, and the calculations are performed both in a commercial and in our own software. Estimated coordinates are compared with the statically calculated coordinates that are determined with the same setups, i.e. the estimated coordinates in kinematic mode that are determined in TTC are compared with the static coordinates from the same software. This is the only fair way to compare the performance of the softwares, since the troposphere is treated differently from software to software, as described previous. We do not study the coordinates itself but instead the difference between coordinates that are transformed into geocentric coordinates with the origin of the coordinates in the static solution. The standards deviation for each kinematic dataset are also calculated and presented in the following sections.

Several different settings are tested in both single and dual frequency mode to see how the result is influenced by the different setups. During the calculations the minimum elevation angle is set either to 10 or 15 degrees. In theory, the result should improve when the lower elevation limit is used, since that more satellites become available. The problem with this approach is that the observations at low elevation angles will be more noisy then the other observations to satellites at higher elevation angles. To compensate for the noise level for these observations the weighting models are presented in Section 6.3.3 are applied in the adjustment.

6.3.2.1 Kinematic results calculated with Trimble Total Control

As a reference for our calculation a conventional software is used to estimate coordinates in kinematic mode. The estimated coordinates are compared with the corresponding static coordinates determined with the same software. The result from these calculations can be found in Table 15. The coordinate differences are given in millimetres between the geocentric coordinates of the static solution and the mean value of the kinematic solution. Also standard deviations are given for the kinematic solution.

Table 15. Coordinate differences between the mean values of the kinematic and the static coordinates together with the standard deviations of the kinematic coordinates

Baseline	Elev.	Type	Mean Value (mm)			STD (mm)		
	(deg)		N	E	U	N	E	U
HIS-ROV1	15	SF	-1.595	-1.386	3.929	2.9	2.0	3.8
HIS-ROV1	10	SF	-0.911	-1.266	3.082	2.8	2.1	3.6
BAG-ROV1	15	SF	-1.653	-0.279	6.167	3.2	4.0	3.9
BAG-ROV1	10	SF	-1.441	-0.229	5.956	3.0	3.8	3.6

As can be seen in this solution, the difference between the static and the kinematic solution is within 1.5 millimetre in the North and East components, but in the Up component the deviation is larger (up to 6 millimetre) on the longest baseline between BAG and ROV1. In general the standard deviations are lower when observations are measured down to an elevation angle of 10 degrees. This is quite obvious, since more observations are accessible when more satellites are above the minimum elevation angle. A disadvantage with the observations at low elevation angles is that their noise level is higher. To overcome this problem one can by apply weighting models, as them introduced in Section 3.3.3. This is probably performed in the kinematic calculation procedure in TTC.

The calculated coordinates that are used to estimate the mean value and standard deviation for the baseline BAG-ROV1, with 10 degree elevation angle, are plotted in Figure 22.

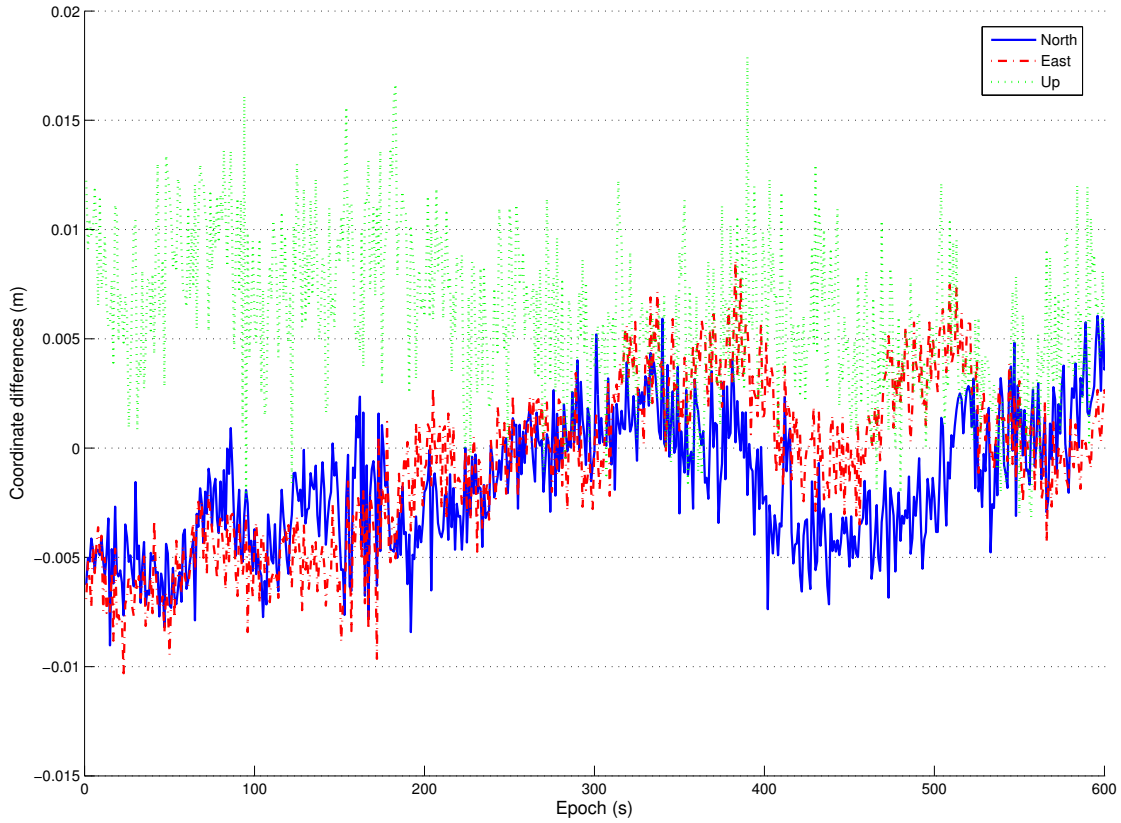

Figure 22. Coordinate differences between the static and kinematic coordinates calculated in TTC for baseline BAG-ROV1.

If we compare the mean values of the kinematic coordinates, given in Table 16, they are closer to the static solution calculated with the undifferenced software, given in Table 14, than the solution that are given by TTC.

Table 16. Mean values of the estimated coordinates from the kinematic solution calculated in TTC. All coordinates are given in WGS84

Baseline	Elev.	Type	X	Y	Z
HIS-ROV1	15	SF	3339138.1047	709216.2783	5369727.7873
HIS-ROV1	10	SF	3339138.1036	709216.2782	5369727.7870
BAG-ROV1	15	SF	3339138.1062	709216.2782	5369727.7913
BAG-ROV1	10	SF	3339138.1058	709216.2783	5369727.7912

This indicates that TTC uses different models for the troposphere in static and kinematic calculations and the one used in kinematic mode could be the same that we are using in our software. No further investigations are done within this subject.

6.3.2.2 Undifferenced GPS in kinematic mode

The kinematic calculations with our undifferenced software start with the short baseline between the stations HIS and ROV1. Calculations are done in both single and dual frequency mode. The lowest elevation angle is set to 10 and 15 degrees. Figure 23 yields a typical result from a kinematic solution. The initial coordinates in the initialisation file is set to the known coordinates, from the static solution, to "help" the software a little bit so that the ambiguity can be solved quicker. This is not necessary in a real setup; navigated coordinates will do, since the solution in the software will converge to the correct coordinates during time and the ambiguities can be fixed. It will however take some more time than in the actual case when the correct coordinates are used as initial coordinates.

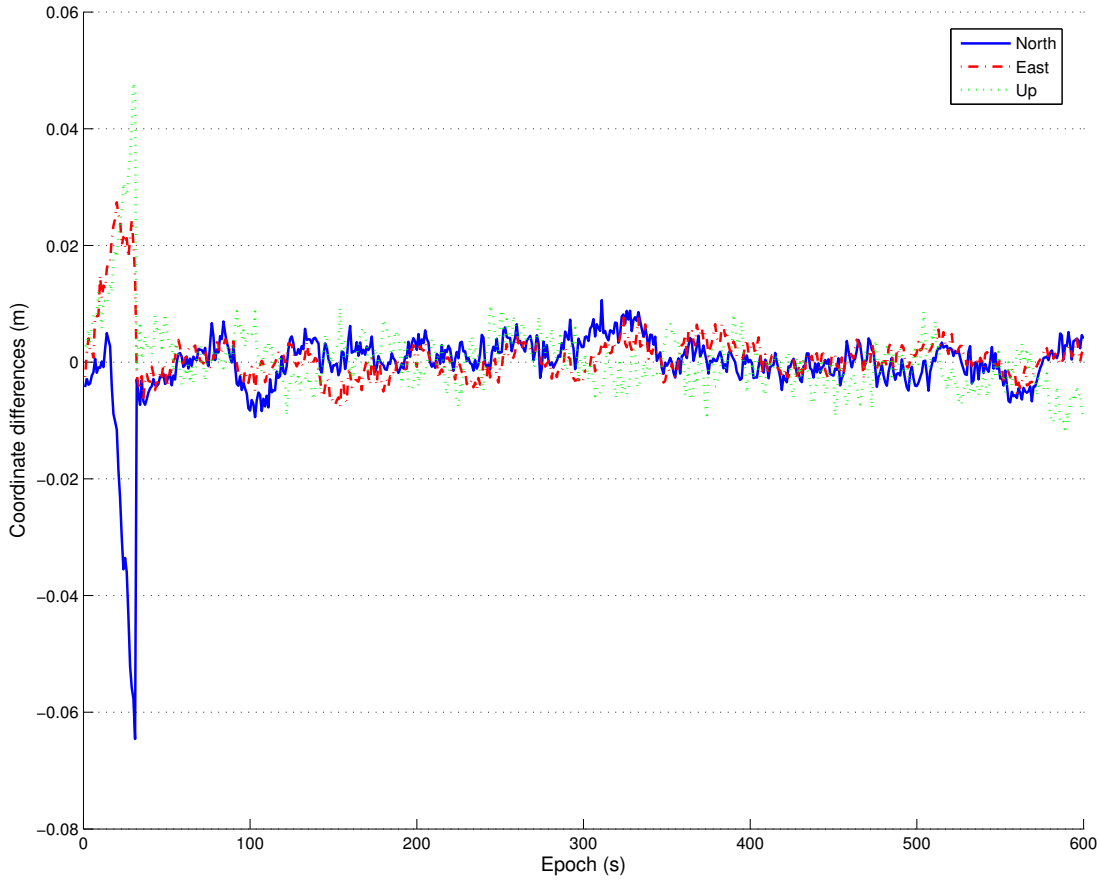

Figure 23. Coordinate differences calculated in undifferenced solution with a 15 degrees elevation limit and single frequency mode

At epoch 30, the ambiguities are fixed in all of the following figures. This can be seen in the coordinate difference plot, Figure 23, when the solution makes a quick jump towards the correct solution. When the ambiguities are fixed, the solution starts to wander back and fourth over the correct solution. This pattern is probably caused by

the multipath or some other none or incorrectly modelled parameter that influences the observations. All estimated coordinate after the ambiguity fixing are used to determine the mean value and the standard deviation for the kinematic solution. The difference between the coordinates calculated in the static solution and the kinematic solution are presented in Table 17. The standard deviations are again lower when the elevation limit is set to 10 degrees; this holds as well for single and dual frequency.

Table 17. Coordinate differences between the mean value of the kinematic and the static coordinates together with the standard deviation of the kinematic coordinates calculated in undifferenced mode

Baseline	Elev.	Type	Mean Value (mm)			STD (mm)		
	(deg)		N	E	U	N	E	U
HIS-ROV1	15	SF	0.5	0.3	-0.4	3.2	2.6	3.9
HIS-ROV1	10	SF	0.0	0.3	0.4	3.7	3.2	3.8
HIS-ROV1	15	DF	-1.3	-0.6	1.5	2.7	1.9	3.6
HIS-ROV1	10	DF	-0.5	-0.4	0.1	2.9	2.2	4.0

It is beneficial to lower the elevation angle, but it also introduces problems as increased observation noise.

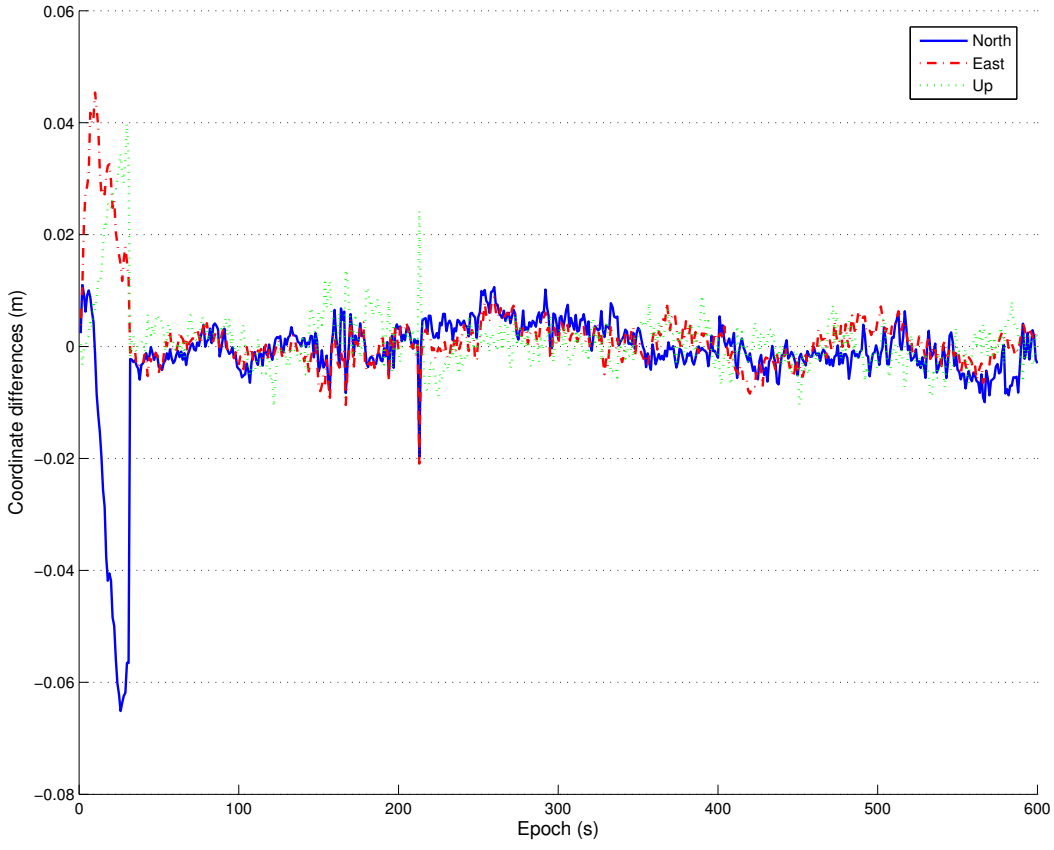

Figure 24. Coordinate difference calculated undifferenced solution of baseline HIS-ROV1, elevation angle 10 degrees, and single frequency

In Figure 24, the differences between the static and the kinematic coordinates, calculated in single frequency, are plotted but now for a minimum elevation angle of 10 degrees. Comparing this figure with the previous, one can observe that the estimated coordinates are more "noisy" between epoch 130 and 230, and that there is a high "spike" at epoch 212. This noisy part of the estimations originates from the fact that the signal to one of the satellites at receiver B is not stabile. The signal appears and disappears with a high frequency, probably caused by some tree at the observation site. Another indication that the signal to this satellite is poor is the C/No value, which is very low for this satellite.

Returning to Table 17 and comparing the standard deviations in single and dual frequency mode, the standard deviations are in general lower in the dual frequency, but the offsets of the mean values are in general larger for these solutions than in single frequency mode.

The same baseline as in Figure 23 and 24 is found in Figure 25, here calculated in dual frequency mode and the outcome from the 10 degree elevation limit. The larger amount of observations calms down the noisy part, compared to the single frequency mode presented in Figure 24, i.e. the spike at epoch 212 is completely removed.

Now we continue with the longer baseline and do exactly the same calculations as for the previous baseline. The result can be found in Table 18, below.

Table 18. Baseline HIS-ROV1 mean values and standard deviation (STD) of the difference between coordinates calculated in kinematic mode and static mode, presented in local horizontal coordinates. The calculations are performed at both 10 and 15 degrees elevation angle and in single frequency (SF) and dual frequency (DF) mode.

Baseline	Elev.	Type	Mean Value (mm)			STD (mm)		
	(deg)		N	E	U	N	E	U
BAG-ROV1	15	SF	-	-	-	-	-	-
BAG-ROV1	10	SF	0.1	0.6	0.7	3.4	3.3	4.3
BAG-ROV1	15	DF	1.2	-0.6	-0.0	2.3	2.6	2.6
BAG-ROV1	10	DF	1.3	-1.0	-0.4	2.8	2.6	3.2

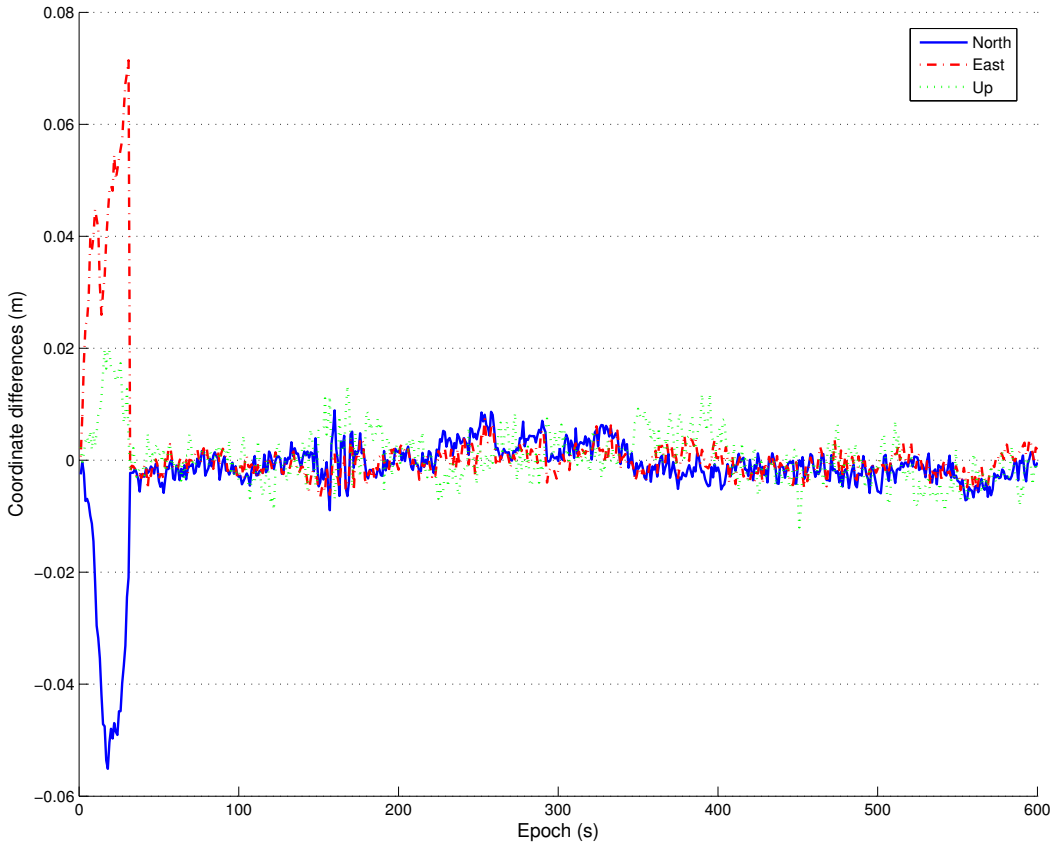

Figure 25. The noisy part is slightly smoothed when dual frequency observations are used. In the figure are the coordinate differences of baseline HIS-ROV1 calculated in dual frequency mode with a 10 degree elevation limit

The undifferenced software did not manage to solve the correct coordinates in single frequency mode when the elevation angle where set to 15 degrees. The geometric precision of dilution value (GDOP) is about 2.5 for the complete set of observations, so it is nothing wrong with the geometry of the 5 available satellites but one of the satellites have a little bit lower C/No value than the other which could result in the incorrect solution. The solution can be found in Figure 26.

The standard deviations in Table 18 do not follow the same pattern as in the former short baseline. Here the standard deviation increases when satellites at lower elevation angles are included. A possible explanation to this result is that the C/No values are very weak for some satellites, which can be seen in Figure 27. Values below 30 dB are normally considered as weak, and in software like TTC these values are removed. Further when studying the C/No plot below one finds that the C/No value sometimes are zero, which indicates that the satellite is lost during the observations. So the number of dual frequency observations is not constant during time and the solution becomes during these times a combination of single and dual frequency observations. The standard deviations in the single frequency calculations are higher than in the dual

frequency, so involving the single frequency observations in the dual frequency solution will in this case introduce some additional errors to the solution.

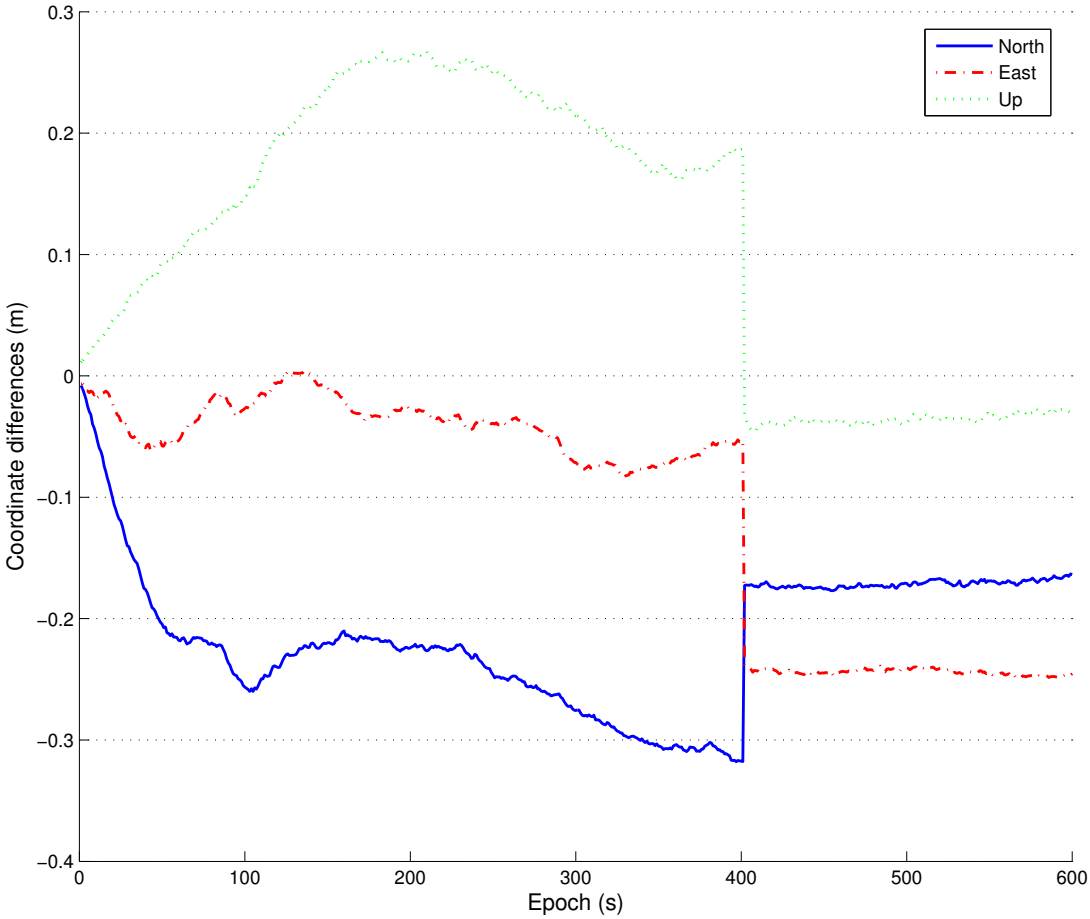

Figure 26. Coordinate differences, baseline BAG-ROV1 calculated in single frequency mode with a 15 degree elevation limit. At epoch 400 the incorrect values of the ambiguity are fixed which results in incorrectly estimated coordinates

Now it is also possible to compare the result from the conventional software TTC and our undifferenced software by comparing the results in Table 15, 17 and 18. In general, the differences between the static solution and the mean values of the kinematic coordinates are smaller in our undifferenced solution, but the standard deviation values, are about 1 mm in all the components independent of whether the single or dual frequency solutions are used. Still we do not know how TTC computes the kinematic coordinates. We do not know if the software applies some weights to the solution or if the solution is smoothed with some kind of filter. We can assume that it uses the complete dataset to solve the ambiguities and to detect cycle slips. This can not be

performed in real-time applications but what we can do is to apply weights to the observations. This is tested in the following section to see if we can improve our result.

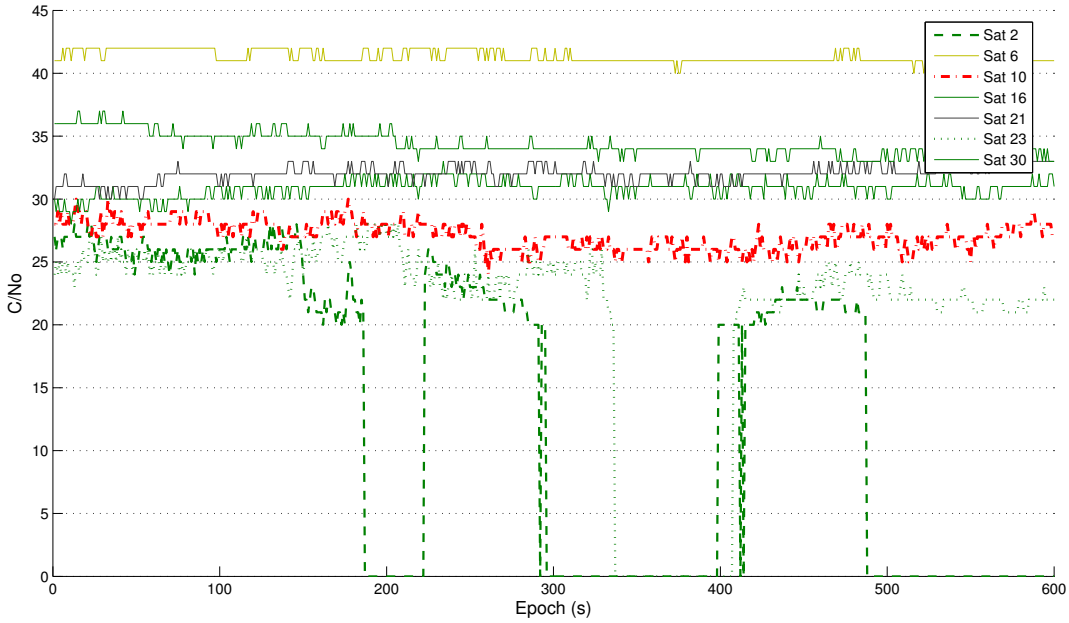

Figure 27. C/No plot for the L2 observations on the ROV1 receiver. The bold lines indicates observations which are below the 30 dB C/No value

6.3.3 Different weighting procedures

The undifferenced solution is sensitive to the number of satellites. To increase the number of satellites one can lower the elevation limit. A problem that then occurs is that noisier observations are included into the filter. Furthermore, the difference in noise between the observations increases and observation weighting becomes necessary. In Section 3.3.3 some different weighting models are presented, and we are going to study the performance of three of them in this section. The equal weighting approach is already used earlier in this chapter. The other two weighting models are the elevation based model presented by Wieser and Gaggl (2005) found in Eq.(124) and the C/No based model presented by Hartinger and Brunner (1999) in Eq.(125).

There is a problem when implementing the last two weight models, which we have ignored in the current phase in the software development. These weighting models are designed for dual frequency observations, and there are some coefficients in each model that are supposed to be estimated with the double difference residuals in a least squares sense. To estimate the coefficients reliably one must use a long observation time, so that observations to all possible elevation angles and all signal to noise levels are covered. This means that at least 24 hours of observations are recommended. Our problem is that the software that we have developed in Matlab is quite time consuming and therefore no observation weights are estimated. Instead we use default values that

are based on the standard accuracy of phase observations that are described in the beginning of Section 3.3.3 as the coefficients in the elevation dependent weighting models. These values seem to correspond to the true values when shorter observation times are used to estimate the coefficients. In the signal to noise dependent weighting models introduced as the sigma-e model by Hartinger and Brunner (1999) we use their estimated value of the variable a_1 ($1.61 \cdot 10^{-4} m^2$). The coefficient a_0 is set to zero just as they did. The results from the weighting procedures are presented in Table 19, where weighting model 1 is equal weighting, model 2 the elevation based weighting and model 3 is based on the C/No values. The calculations are made in both single and dual frequency mode, and the elevation limit is set to 10 degrees.

Table 19. Different weighting models are applied in the kinematic calculations of the baselines. Model 1 is equal weighting, model 2 elevation dependent weighting and model 3 is C/No based weighting

Baseline	Weight	Type	Mean Value (mm)			STD (mm)		
	Model		N	E	U	N	E	U
HIS-ROV1	1	SF	0.0	0.3	0.4	3.7	3.2	3.8
HIS-ROV1	2	SF	-0.1	0.4	-0.2	3.9	2.6	3.9
HIS-ROV1	3	SF	0.2	0.3	-0.1	3.3	2.8	3.4
HIS-ROV1	1	DF	-0.5	-0.4	0.1	2.9	2.2	4.0
HIS-ROV1	2	DF	-0.4	0.3	-0.4	3.6	2.7	3.8
HIS-ROV1	3	DF	-0.4	0.1	-0.4	2.8	2.4	3.5
BAG-ROV1	1	SF	0.0	0.6	0.7	3.4	3.3	4.3
BAG-ROV1	2	SF	1.1	1.0	0.2	2.9	3.4	3.2
BAG-ROV1	3	SF	1.6	-0.8	-1.7	2.8	2.6	3.2
BAG-ROV1	1	DF	1.3	-1.0	-0.4	2.8	2.6	3.2
BAG-ROV1	2	DF	1.3	-0.3	0.1	2.6	3.2	2.1
BAG-ROV1	3	DF	0.0	0.6	1.5	3.3	3.7	3.4

More or less generally one can say that the C/No based weighting approach gives the best result in the single frequency (SF) calculations. There are some exceptions, take as an example the standard deviation value of the east component of the baseline HIS-ROV1, where the best weighting procedure are given by the second weighting model. But if the complete sets of standard deviations in all the components are treated we get a different result where the C/No based weighting procedure gives the best result.

In the dual frequency mode, the results are not that convincing as in the single frequency mode. Here the C/No weighting procedure gives the worst result even worse than the equal weighting procedure.

With the result from these tests, one can conclude that there is a great potential in improving the result by applying weights to the observations. This is especially obvious in the single frequency mode where the standard deviation became lower by applying

weights. The mixed result in the dual frequency mode is likely due to the parameters that are used in the weighting functions, which not are estimated correctly. With a long set of observations, one could determine a better value for this constant, but as mentioned before, we do not have the options to calculate these observations yet.

Interesting to see is that the noisy part in Figure 24 is removed when using the C/No weighting; see Figure 28, below.

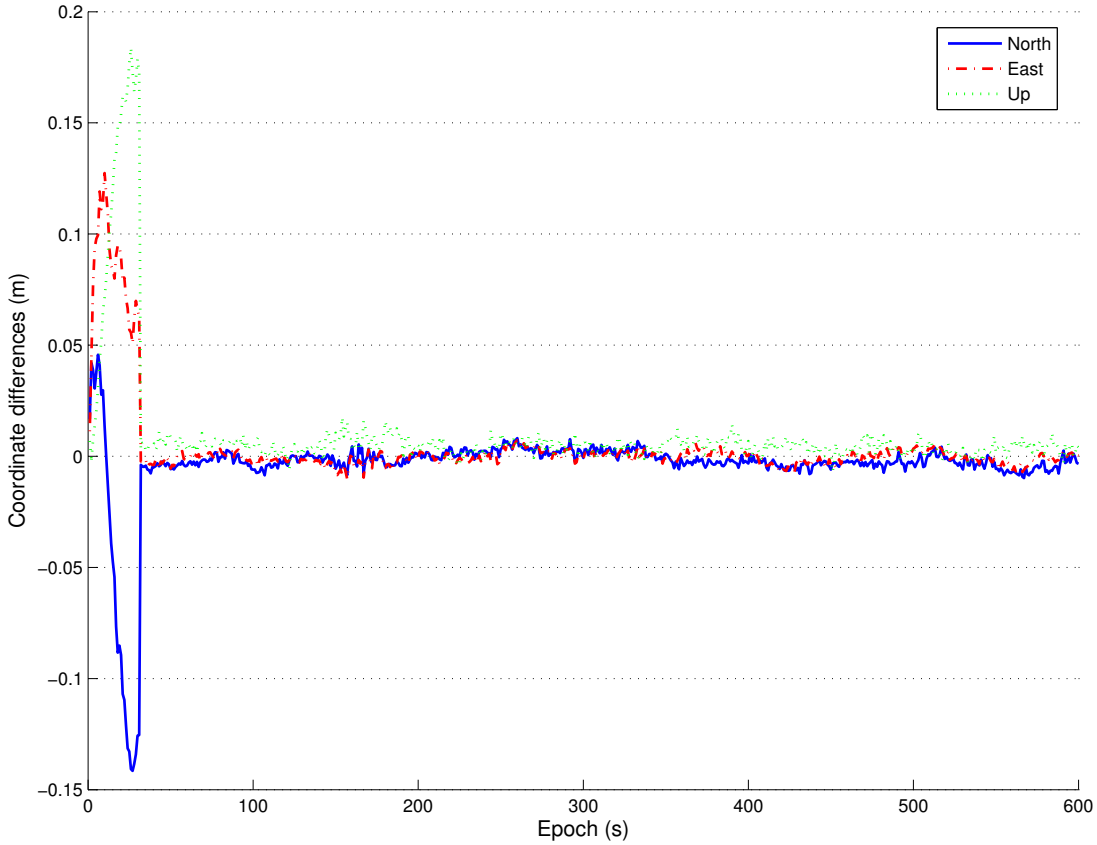

Figure 28. Coordinate differences calculated undifferenced solution of baseline HIS-ROV1, elevation angle 10 degrees, single frequency and C/No weighting according to Hartinger and Brunner (1999)

The improvements that are seen in these initial tests with weighting of observations indicate that there are great potentials left to improve the result in the undifferenced approach.

6.3.4 Deformation detection with real observations

To verify that it is possible to detect deformations with the developed software, the deformations are generated by simply moving an antenna at a rover station linearly a known distance. This is done at rover station ROV2 during the field observations in Gothenburg. As described before in the presentation of the observations, the antenna of

ROV2 is placed on top of a sliding platform, which is used to generate a deformation. The deformation was generated at epoch 393 by moving the antenna horizontally 0.360 metres towards south on the sliding platform.

Calculations of the observations are performed in the undifferenced software in dual frequency mode with a 10 degree elevation limit and with equal weighting and in TTC. The result can be found in Figure 29, the epoch with the deformation is well marked since the coordinate's changes in this epoch. One can assume that only the north coordinates would change during the deformations but there is also a small deformation in the easting component. This deformation depends on the fact that the sliding platform was not set up exactly in a north-south direction.

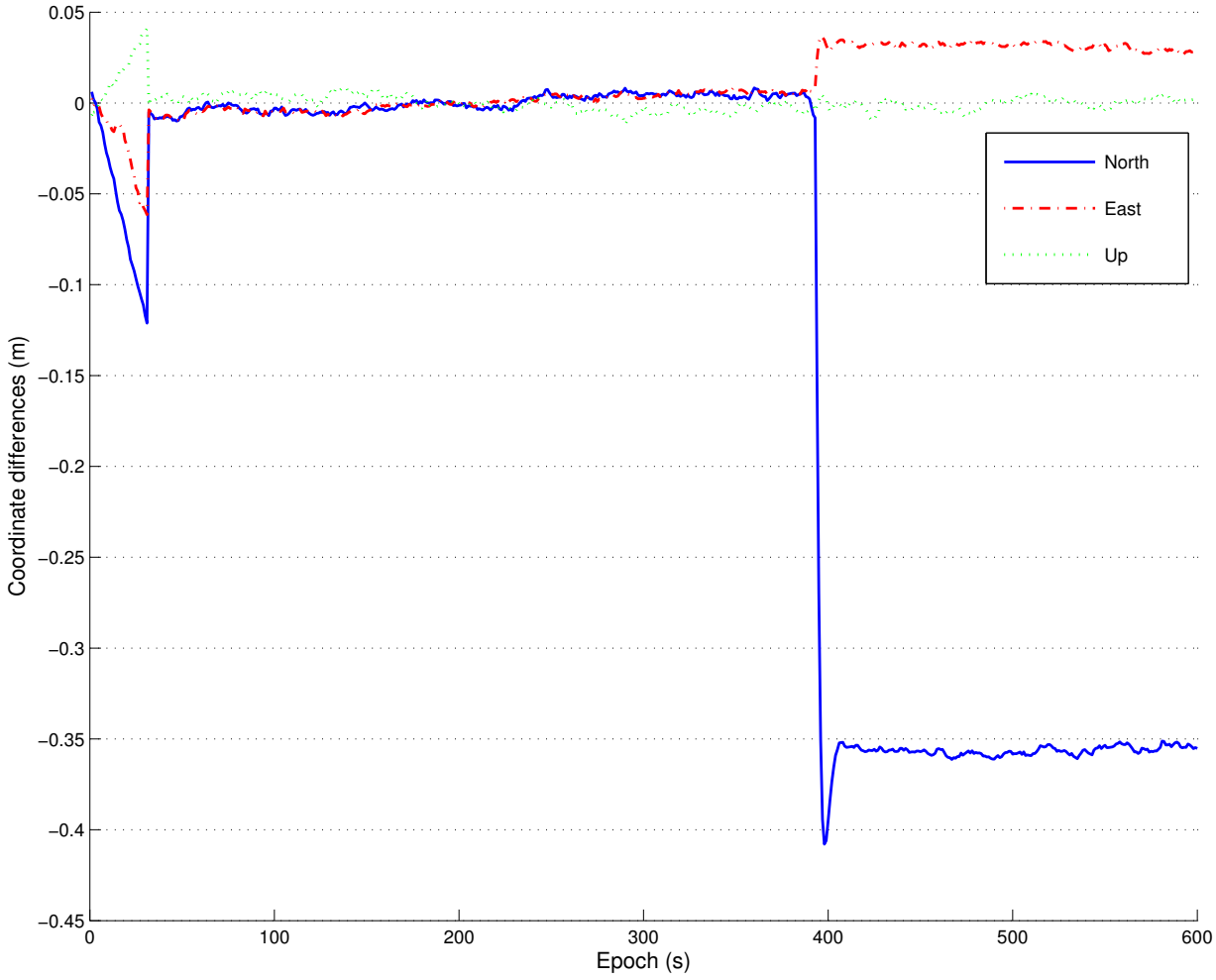

Figure 29. Result from the generated deformations, baseline HIS-ROV2

Comparing this result with the result that we got when the simulated observations were used, we see the same pattern. There will be a lag in the coordinate estimations after the deformation which, depends on the value of the PSD-acceleration value.

If the mean value of the coordinates is determined from the kinematic solution before and after the deformation one can determine the size of the deformation to 0.361 metres. This is the same value that we get if the size of the deformation is calculated in TTC. The only difference between these two solutions is that there is no lag directly after the deformation caused by the Kalman filter in the TTC solution, since no Kalman filter is applied in this solution. The result from this test shows that the undifferenced approach will work in deformation monitoring purposes.

7 Summary, Conclusions and Further Research

7.1 Summary and Conclusions

There are several possible surveying methods to measure movements and detect deformations, both absolute and relative ones. The relative methods detect the deformations without relating the observations to some fix object outside the actual monitored object. In the absolute methods at least one measuring device is placed at a fix point outside the moving area.

Among the relative methods, deformation monitoring systems based on GPS observations are good alternatives since, they provide the opportunity to measure with high precision and over long distances without the condition that there must be a line of sight between the reference point and the moving objects.

Traditionally, monitoring systems based on GPS observations are based on algorithms that create double differences in the observation equations. Double differences remove all parameters related to the satellite and receiver clocks each at epoch and the singularity in the observation equations is also removed, other error sources are typically reduced. This is a good result but, it will not come without some disadvantages. Correlations are introduced among the double differences since they are combinations of four observations, recorded at two stations towards two satellites. The situation becomes even more complicated when more than one reference station is used. These introduced correlations are difficult to model correctly, and they are therefore often ignored within traditional GPS calculations based on double differences.

In this thesis an alternative method is introduced based on undifferenced GPS-observations. The method is mathematically based on a state space approach, where the correlation in time for each parameter is used instead of eliminating the parameters as in the previous case. This is done in a Kalman filter, where all unknown parameters are estimated together at each epoch. The benefit with the method is that no correlations are introduced into the observations, and that most of the estimated parameters are the true parameters and not parameters that are combinations of several parameters as in the case when double differences are used. The main problem with the methods is that all parameters must be modelled correctly. If not, biases will be introduced in the other modelled parameters caused by the unmodelled parameters. In the undifferenced approach it is easy to add additional reference receivers without having the problem with correlations that occurred when double differences were used.

Our hypothesis in this thesis is that we assume that one can estimate the coordinates in real-time based on the undifferenced algorithm with the same precision or better than in the traditional algorithms based on double differences. The main argument that we base our hypothesis on is the fact that we use the correlation in time for all unknown parameters instead of eliminating them and that all correlations between the epochs are used in the estimation.

To evaluate the hypothesis, we have developed a post processing software in Matlab. The software is designed so that it easily can be transformed into a real-time application in the future. The Kalman filter is presented in Chapter 3 together with all deterministic models for the unknown parameters in the filter. Two new algorithms are also introduced in this chapter. One algorithm that unifies the calculation of satellites coordinates for precise and broadcast ephemerides are presented developed by Horemuz and Andersson (2006). The other new algorithm is generated to adopt the NGS-antenna parameters so that it can be used on an antenna that is rotated in an arbitrary direction. This algorithm seems to be very useful in engineering applications.

In Chapter, 4, the implementation details of the software are described. Traditional cycle slip detection algorithms are presented as well as the Lambda method, which is used for the phase ambiguity fixing. Several different observation weighting procedures are also introduced in this chapter based on the quality indicators as the elevation angle and the C/No value that are available from the instruments.

A simulator to generate observations is developed to perform debugging and tests in a known environment. All unknown parameters that are estimated in the state vector of the Kalman filter are included in the simulator, which is described in Chapter 5.

In Chapter 6 the result from different tests are presented. The tests are performed with both simulated and real observations. The real observations are calculated both in our own developed software and the commercial software as Trimble Total Control and Leica SKI PRO. The first tests where performed with simulated observations to study the deformation monitoring performance of the developed software and to analyse the influence of the antenna parameters and influence of incorrectly orientated antennas.

The results from these tests prove that the undifferenced software is suitable for deformation monitoring, and it is necessary to use correctly orientated antenna parameters if the true coordinates of the physical centre is wanted. The results from the tests with real observations and generated deformations show that comparable results are achieved with our software as in the conventional software Trimble Total Control (TTC).

From the observations with the generated deformation we conclude that a deformation can be found by studying the change in the coordinates or the velocity. A deformation occurs distinctly in coordinate estimates as a jump from one stable coordinate to another. In the velocity estimates the corresponding deformations can be found as a sudden spike. Here is a potential research area in the future, to develop an algorithm that identifies deformations based on the output from the software in a real-time.

In the second investigation with simulated observations the algorithm to modify the NGS-antenna parameters was tested. In the simulator with where observations generated with incorrectly orientated antennas. These observations where then used to calculate coordinates, without and with antenna parameters which was modified and unmodified according to the presented algorithm. The result showed that if no antenna model is used then the estimated position is displaced with several centimetres. If incorrect orientated antenna parameters are used then are coordinates incorrect only in the horizontal direction, and, finally, if the correct antenna parameters were used then the correct coordinates are estimated. These tests show how the importance of using the correct antenna parameters.

To get an indication of the performance of the software, we use real observations, and we compute them both in our and in conventional softwares. The calculations are performed in both static and kinematic mode. The real observations contain 600 epochs are recorded with 1 second intervals. The result from the static calculations showed that the coordinate differences between our and the conventional softwares differenced a few millimetres, especially in the X and Z component (WGS 84). We concluded that one reason for this difference could be different modelling of the troposphere or depending on the weighting procedures. In general it is rather difficult to model the influence of the troposphere if the height difference between the stations is large. In our case is the height difference about 89 metres. This is why we assume that the troposphere is the reason to the coordinate differences. Here we got another potential work in the future, to study different tropospheric models and different optimal setups of the reference receivers to be able to estimate the correct troposphere.

The results in kinematic mode have been compared by the same method as the static. Kinematic coordinates were calculated in both conventional and the undifferenced software. The mean values of all kinematic solutions are compared with the static result from the corresponding static solution.

Surprisingly large difference occur between the static and the kinematic solution when the conventional software where used. It is obvious, that the algorithms are different. It is again especially the height components that differ from the traditional solution. Again we suspect that the troposphere or the weighting procedures causes these offsets.

When comparing the same solutions in the undifferenced mode, the differences are much smaller. The reason to this is that the solutions both are based on the same algorithms and therefore are approximately the same result achieved.

The accuracy in the undifferenced software is not yet optimal. This is clear when the result from the conventional software were compared with the undifferenced solution. The standard deviation is about 1 mm higher in all components in the undifferenced solution, but one should notice that this solution corresponds to the solution that one gets in a real-time application. We do not know exactly, but one can assume that the conventional software uses the complete dataset in some kind of pre processing when the kinematic calculations are performed which is not possible in a real-time application, where observations are only available up to the last epoch.

During the kinematic calculations a problem occurred. In one of the baselines the undifferenced software did not find the correct phase ambiguities, which lead to incorrectly estimated coordinates. This is a situation that obviously can occur even if the satellite geometry is good. One problem with the actual data set was that the signal quality was quite poor to some of the satellites. Therefore an improved algorithm to test the phase ambiguities is needed. In the current version of the software we test the ambiguity candidates using observations only from one epoch. This algorithm can be improved so that more epochs are involved in the ambiguity testing.

It is well known that the influence of noise on the signal becomes higher when the elevation angle towards the satellite becomes lower. To improve the results in the undifferenced software some initial tests were performed with different observation weighting approaches. The results from these tests indicate that it is possible to improve the result by applying weights. All the tested observation weighting methods are dependent on the combination of receiver and antenna. This is not considered during our tests, where we have used only default values taken from other research groups, which means that it is possible to improve the result by studying this subject further.

7.2 Further developments and research

This thesis proves the hypothesis that it is possible to determine deformations with undifferenced GPS-observations. The estimated accuracy that we got so far in our undifferenced software is not as good as the same as in traditional kinematic calculations based on double differences, but there are several potential factors left that can improve the result. We have already in the previous section mentioned that the influence of the troposphere is one of the factors that can be studied further as well as different weighting procedures. The following developments can be implemented to

improve the result; a more stabile ambiguity testing algorithm which uses more than one epoch to fix the ambiguities, a correct weighting algorithm for the observations.

One of the main purposes with this project is to see if it is possible to improve the result by using several reference stations in a multipoint solution. This is not done yet and therefore, this is one of the main target in the continuation of the project.

Our goal in the project was to generate a real-time software. To reach this goal we need to change the programming language to a language that are better adopted for real-time applications. The code is so far written in Matlab which is a very good language when developing and testing applications, but Matlab is not suited for real-time applications.

8 References

Beutler G, Gurtner W, Bauersima I, and Rothacher M (1986). Efficient computation of the inverse of the covariance matrix of simultaneous GPS carrier phase difference observations. Manuscripta geodetica Vol. 11: 249-255

Beutler G, Bauersima I, Gurtner W, and Rothacher M (1987). Correlations between simultaneous GPS double difference carrier phase observations in multistation mode: Implementation considerations and first experiments, Manuscripta geodetica, Vol. 12: 40-44.

Bjerhammar A (1973), Theory of Errors and Generaized Matrix Inverses, Elsevier Scientific Publishing Company. Amsterdam, London, New York, ISBN 0-444-40981-5

Brown R. G., Hwang Y.C. P. (1992), Introduction to Random Signals and Applied Kalman Filtering, Second Edition, John Wiley & Sons, New York, ISBN 0-471-52573-1

Brown R G, Hwang Y C P (1997), Introduction to Random Signals and Applied Kalman Filtering, Third Edition, John Wiley & Sons, New York, ISBN 0-471-12839-2

Brunner F K, Hartinger H, Troyer L (2000), GPS signal diffraction modelling: the stochastic SIGMA-Δ model. Journal of Geodesy, 73: 259-269

Collins J P, Langley R B, (1999), Possible weigthing schemes for GPS carrier phase observations in the presents of multipath, Contract report for the United States Army Corps of Engineers Topographic Engineering Center, No. DAAH04-96-C-0086 / TCN 98151

Davis J L, Herring T A, Shapiro I I, Roger A E E, Elgered G (1985), Geodesy by Radio Interferometry: Effect of Atmospheric Modelling Errors on Estimates of Baseline Length. Radio Science, 20(6):1593-1607

Fan H (2001), Theoretical Geodesy, Lecture Notes, Division of Geodesy Report No.2016, Royal Institute of Technology, Sweden, ISBN 91-7170-646-1

Fan H (2003), Theory of errors and Least Squares Adjustment, Lecture Notes, Report No.2015, Royal Institute of Technology, Sweden., ISBN 91-7170-200-8

Farrell J, Barth M, (1999), The Global Positioning System and Inertial Navigation, McGraw-Hill Publishing Co New York, ISBN-0-07-022045-X

Frei E, Beutler B (1990). Rapid static positioning based on the fast ambiguity resolution approach "FARA": theory and firstresults. Manuscripta Geodaetica, 15(4):325-356.

Gassner G, Wiesner A, Brunner F K (2002), GPS software Development for Monitoring of Landslides. FIG XXII Congress Washington, D.C. USA.

Gurtner W (2001), RINEX: The Receiver Independent Exchange Format Version 2.10, Astronomical Institute, University of Berne

Halliday D, Resnick R, Walker J (2001), Fundamentals of Physics, Six Edition, John Wiley & Sons, Inc. ISBN 0-471-33235-6,

Hartinger H, Brunner F K (1999), Variances of GPS Phase Observations: The sigma-ε Model. GPS-solutions, Vol.2, No.4:25-43

Hoffmann-Wellenhof B, Lichtenegger H, and Collins J (2001), GPS Theory and Practice, Fifth Edition, Springer-Verlag, Wien New York, ISBN 3-211-83534-2

Hopfield H S (1969), Two-quartic Tropospheric Refractivity Profile for Correcting Satellite Data, Journal of Geophysical Research 74(18):4487-4499

Horemuz M, Sjöberg L E (2002), Rapid GPS ambiguity resolution for short and long baselines. J Geod.76 (2002), 6-7: 381-391

Horemuz M, Andersson J V (2006), Polynomial interpolation of GPS satellite coordinates, GPS-solutions, Vol.10, No.1:67 - 72

ICD-GPS-200C (1999), Interface Control Document ICD-GPS-200, Revision C, IRN-200C-004, ARINC, Incorporated. El Segundo, CA

Ifadis I (1986), The Atmospheric Delay of Radio Waves: Modelling The Elevation Dependence on a Global Scale. Licentiate Thesis, Technical Report No 38L, Chalmers University of Technology, Gothenburg, Sweden, 1986

Ifadis I (2000), A new approach to mapping the atmospheric effect for GPS observations. Earth Planets Space, 52:703-708

Ince C D, Sahin M (2000), Real-time deformation monitoring with GPS and Kalman Filter. Earth Planets Space, 52:837-840

Jansson P (1998), Precise Kinematic GPS Positioning with Kalman Filtering and Smoothing, Doctoral Dissertation, Division of Geodesy Report No.1048, Royal Institute of Technology, Sweden, TRITRA-GEOFOTO 1998:7

Jin X X, de Jong C D (1996), Relationship between satellite elevation and precision of GPS code observations, Journal of Navigation, 49:253-265

Jäger R, Kälber S (2004), GNSS / GPS / LPS based Online Control and Alarm System (GOCA). Proceedings WEPES 2004, Workshop on Environmental Problems and Ecological Safety, Germany, Wiesbaden, Sept. 29- Oct. 1, 2004

de Jonge P, Tiberius C (1996), The LAMBDA method for integer ambiguity estimation: implementation aspects. Publications of the Delft Geodetic Computing Centre, LGR-Series No.12

Joosten P, (2001), The LAMBDA-Method: Matlab Implementation Version 2.1 12th March 2001. Delft University of Technology

Klobuchar J (1987), Ionospheric Time-Delay Algorithm for Single-Frequency GPS Users, IEEE. Transactions on aerospace and electronic systems vol. AES-23, No. 3

Klobuchar (2001), Eye on the Ionosphere: Correction Methods for GPS Ionospheric Range Delay, GPS-solutions, Vol. 5, No. 2: 91-92

Koch K-R, (1997), Parameter Estimations And Hypothesis Testing in Linear Models, Springer-Verlag, Berlin Heidelberg New York, ISBN 3-540-65257-4

Leick A, (2004), GPS Satellite Surveying, Third Edition, John Wiley & Sons, ISBN 0-471-05930-7

Mader G L (2002). GPS Antenna Calibration at the National Geodetic Survey, U.S. National Geodetic Survey

Marini J W (1972), Correction of satellite tracking for an arbitrary atmosphere profile. Radio Sci., 7:223-231

Mendes V B, Langley R B (1994), A Comprehensive Analysis if Mapping Functions Used in Modelling Tropospheric Propagation Delay in Space Geodetic Data, KIS94, International Symposium on Kinematic Systems in Geodesy, Geomatics and Navigation, Banff, Canada, August 30 – September 2, 1994

Mendes V B, Langley R B (1999), Tropospheric Zenith Delay Prediction Accuracy for Airborne GPS High-Precision Positioning. Navigation 46(1):25-34

Niell A E (1996), Global mapping functions for the atmosphere delay at radio wavelength. Journal of Geophysical Reseach, Vol. 101, No.B2:3227-3246

Råde L, Westergren B (1998), Mathematics Handbook for Science and Engineering, Studentlitteratur, Lund, Sweden, ISBN 91-44-00839-2

Saastamoinen J (1973A), Contributions To The Theory of Atmospheric Refraction, Bulletin Géodésique, No 105: 279-298

Saastamoinen J (1973B), Introduction to Practical Computation of Astronomical Refraction, part 1, Bulletin Géodésique, No 106: 383-397

Saastamoinen J (1973 C), Introduction to Practical Computation of Astronomical Refraction, part 2, Refraction Corrections in Satellite Geodesy, Bulletin Géodésique, No 107:13-34

Satirapod C & Wang J (2000): Comparing the quality indicators of GPS carrier phase observations, Geomatics Research Australasia, 73:75-92.

Schön S,Wieser A, Macheiner K (2005), Accurate tropospheric corrections for local GPS monitoring networks with large height differences, ION GNSS 2005, Session D1 " Atmospheric Effects on GNSS by Troposphere & GNSS Metrology Applications

Seeber G (1993), Satellite Geodesy, Foundations, Methods, and Applications, Walter de Gruyter, Berin New York ISBN 3-11-012753-9

Sjöberg L E (1997). On optimality and reliability for GPS base ambiquity resolution by combined phase and code observables, Zeitschrift für Vermessungswesen, Vol. 122, No. 6:270-275

Sjöberg L E (1998A), A new method for GPS phase base ambiguity resolution by combined phase and code observables. Survey Review Vol. 34, No. 268:363 – 372

Sjöberg L E (1998B), Linear estimation of GPS phase ambiquities from dual frequency code and phase observables. Division of Geodesy Research Report No. 1049, Royal Institute of Technology, Stockholm, December, 1998

Sjöberg L E, Horemuz M (1999). Quick GPS ambiguity resolution for short and long baselines, Division of Geodesy Report No. 1051, Royal Institute of Technology, Sweden, TRITA-GEOFOTO 1999:3

Sjöberg L E (2005), Theory of Satellite Geodesy, Lecture notes, Division of Geodesy, Royal Institute of Technology, Sweden

Thayer, G D (1974), An Improved Equation for Radio Refractive Index of Air, Radio Science, 9(10):803-807

Teunissen, P J G (1994), A new method for fast carrier phase ambiguity estimation, Proceedings of IEEE PLANS'94:562-573.

Wanninger L, Frevert, V, Wildt S (1999), Mitigation of signal Diffraction Effects on Precise GPS-positioning. Poster presented at the XXII. General Assembly of the IUGG, Birmingham (1999)

Wieser A, Brunner F K (2000), An extended weight model for GPS phase, Earth Planets Space, 52, 777-782, 2000

Wieser A, Gaggl M (2005), Improved positioning accuracy with high-sensitivity GNSS receivers and SNR aided integrity of pseudo-range observations. Reprint of paper at ION GNSS, Long Beach, CA, Sept 13-16

Witchayangkoon B, (2000), Elements of GPS Precise Point Positioning, PhD dissertation at The University of Maine

Wübbena G, Menge F, Schmitz M, Seeber G, Völksen C (1996), A New Approach for Field Calibration of Absolute Antenna Phase Centre Variations, Proceedings International Technical Meeting, IONGPS−96, Kansas City, Missouri:1205−1214.

Homepages on internet:

Swedish Road Administrations www.vv.se (2006-05-19)

Geo++®, www.geopp.de (2006-05-19)

Trimble navigation, www.trimble.com, (2006-05-19)

9 Appendix A

Coefficients of the hydrostatic mapping function developed by Niell (1996)

Average

Latitude	$\tilde{a}$	$\tilde{b}$	$\tilde{c}$
15	1,2769934E-03	2,9153695E-03	6,2610505E-02
30	1,2683230E-03	2,9152299E-03	6,2837393E-02
45	1,2465397E-03	2,9288445E-03	6,3721774E-02
60	1,2196049E-03	2,9022565E-03	6,3824265E-02
75	1,2045996E-03	2,9024912E-03	6,4258455E-02

Amplitude (hydrostatic)

Latitude	a	b	c
15	0,000	0,000	0,000
30	1,2709626E-05	2,1414979E-05	9,0128400E-05
45	2,6523662E-05	3,0160779E-05	4,3497037E-05
60	3,4000452E-05	7,2562722E-05	8,4795348E-04
75	4,1202191E-05	1,1723375E-04	1,7037206E-03

Amplitude (wet)

Latitude	a	b	c
15	5,8021897E-04	1,4275268E-03	4,3472961E-02
30	5,6794847E-04	1,5138625E-03	4,6729510E-02
45	5,8118019E-04	1,4572752E-03	4,3908931E-02
60	5,9727542E-04	1,5007428E-03	4,4626982E-02
75	6,1641693E-04	1,7599082E-03	5,4736038E-02

Height correction

a_h	b_h	c_h
2,5300000E-05	5,4900000E-03	1,1400000E-03